DESIGN AND AN AUTOMATED PARAMETRIC STUDY OF GEODESIC DOMES

by

Cecil Allen Jones

Thesis submitted to the Graduate Faculty of the
Virginia Polytechnic Institute and State University
in partial fulfillment of the requirements for the degree of
MASTER OF SCIENCE
in
Civil Engineering

APPROVED

S./M. Holzer, Chairman

R. H. Plaut

D. A. Garst

June, 1978

Blacksburg, Virginia

ACKNOWLEDGEMENTS

The author wishes to express his sincere appreciation and thanks to Dr. S. M. Holzer for his encouragement and support in the development of this thesis. An additional thank you is extended to Prof. D. A. Garst, Dr. R. H. Plaut, and Prof. O J. Blake for their advice, comments and contributions in the preparation of the material contained herein.

The author offers his appreciation and thanks to

, , , and for

their invaluable assistance in typing the text.

TABLE OF CONTENTS

TABLE OF CONTENTS (continued)

TABLE OF CONTENTS (continued)

LIST OF FIGURES

LIST OF FIGURES (continued)

LIST OF FIGURES (continued)

LIST OF TABLES

NOMENCLATURE

The following is a list of variables used in the text.

(,)	matrix dimensions (# rows, # columns)
A	area of lattice element, area of triangular face
B	Compatiability transformation matrix
c_k	cosine of rotation angle
d	direction of design change
e	number of degrees of freedom
E	modulus of elasticity
E'	modulus of elasticity of equivalent shell element
g_i, g_j	equality constraint function, inequality constraint function
i_j	unit vector on the j-local axis
k	cycle of iterative analysis
ℓ	projection length of discrete element in space
L	length of member
n	number of members in a structure
P	equivalent concentrated load
P_x, P_y	applied joint loads in x and y directions
q	distributed load
q'	equivalent distributed load
r	order of indeterminacy of a structure
r_g	radius of gyration of lattice element
s_k	sine of rotation angle
S	matrix product of modulus of elasticity and B matrix

NOMENCLATURE (continued)

S_a, S_b	partioned forms of matrix S
t'	thickness of equivalent shell element
u	elongation of member in x-direction
U	global displacement vector
U_a, U_b	partitioned forms of matrix U
v	elongation of member in y-direction
x	design variable vector, vector in local coordinates
x_i	design variable of member i
X	vector in global coordinates
X_{mn}	coordinate of joint m in the n direction
α	amplitude of directed design change
β	overrelaxation factor, horizontal plane angle
ε	strain vector
θ	slope of triangular face
λ	coordinate transformation matrix
ν'	poisson's ratio of equivalent shell element
σ	actual stress vector
σ_a, σ_b	partioned forms of stress vector
$\bar{\sigma}$	maximum allowable stress vector
ϕ	angle between members
Φ	rotation angle

CHAPTER 1

INTRODUCTION

1.1 Objectives

Many of the modern structures under construction today are very complex and sophisticated in design. In many of these designs, engineers have utilized the theoretical ideas of shells and the creativeness of concrete. But the disadvantages of forming and the excessive weight of the concrete have caused many designers to seek more economic options afforded by utilizing lightweight, high strength steels and metal alloys. In particular, many of the modern lattice or reticulated domes have employed these materials in achieving satisfactory results [1,3,18,24, 26,28,35].

In addition to being lightweight, these structures have been reported to possess excellent load distribution characteristics and can sustain eccentric as well as symmetrical loads [26,34]. It is the objective of this thesis to a) investigate the three-dimensional load distribution characteristics of reticulated domes via a parametric study and b) illustrate automated methods for the structural analysis and design of these structures.

To perform the parametric study, a space truss and a space frame structural analysis computer program are assembled to analyze the framework of a geodesic dome (a particular form of lattice dome). The solution algorithm employed in the analysis portion of these programs is based on the stiffness method of matrix structural analysis. The

automated space truss program is modified to incorporate a fully-stressed design procedure via the stress-ratio method. This is done to permit the study of the use of automated methods for interactive computer design for reticulated structures. The contents of chapters 2 and 3 are devoted to a discussion of these topics.

In chapter 4, various industrial and domestic applications for geodesic domes are presented. This is followed by an introduction to geodesic terminology and a general description of geodesic geometry.

A brief description of the assembled WATFIV/FORTRAN computer code and its capabilities is given in chapter 5. This is accompanied by descriptions of several demonstration problems and actual numerical results obtained using the WATFIV/FORTRAN computer code.

Finally, chapter 6 contains a summary of the numerical results presented in chapter 5 as well as conclusions drawn from these results. In addition, several suggestions for further study are discussed.

A mathematical derivation of the coordinate transformation matrix, miscellaneous sample preliminary calculation procedures, and results obtained from an automated design of one of the demonstration problems are placed in the appendix.

CHAPTER 2

THE STIFFNESS METHOD OF MATRIX STRUCTURAL ANALYSIS

2.1 Introduction

Matrix algebra has become a very powerful mathematical tool for the structural engineer. When the structural engineer is required to obtain a solution for a structural problem, he must decide upon an approach which is both easy to use and theoretically applicable to the problem under consideration. For the analysis of skeletal structures (such as space trusses and frames), an approach using the techniques of matrix algebra has several advantages. First, the notation provides a precise compact symbolism for the presentation of basic structural principles. Secondly, it aids the development of mathematical procedures which are applicable to a wide range of structures [14].

The systematic processes of matrix manipulation which may be developed reduce the elaborate numerical operations required in the analysis of any given structure [14]. If performed by hand, these processes become tedious and unwieldly to use for large complex structures. However, if the systematic matrix manipulations are carried out by a digital computer they become a powerful tool. Thus, because of the computer, matrix methods have found a major application in the field of structural engineering.

Realizing the advantages to be gained in using the matrix approach in the analysis of large intricate structures, the author has decided to implement the method in a computer code for the analysis of space

trusses and space frames. But before the approach can be formulated into a computer code, some specific aspects of matrix structural analysis must be considered.

2.2 Stiffness Approach vs. Flexibility Approach

There are basically two approaches to matrix methods of structural analysis which are closely related. These two approaches have come to be known as the stiffness [10] (equilibrium [14], displacement [22]) method and the flexibility [10] (compatibility [14], force [22]) method. In the matrix analysis of skeletal structures, if one wishes to work in terms of the joint displacements, which are the more physically obvious variables, one would tend to choose the stiffness method of matrix analysis [14]. The flexibility method on the other hand involves an investigation of the degree of indeterminacy of a structure to ascertain the basic variables which are self-equilibrating redundant load-pairs [14].

The basis for choosing one approach over the other centers around the desire for a general purpose program for structural analysis. The unkown quantities in the stiffness method (the displacements of the joints) may become quite numerous, especially in the analysis of large intricate structures. The number of unkowns in the flexibility method (the redundant load-pairs) are generally less than those found in the stiffness method [29]. Thus, for large structural systems, one might at first glance choose the flexibility method over the stiffness method for ease of solution. But a major difficulty in the flexibility method arises when a general purpose program is to be assembled for the analysis

of different types of structures. The choice of redundants in the flexibility method becomes a difficult task to accomplish in automated programs [29]. If programs are written for a particular type of structure this problem is easily overcome, as the same basic form of the primary structure would be used [29]. But it is more desirable to assemble general purpose programs which can be employed in the analysis of a variety of complex structures. In the case of the stiffness method, the unknowns are always the joint displacements regardless of the type or structure size under investigation. And since interest is largely centered on the displacements of the joints in skeletal structures [14], it seems more logical and judicious to consider the stiffness method over the flexibility method. Once the joint displacements are determined, it is no great effort to find the joint forces associated with the displacements. Internal forces within the skeletal member itself are then easily obtained from the member end-forces employing traditional classical procedures [22]. Recognizing the advantages of applying such a method to any arbitrary skeletal structure, one should naturally choose the stiffness method over the flexibility method and its inherent limited scope of application in general purpose programs. For this reason, the stiffness method of matrix structural analysis has been selected by the author as the basis for the development of the automated procedure for the analysis of space trusses and space frames. It is the author's assumption that the reader possesses a sufficient background in the mathematical development of the stiffness method of structural analysis to understand

the solution algorithms incorporated in the computer code, as these algorithms are based on the mathematical procedures presented in the matrix structural analysis courses taught in the Civil Engineering Department at VPI & SU [10]. Further, it is assumed that the reader is familiar with all of the important theoretical assumptions such as the linear elastic small-deflection theory upon which the matrix methods of structural analysis are founded. But in the event that the reader should require a quick review of the basic components of the stiffness method, a flowchart of the method has been presented in Fig. 1.1.

In this chapter, the analysis procedure for space trusses and space frames has been described along with basic assumptions. It is appropriate to move to a discussion of the procedures that will effectively utilize the information provided by this important component of the design process.

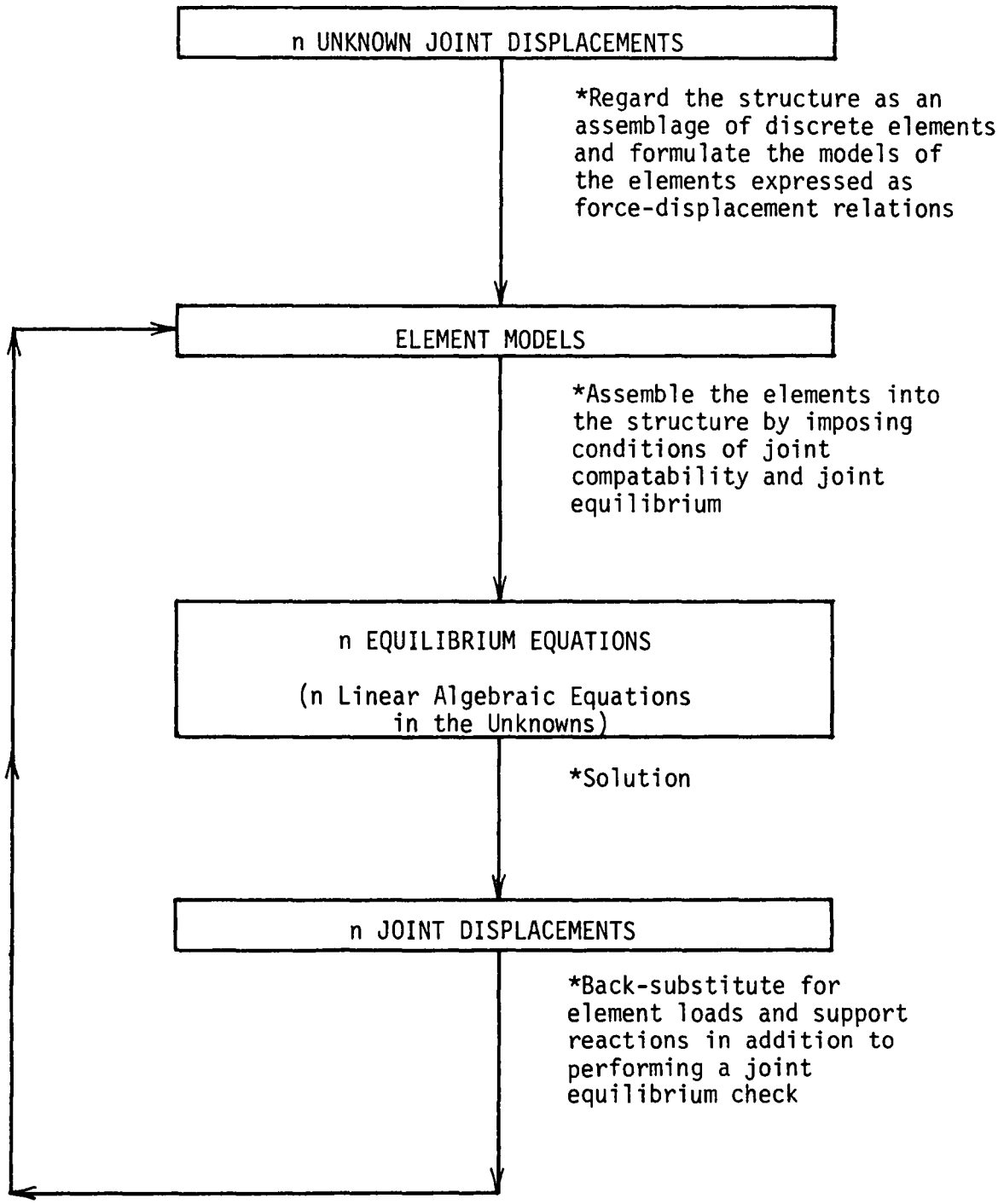

FIG. 1.1 - Flowchart of the Stiffness Method [10]

CHAPTER 3

THE FULLY-STRESSED DESIGN OF SKELETAL STRUCTURES VIA THE STRESS - RATIO METHOD

3.1 Introduction

In conventional structural design, an engineer attempts to produce a structure that is safe, functional, economical and satisfies a specific need [11]. The conventional structural design process begins when there is a recognized need for a structure. A structural form or scheme is drawn up satisfying specified design criteria. A trial design is then chosen from a preliminary analysis of the structural form. Actions are imposed on the initial trial design and a structural analysis is performed. From this analysis, the engineer obtains a response, usually in the form of displacements at the joints of the structure. From these displacements, member forces and stresses may be obtained. In the design process, limitations are placed on the design variables in the form of allowable stresses and minimum gauge sizes which are referred to as design constraints [11,31]. The minimum gauge sizes are necessary to prevent stability and serviceability problems that may occur if there were no such constraints. The designer is thus provided the necessary information to decide if the design meets code requirements [31] and is a feasible design. If the design is not feasible, adjustments in the design variables of the structure are carefully considered until a feasible design is obtained which minimizes (optimizes) a given cost function. The cost function is usually formulated in terms of specific structural parameters such as material

density and cross-sectional area of the members [8].

For the complex space truss structure considered in this discussion, the constraints are visualized as being upper bounds on the stresses and lower bounds on the cross-sectional areas of individual members [2]. It is thus possible to create a structure in which all the design variables lie within the upper and lower bounds of the design constraints. Some authors of recent optimum design publications feel that when the design variables are controlled by stress constraints alone the design should be referred to as "fully-stressed" [2]. Where the structure is subjected to multiple loading conditions, a fully-stressed design is one in which the design variables are stress-constrained for at least one of the applied loads [2,8]. When the design variables are either stress or gauge constrained, a "fully-constrained" design is obtained [2]. It may happen that many fully-constrained designs are also optimal designs. If it is known ahead of time that the resulting optimal design is a fully-constrained design, it is then possible to find the optimizing values for the design variables by seeking to satisfy the constraints only without considering a cost function [2]. For statically determinate structures, a fully-stressed design procedure involving a "stress-ratio" formula can achieve the desired results. But for indeterminate structures, it becomes necessary to use an iterative procedure to obtain a fully-constrained design [2]. The latter case involves devising algorithms based upon either the simple "stress-ratio" or the more sophisticated Newton procedures [2,8].

According to theory, these procedures should converge towards the

optimal design if the resulting optimal design is fully-constrained. But some structures do not have optimizing design variables which are controlled by constraints and are referred to as non fully-constrained optima [2]. Certain authors [19,25] have shown that such optima can be identified by the occurrence of negative Lagrangian multipliers. For such cases, new methods which depart from the fully-constrained criterion are required, permitting the selection of improved designs [2].

Such discussions are more concerned with the realm of optimal design and involve elaborate techniques for arriving at minimum weight designs for structures subjected to multiple loadings. The automated design process used in the design of the statically indeterminate space truss presented in Appendix C is based on the simple stress-ratio algorithm in which the design variables are assumed to be fully-constrained. No effort is made to determine if the resulting design is an optimal design as this would involve the minimization of a cost function and the employment of the techniques mentioned above [19,25].

The remainder of this chapter is devoted to investigating various aspects of the fully-stressed criterion in some detail. Basic definitions of associated terms are presented next. This is followed by a discussion devoted to the stress-ratio method for obtaining a fully-stressed design. The necessary conditions for a fully-stressed design to be feasible is investigated next with a brief review of the relationship of fully-stressed design and optimal design to follow. The chapter concludes with some remarks concerning the role preliminary design plays in the automated design process.

3.2 Basic Definitions

The following is a presentation of the definitions which are associated with the fully-stressed design procedure.

> STRUCTURAL OPTIMIZATION is the selection of design variables which satisfy the limits (constraints) placed on the structural behavior, geometry, stability or other criteria in attaining an optimum state defined by the objective function for specified loadings or environmental conditions [8].

> DESIGN VARIABLE is a term used to describe the size of a member, representing the cross-sectional area of a truss member or the moment of inertia of a flexural member [8].

> DESIGN SPACE is described by axes representing the respective design variables. Fig. 3.1 shows a three-variable or three dimensional design space. The number of design variables "n" is generally greater than three and the n-dimensional space is termed a "hyperspace" [8].

> DIRECT SEARCH is the strategy used in design algorithms in which a series of directed design changes are made between successive points in design space. A typical change is between the

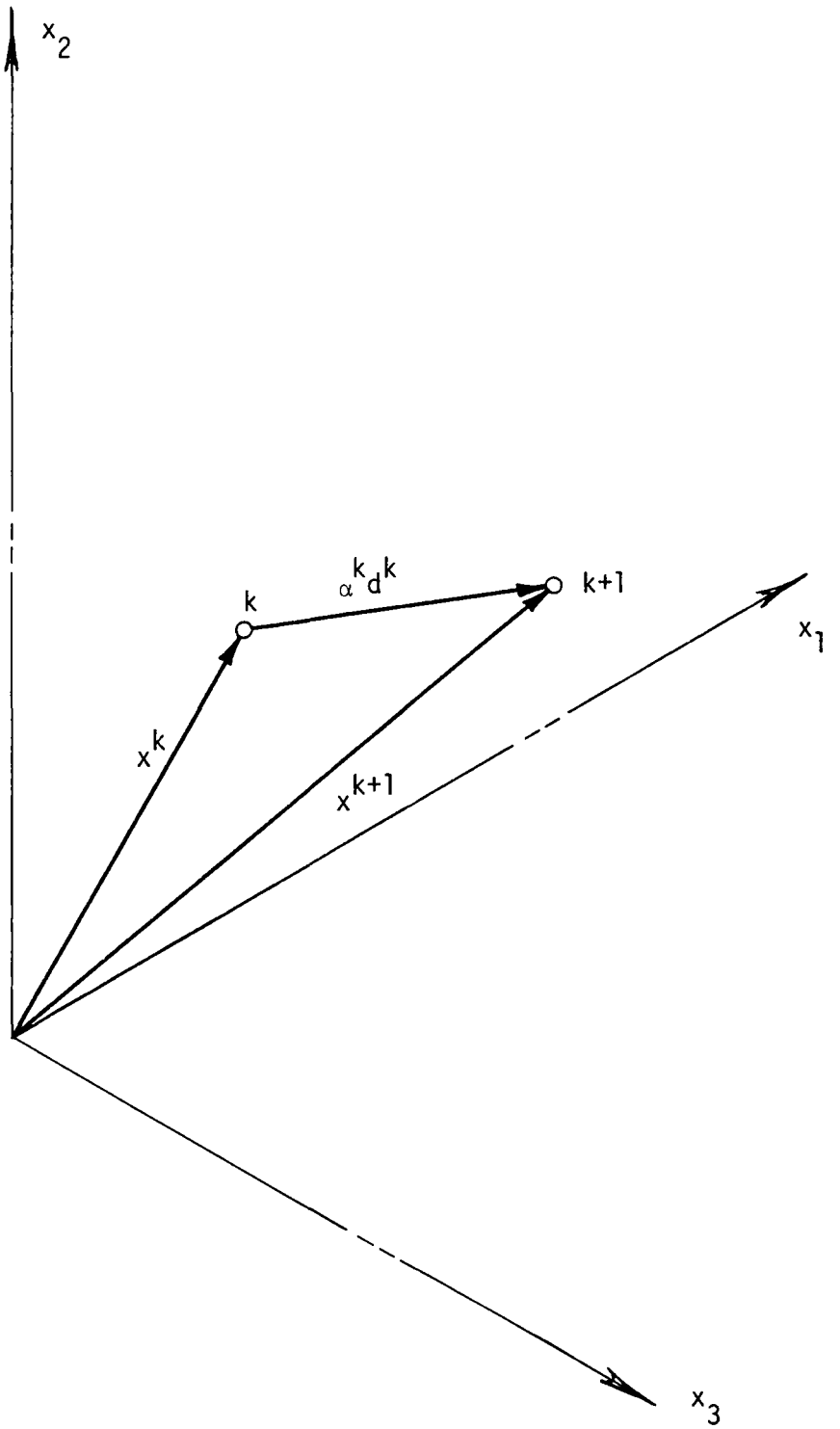

FIG. 3.1 - Three Variable Design Space with Design Points "k" and "k+1"

kth and (k+1)th design points given by the equation

$$x^{k+1} = x^{k} + \alpha^{k} d^{k} \tag{3.1}$$

in which x^k = the design variable vector in the kth cycle of iterative analysis; x^{k+1} = the design variable vector in the (k+1)th cycle of interative analysis; d^k = a vector which defines the direction of the change; and α^k = the amplitude of d^k [8]. This idea is presented graphically in Fig. 3.1.

OBJECTIVE FUNCTION (cost function or merit function) is a scalar function of the design variables whose extreme value is sought in an optimization procedure and constitutes a basis for the selection of one of several alternative acceptable designs [8].

CONSTRAINT is a restriction to be satisfied so that the design may be acceptable [8].

EXPLICIT CONSTRAINT is a limitation imposed directly on a design variable or group of design variables [8].

IMPLICIT CONSTRAINT is a limitation on quantities whose dependence on the design variables cannot be stated directly [8].

EQUALITY CONSTRAINT is a constraint designated by the

the equality sign which may be either explicit or implicit [8].

INEQUALITY CONSTRAINT is a constraint designated by the inequality sign and may be either explicit or implicit [8].

SIDE CONSTRAINT is an explicit constraint that is a specified limitation (minimum or maximum) on a design variable or a relationship which fixes the value of a group of design variables (see Fig. 3.2 where $g_i(x)$ represents a constraint function) [8].

BEHAVIOR CONSTRAINT is either an explicit or implicit constraint which is a limitation on the stresses or displacements of a structure (see Fig. 3.2) [8].

FEASIBLE DESIGN POINT is a design point in design space which satisfies the constraints [8].

INFEASIBLE DESIGN POINT is a design point that represents a violation of constraints [8].

3.3 Fully-Stressed Design via the Stress-Ratio Method

As stated in the introduction to this chapter, a fully-stressed design, hereafter referred to as f.s.d., is a design in which each structural member sustains a limiting allowable stress under at least one of the specified loading conditions [2,8]. Analysis is restricted

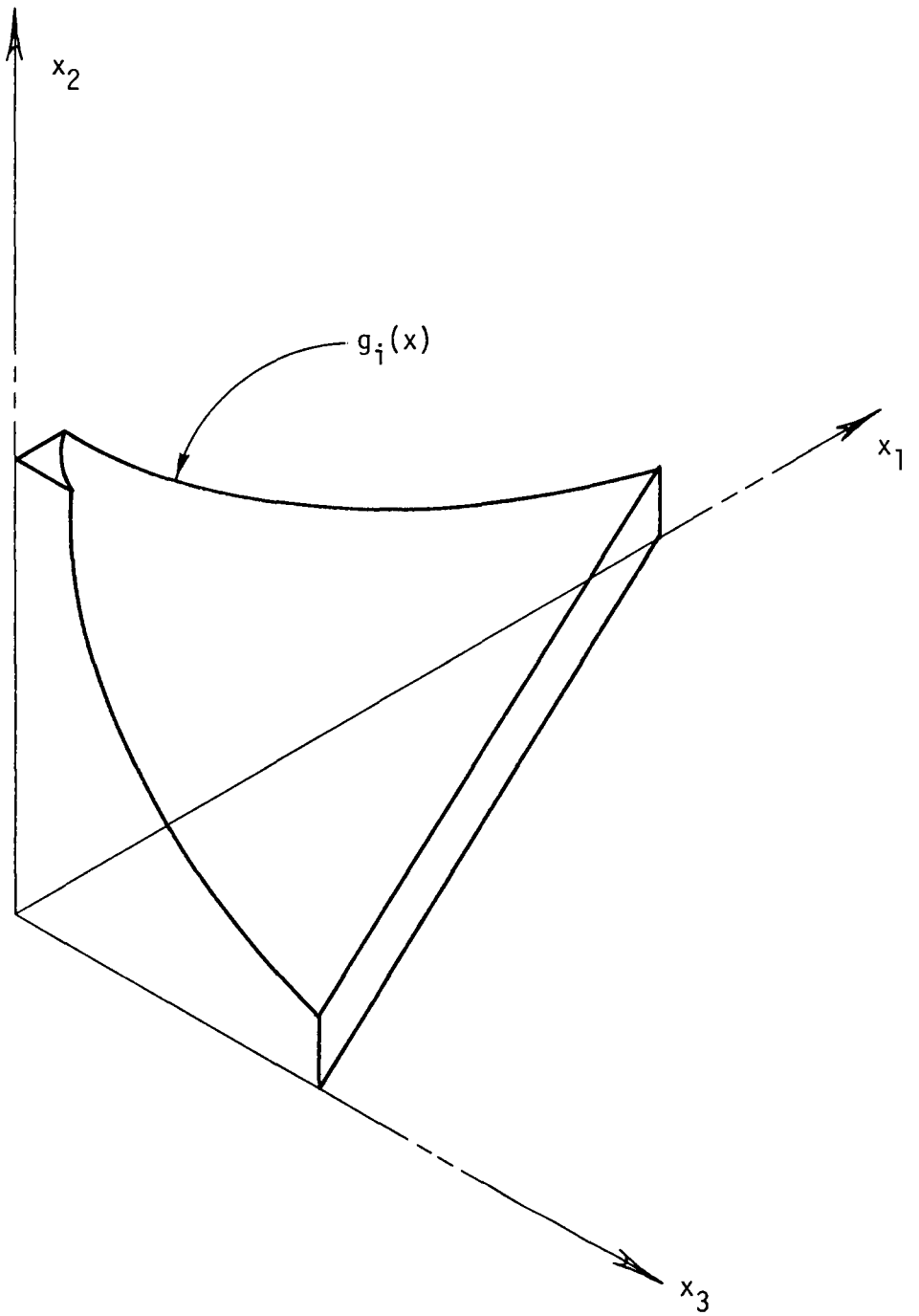

FIG. 3.2 - Three Variable Design Space with Typical Side and Behavior Constraints

to the selection of member sizes for a fixed structural geometry and specified materials [8]. No consideration is given to displacement or stability limitations. If maximum or minimum member-size limitations are considered, the affected members may not be fully-stressed [8].

According to Gallagher, the f.s.d. procedure owes its significance to its intuitive appeal in the design of optimal structures [8]. An f.s.d. analysis provides structural proportions which can be proved to be optimal under certain circumstances [8].

Also, it is relatively inexpensive in application when compared with other methods derived from mathematical-programming concepts [8]. In order to gain a better understanding of the general nature of an f.s.d. analysis, it is important to begin a discussion of the procedure by defining its relationship to the more general type of optimal-design analysis.

3.3.1 Characteristics of F.S.D.

In an f.s.d. analysis one does not seek an extreme value for an objective function as in an optimal design procedure. An f.s.d. analysis does not contain an objective or merit function, which must be extremized [8].

It is also observed that an f.s.d. is not unique [8]. Since every statically determinate structure can be proportioned directly to yield an f.s.d., if the members of an initially prescribed statically indeterminate structure are allowed to assume zero size, each subsidiary statically determinate form of the structure is an alternative f.s.d. [8].

Finally, there is no assurance that the algorithm for the calculation of an f.s.d. will converge to the minimum-weight f.s.d. since the minimum-weight merit function is absent from the algorithm [8]. This algorithm will now be reviewed in some detail.

3.3.2 The Algorithm for the Calculation of an F.S.D.

The algorithm used for calculating an f.s.d. is an interative analysis procedure in which the results from a given cycle are used to scale the members to the fully-stressed state. These scaled sizes are then used in the next cycle of analysis. This process can be written in algebraic form as

$$x_i^{k+1} = x_i^k(\sigma_i^k/\bar{\sigma}_i^k) \tag{3.2}$$

in which x_i^k = the design variable of the ith member in the kth cycle of iterative analysis; x_i^{k+1} = the design variable of the ith member in the (k+1)th cycle of iterative analysis; σ_i^k = the actual stress in the ith member in the kth cycle of iterative analysis; and $\bar{\sigma}_i^k$ = the maximum allowable stress in the ith member in the kth cycle of iterative analysis. Eq. (3.2) is referred to as the stress-ratio algorithm for the computation of an f.s.d. The process is continued until convergence to an f.s.d. state is attained unless this convergence is impossible because of relationships between the indeterminacy of the structure and the number of load conditions [4,8]. This problem is discussed in the next section of this chapter.

The convergence may be hastened by employing the idea of "over-relaxation" which is based on the fact that an increase in size of a

member will draw more load to that member and a decrease in size will relieve the amount of carried load [8]. Eq. (3.2) may be rewritten in the form

$$x_i^{k+1} = x_i^k(\sigma_i^k/\bar{\sigma}_i^k)^\beta \tag{3.3}$$

where β = the overrelaxation factor greater than unity.

Eqs. (3.2) and (3.3) represent the approach used in the design portion of the automated program discussed in chapter 5. However, more sophisticated f.s.d. algorithms than the stress-ratio method presented in Eqs. (3.2) and (3.3) may be used to obtain a more rapid convergence to the f.s.d state. It has been proven that a "mixed-mode" approach, coupling the idea of the stress-ratio method with the Newton method, results in convergence to an f.s.d. state in relatively few cycles of iterative analysis [2,8]. Though the potential value of a "mixed-mode" approach can be easily seen from the results obtained, a preference for a single-mode scheme may result when software costs and other complexities of a given problem (e.g. the availability of good initial design variable estimates) are taken into consideration [8].

To aid the reader in comprehending the stress-ratio algorithm as incorporated in the automated program described in Chapter 5, a simple flowchart of the procedure is presented in Fig. 3.3.

3.4 Feasibility of Convergence to an f.s.d.

Convergence to an f.s.d. is only feasible under certain conditions associated with the number of load conditions, the order of indeterminacy, and the topology (geometry) of the structural layout [4].

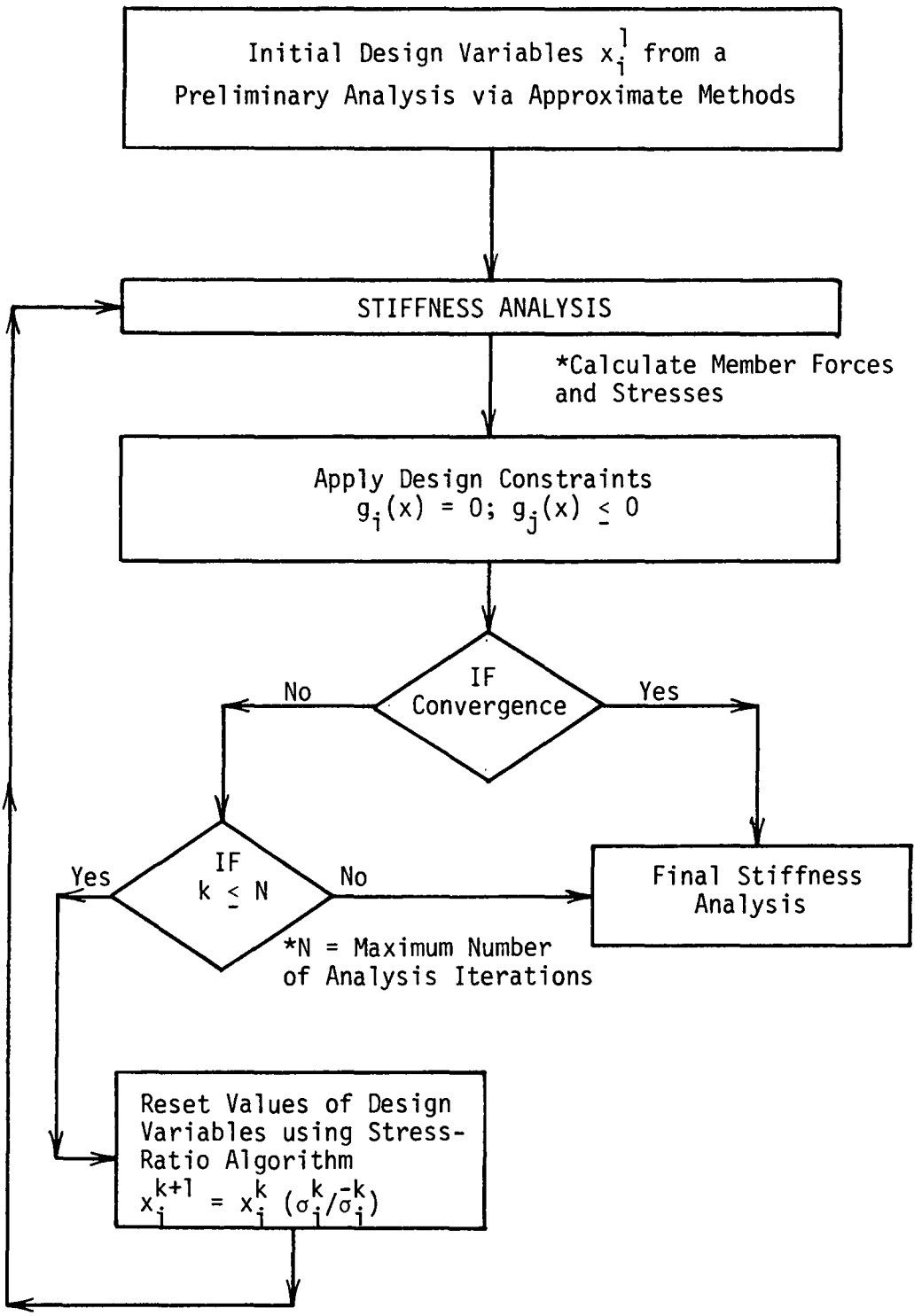

FIG. 3.3 - Flowchart of Fully-Stressed Design via the Stress-Ratio Method

To investigate the problem a little closer, consider a three-bar truss acted upon by a vertical load P_y with $P_x = 0$ as in Fig. 3.4 [8]. If member 2 is subjected to a stress, σ, the elongation, v_2, may be written as

$$v_2 = (\sigma/E)L_2 \tag{3.4}$$

If members 1 and 3 (having the same modulus of elasticity, E, as member 2) were also stressed to σ, then the elongations would be

$$v_1 = v_2 = (\sigma/E)(L_2/\cos\phi) \tag{3.5}$$

Applying compatibility of displacement at joint A dictates that

$$v_1 = v_3 = v_2 \cos\phi \tag{3.6}$$

From Eq. (3.5) it follows that

$$\sigma_1 = \sigma_2 \cos^2\phi \tag{3.7}$$

Therefore, the stress in the inclined bars must be less than the stress in the vertical member which is fully-stressed and an f.s.d. is not possible for a single choice of material [8].

The simple problem presented in Fig. 3.4 clearly demonstrates that the f.s.d. of a statically indeterminate structure is not feasible for a single load condition. But convergence to an f.s.d. can be obtained if the proper number of multiple load conditions is applied [4,8]. There exists a relationship between the number of load conditions and the order of indeterminacy of a structure which can determine the feasibility of convergence to an f.s.d. [4,8,11].

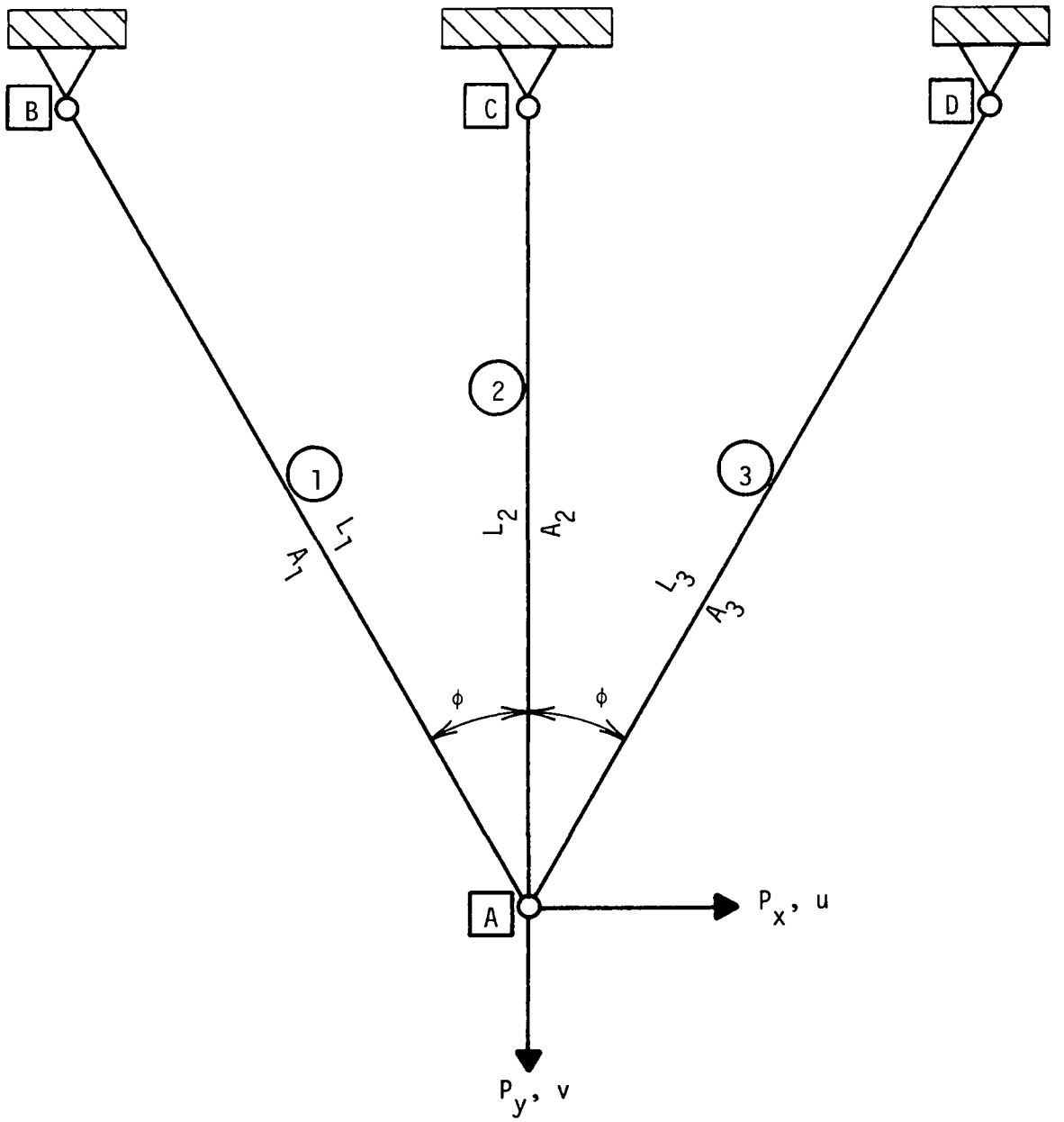

FIG. 3.4 - Three Bar Truss

To develop the relationship, consider the case of an indeterminate plane or space truss structure subjected to a single load condition [4,11]. From elastic deformation compatibility it is possible to write

$$\underset{(n,1)}{\varepsilon} = \underset{(n,e)}{B}\,\underset{(e,1)}{U} \tag{3.8}$$

where ε = the strain vector of discrete elements; B = the compatibility transformation matrix, U = the global displacement vector; n = the number of discrete elements in the structure; and e = the number of degrees of freedom of the structure.

From the constitutive law,

$$\sigma = E\varepsilon \tag{3.9}$$

in which E = modulus of elasticity; and σ = the stress vector associated with the strain vector, ε. Combining Eq. (3.8) and Eq. (3.9),

$$\sigma = EBU \tag{3.10}$$

or

$$\underset{(n,1)}{\sigma} = \underset{(n,e)}{S}\,\underset{(e,1)}{U} \tag{3.11}$$

Eq. (3.11) expresses n discrete element stresses in terms of e displacements of the joints of a structure. Writing Eq. (3.11) in partitioned form

$$\begin{bmatrix} \sigma_a \\ \sigma_b \end{bmatrix} = \begin{bmatrix} S_a \\ S_b \end{bmatrix} \begin{bmatrix} U_a \\ U_b \end{bmatrix} \tag{3.12}$$

or

$$[\sigma_a] = [S_a][U_a] \tag{3.12a}$$

$$[\sigma_b] = [S_b][U_b] \tag{3.12b}$$

Eq. (3.12a) represents a set of algebraic equations which can be solved to obtain U_a if S_a is nonsingular (i.e. $|S_a| \neq 0$). This means that for any one load condition, there exists a unique U containing e number of displacements of the structure. Therefore only e discrete element stresses may be arbitrarily selected as being fully stressed while the remaining (n-e) discrete element stresses are automatically defined by Eq. (3.12b) [4,11]. Hence, for a structure subjected to a single load condition, an f.s.d. is not feasible unless the number of degrees of freedom e is greater than the number of discrete elements n. This can be written as

$$e \geq n \tag{3.13}$$

In the case of statically indeterminate truss structures, this cannot be true since the number of degrees of freedom e is less than the number of discrete elements n.

However, considering a truss whose order of indeterminacy r is given by (n-e) and knowing that there must be (n-r) independent element equilibrium equations for each applied load condition, it is possible to write (using Eq. (3.13) [8])

$$p(n-r) \geq n \tag{3.14}$$

in which p = the number of loading conditions; n = the number of discrete elements; and r = the order of indeterminacy. Substituting the value (n-e) for r, Eq. (3.14) becomes

$$p(e) \geq n \tag{3.15}$$

or

$$p \geq n/e \tag{3.16}$$

If all n discrete elements in a statically indeterminate structure are to be fully-stressed, then the minimum number of applied load conditions is given by Eq. (3.16) [8]. From Eq. (3.16) it can be seen that more than one load condition is necessary for any redundant structure before the determination of member sizes can be accomplished on a truly independent basis [8].

3.5 The Relationship between F.S.D. and Optimal Design

As stated before, an f.s.d. is not unique [8] and may not always converge to an optimal design. But it is often desirable to determine if it is indeed an optimal design. The analytical procedure usually employed to perform this task is known as the Kuhn-Tucker optimality condition which is relatively inexpensive to apply [8,25].

Although the Kuhn-Tucker optimality condition provides a perfectly valid criterion for testing optimality, it does not help with the selection of improved designs for non-optimal cases. A failure of the test will not disclose the gap between the f.s.d and the optimal solution, nor will it disclose the relative proportions of members

for an optimal design [8]. Gallagher [8] addresses this problem and suggests several methods for its solution. However, Gallagher also states that available numerical evidence indicates that the gap between the best f.s.d. and an optimal design is often quite small for many classes of real problems.

Accordingly, the f.s.d. approach to structural design is often the most efficient and economical method of calculating sizes for structural members. If the relationship between the number of members, redundants and load conditions permits, and if the mode of structural action is simple, solutions can be obtained in relatively few cycles [8]. In addition, the f.s.d method is a good starting point for applications of mathematical programming methods for optimal structural design [8].

3.6 Remarks Regarding Preliminary Design

To begin the iterative f.s.d. process via the stress-ratio method, a suitable initial design variable must be chosen. The selection of the initial design variable is very important for it affects the rate of convergence to an f.s.d [8]. Thus, it is desirable to choose a value for the initial design variable which will necessitate relatively few iterations of the stress-ratio algorithm before an f.s.d. is obtained.

The methods employed in acquiring the initial design variables are approximate in nature. A discussion of approximate methods of structural analysis for indeterminate structures may be found in certain references [11,22]. In the case of lattice domes, many authors [23,27] have used the popular idea of approximating the

behavior of these structures by considering a similar continuum structure. The key to approximating a lattice by a continuum involves the relationship of properties of the two systems [36]. There are several approaches which are used to determine the appropriate relations. One particular method treats a lattice composed of equilateral elements having identical properties as a shell element using the following relations [31,36]:

$$E' = 2AE/(3)^{\frac{1}{2}}\ Lt' \tag{3.17}$$

$$\nu' = 1/3 \tag{3.18}$$

$$t' = 2(3)^{\frac{1}{2}}\ r_g \tag{3.19}$$

$$r_g = L/200 \tag{3.20}$$

where E' = the elastic modulus of the equivalent shell element; ν' = the Poisson's ratio of the equivalent shell element; t' = the thickness of the equivalent shell element; A = the area of the lattice element; E = the elastic modulus of the lattice element; L = the length of the lattice element; and r_g = the radius of gyration of the lattice element.

These are the relationships employed to obtain the initial cross-sectional area of the lattice elements which compose the framework of the demonstration problem for the fully-stressed design procedure described in Chapter 5 and Appendix C. However, Eq. (3.17) has been slightly altered upon discovery of a small printing error. The author compared the incorrect version of Eq. (3.17) as provided in reference [36] with similar equations for lattice structures as presented by Schnobrich [27] and corrected the error. Thus Eq. (3.17) as shown is in complete agreement with the relationship devloped by Schnobrich.

CHAPTER 4

GEODESIC DOMES

4.1 Introduction

The previous two chapters have been devoted to the discussion of automated methods for structural analysis and design which are suitable for incorporation in a computer code. These methods are used in the analysis and design of several demonstration problems which are quantitatively and descriptively defined in the next chapter of this discussion. But before this is done, it is important to physically comprehend and visualize the problems which are to be studied. To achieve this goal, the present chapter has been devoted to the geometric development of geodesic domes and the important characteristics which distinguish them from all other forms of structures. An an introduction, a brief historical review is presented along with some of the more important uses of the dome. This is followed by a study of the advantages and disadvantages associated with their use. Finally, a description of the geometric development is presented and appropriate geodesic terminology is defined.

4.2 A Brief History of the Development of Geodesic Domes

The introduction of iron opened up a new era of steel-braced domes in the eighteenth and nineteenth centuries [18,36]. The lightweight and high strength of these structures permitted the enclosure of large spaces [18]. One particular inventor recognized the advantages to be gained from pre-fabrication and mass production, and created a dome

consisting of identical elements joined together by simple connections. This inventor's name was R. Buckminster Fuller and the structure he invented was called a geodesic dome. Fuller created the design in 1949 and acquired a government patent in 1954. He developed the triangulated design of the dome by projecting the faces of an icosahedron onto the surface of a circumscribed sphere, creating a spherical icosahedron. The original Fuller domes consisted of two parts, a skeleton framework and a superimposed skin of plastic or mylar [7,18]. The skin was erected separately and did not contribute to the strength of the dome. For large spans, the arrangement of the bars in the single layer framework resulted in stability problems [18]. To avoid this, Fuller suggested forming "dimples" by inwardly offsetting the vertices of the pentagons and adjoining hexagons which considerably stiffen the structure [7,18]. But for very large spans, double-layer domes have become the only answer [18].

The increased popularity of the geodesic domes in recent years has resulted in a variety of uses for the structure which range from homes for domestic living to industrial applications.

4.2.1 A Review of Domestic and Industrial Applications for Geodesic Domes

Geodesic domes are becoming very popular in the area of housing. Peter Tobia of the New Jersey-based Geodesic Structures, Inc. claims that the market for geodesic domes is booming [33]. The interior space provided by these structures makes them an ideal choice for homes and hunting cabins. Someday they may even be used to enclose entire

cities [6]. Some are used as green houses, such as the Climatron in St. Louis [1]. Geodesic domes create a unique micro-climate completely immune from all outside atmospheric conditions [1,6]. Others are used as Antaractic scientifc research stations, providing protection from extreme cold temperatures, snow, ice and wind. One such dome was designed and built by Temcor for the U. S. Navy on the South Pole [26].

The Union Tank Car Company of Baton Rouge, Louisiana implemented the first major industrial application of the dome in the construction of a railroad tank car repair and maintenance depot [17,24]. Another important industrial use has been in the field of wastewater treatment. Many sanitary treatment facilities of various cities across the country employ the Polyframe Dome supplied by Temcor as process tank coverings, improving operating efficiency and odor control [3,34]. Similar domes enclose water storage tanks, insuring the safety and purity of drinking water [35]. The Polyframe Dome can also provide a very effective means of protecting chemicals, granular and solid materials as well [34].

One of the more spectacular uses of the geodesic dome was seen at EXPO '67 in Montreal, Canada [6,24]. The U. S. Pavilion was housed in a 5/8 sphere version of the geodesic dome which used a double layer space frame system consisting of a hexagonal inner layer and a triangulated outer layer to reduce stability problems [24].

Recently, the geodesic dome has also been considered as a possible means of enclosing football stadiums and coliseums [28].

These are just a few of the uses which can be found for geodesic domes. The number of uses will grow as the advantages afforded by

using such structures are realized by designers. In the next section, a few of these advantages are recognized along with some important disadvantages as well.

4.3 Advantages and Disadvantages Associated with the Use of Geodesic Domes

One of the most important advantages to be gained from the use of a geodesic dome is the ability to enclose large amounts of space without interior supporting columns. This provides a completely unobstructed inner space which is very desirable from a designer's point of view.

Secondly, geodesic domes have been reported to possess great stiffness and strength [26,34]. This is a result of the regular geometric nature of the geodesic framework which allows uniform stressing of members [18,36]. Computer studies have shown that the geodesic framing system is very effective in carrying symmetric as well as eccentric loads which occur during windstorms, ice buildup and snow drifts [18,26]. An important characteristic of the framework is a horizontal tension ring at the periphery of the dome which reduces the horizontal thrusts at the base, eliminating the need for construction of heavy foundations to resist these thrusts [18,30,34]. This can reduce foundation construction costs considerably.

Another important advantage to be gained from the use of geodesic framing systems is the reduction in fabrication, construction and maintenance costs [26,34]. The nearly identical elements and simple connections permit easy fabrication and mass production. The resulting

structure is extremely light compared to other similar concrete structures [36]. The use of lightweight structural elements and simple joint connections permits easy handling, shipping and quick erection without the employment of expensive scaffolding. This means a significant savings in construction, shipping and handling costs. If the framework members are manufactured from lightweight aluminum alloys, the resulting structure is corrosion resistant and maintenance free as well.

Economy is also realized in the heating and cooling of the interior of geodesic domes. The dome easily controls and maintains any desired temperature [1,6,30]. This reduces excessive heating and cooling costs [33]. The energy-saving, spherical geodesic dome has been shown to be more economical to heat and cool than the more conventional rectilinear homes [33].

Industry can find the dome advantageous to use because of the lightweight construction. This permits the entire removal of the dome as a single unit allowing easy access to the interior of the tanks which the dome may be used to cover [34,35]. When the removal of the entire dome is infeasible or undesirable, the lightweight triangular panels may be individually removed to permit easy access. Doors and hatches can be conveniently added as needed even after construction is complete [34].

Although there are many advantages in using the geodesic dome, there are several disadvantages which should be recognized as well. Stability is one of the main problems associated with the very large

domes [7,18,26,36]. The arrangement of framework members in a single layer may cause snap-through of a single joint [18]. Problems may occur as a result of the increase in the number of members in a single layer dome. The members joining any individual joint lie almost in the same plane when the dome is viewed in section. If the structure is pin-connected, the joint can easily snap-through [18,36]. This is referred to as local instability [36]. As mentioned before, Fuller suggested forming "dimples" in the dome's surface to prevent this type of instability [7,18]. But many large domes have adopted a very effective double-layer system to prevent snap-through problems [18,24]. Other dome systems make the joints as rigid as possible and stiffen the basic hexagonal unit with additional struts and cables [18, 30]. The problem of snap-through is discussed in several references [12,13,36].

Another disadvantage is the need for maintaining strict control over fabrication and erection tolerances [26,36]. If this is not done, the members may not meet properly. This can induce stress in the members which was not accounted for in the original design [26,36]. The possibility of snap-through of the joints is also enhanced [36].

In addition, not much is known about the dynamic effects on geodesic domes [36]. Much study is required in the area of wind loading and earthquake analysis of lattice structures before the dynamic response can be satisfactorily predicted [26,36].

Some geodesic domes have been reported to leak at the seams where the triangulated panels meet or where they frame into the struts of the dome [30,36]. There are many types of sealants on the market which

may be used to remedy the problem. If the struts possess grooves into which the triangulated panels may be snugly fitted and sealed, this can significantly reduce the possibility of leaks as well.

The geodesic dome can be noisy because of the lack of partitions to muffle the sounds from other parts of the interior [30].

The lack of curvilinear furniture suited for use in a circular room is also another disadvantage. Most furniture is designed for the more conventional rectilinear home [30,33].

Even though there are several disadvantages that cannot be overlooked, the geodesic dome can still provide a very effective and economical means for enclosing space.

4.4 Geodesic Geometry and Related Terminology

According to Popko [24], the term geodesic is a geometric title given to the arcs on a spherical surface which represent the shortest distance between any two points on that surface. In architecture, it is a framework of generally spherical form in which the main structural elements are interconnected in a geodesic pattern of approximate great circle arcs intersecting to form a three-way grid [7,18].

Fuller used the spherical version of the icosahedron as a basis for the geometric development of the three-way grid. All geodesic developments are based on the spherical versions of basic polyhedra. The five platonic solids of Fig. 4.1 are the most basic of polyhedra possessing regular congruent faces, equal face angles and equal dihedral angles between the faces [24]. Fuller chose the icosahedron because of the five platonic solids with triangular faces, it most closely

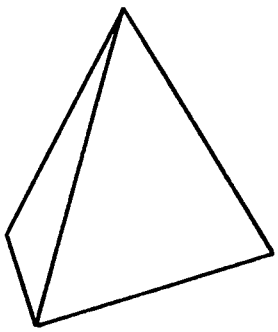

TETRAHEDRON

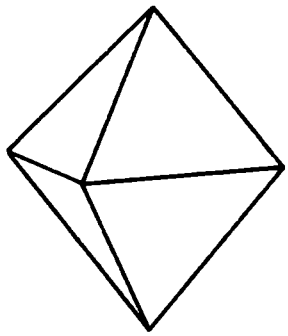

OCTAHEDRON

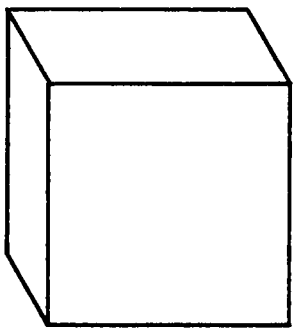

HEXAHEDRON

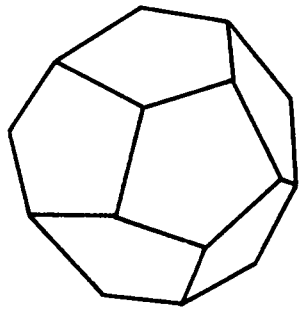

DODECAHEDRON

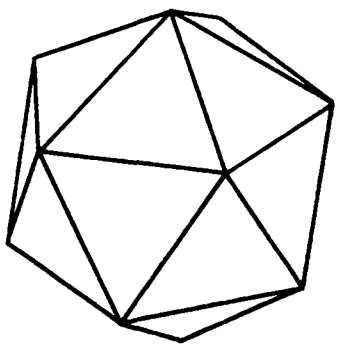

ICOSAHEDRON

FIG. 4.1 - Basic Polyhedra - Five Platonic Solids

approximates a sphere and offers a great degree of regularity and symmetry when transformed into a spherical form [7,30].

In the geometric development, Fuller projected the icosohedron onto the surface of a sphere dividing the sphere into 20 equilateral spherical triangles (see Fig. 4.2). Each of these triangles are, in turn, divided by median lines and bisectors forming six additional equlilateral spherical triangles. The medians used to divide the triangle lie on great circles which are extensions of the sides of the basic equilateral triangles of the spherical icosahedron [18]. Fifteen such great circles are regularly arranged on the surface of the sphere [24, 30]. The fifteen great circles divide the surface of the sphere into 120 identical spherical triangles. This is the maximum number of identical subdivisions possible on the surface of a sphere [30].

In reducing the icosahedron to nearly equal subdivisions, there are two basic breakdown methods which are available [24,30]. Using the Triacon method, the icosa face is divided about its median lines as shown in Fig. 4.3. The Triacon method, in its most basic form, distributes two near equilateral faces over every icosa edge and the icosa edge no longer remains a part of the final form [24,30]. In the Alternate method, the icosa face is subdivided by faces whose edges are parallel to the icosa edge as shown in Fig. 4.4. Unlike the Triacon breakdown, the icosa edge remains a part of the final form [24,30].

The breakdown process merely reduces the icosahedron to smaller and smaller nearly identical pieces. The more subdivisions there

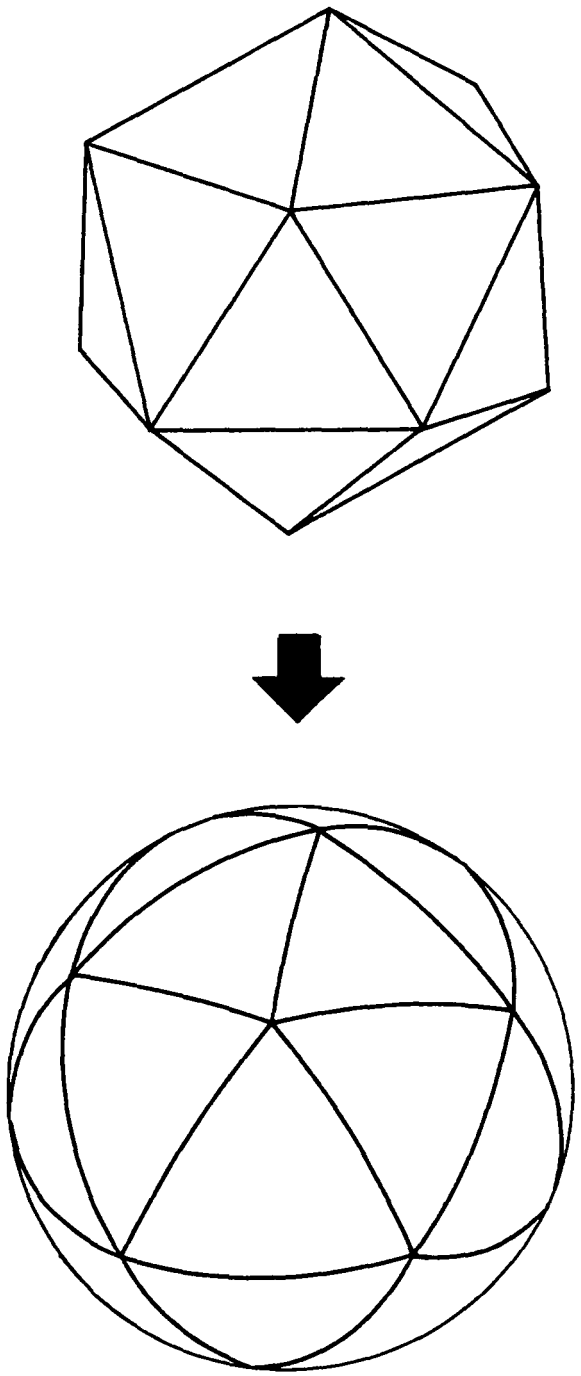

FIG. 4.2 - Planar and Spherical Icosahedron

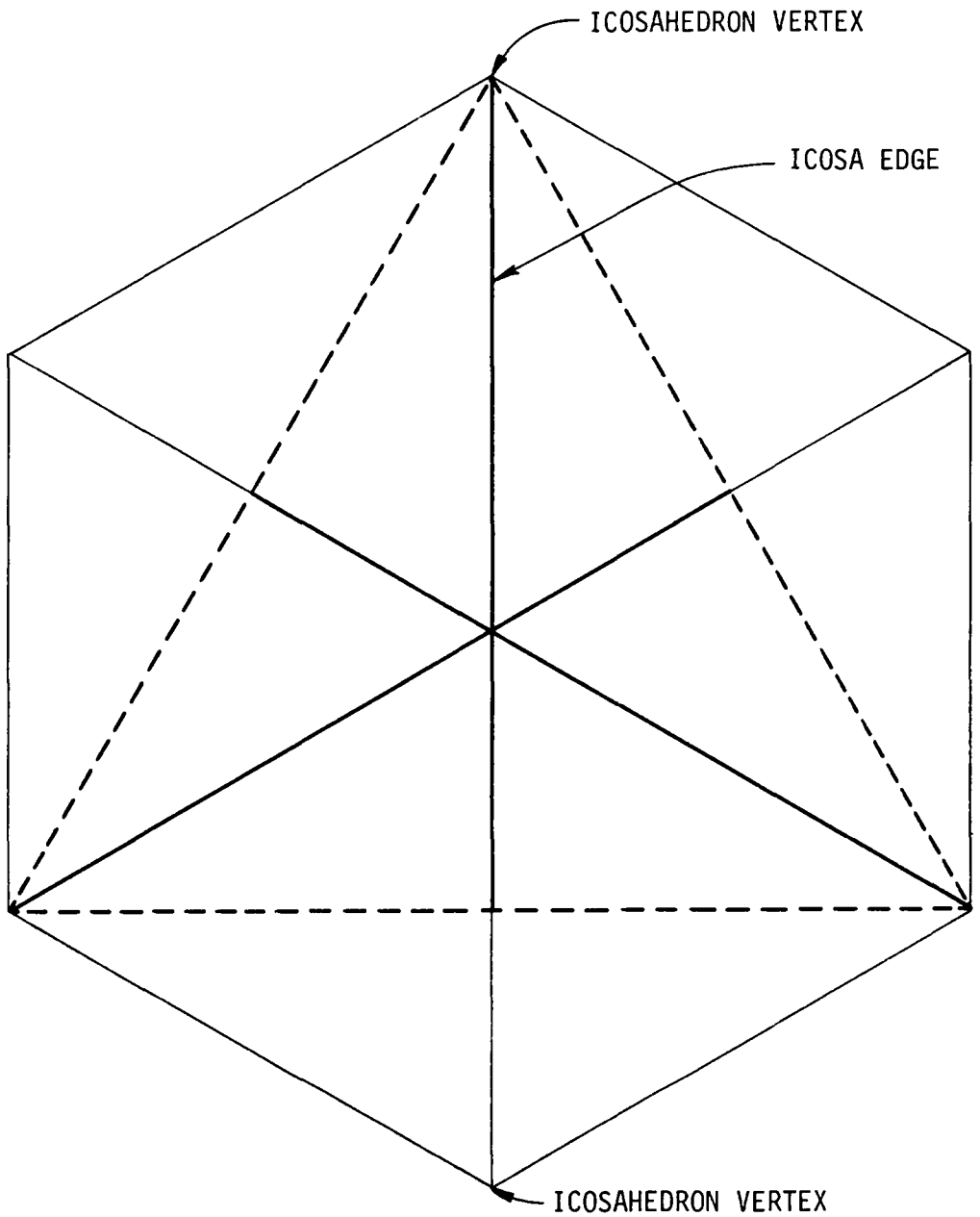

FIG. 4.3 - 2^V Triacon Breakdown

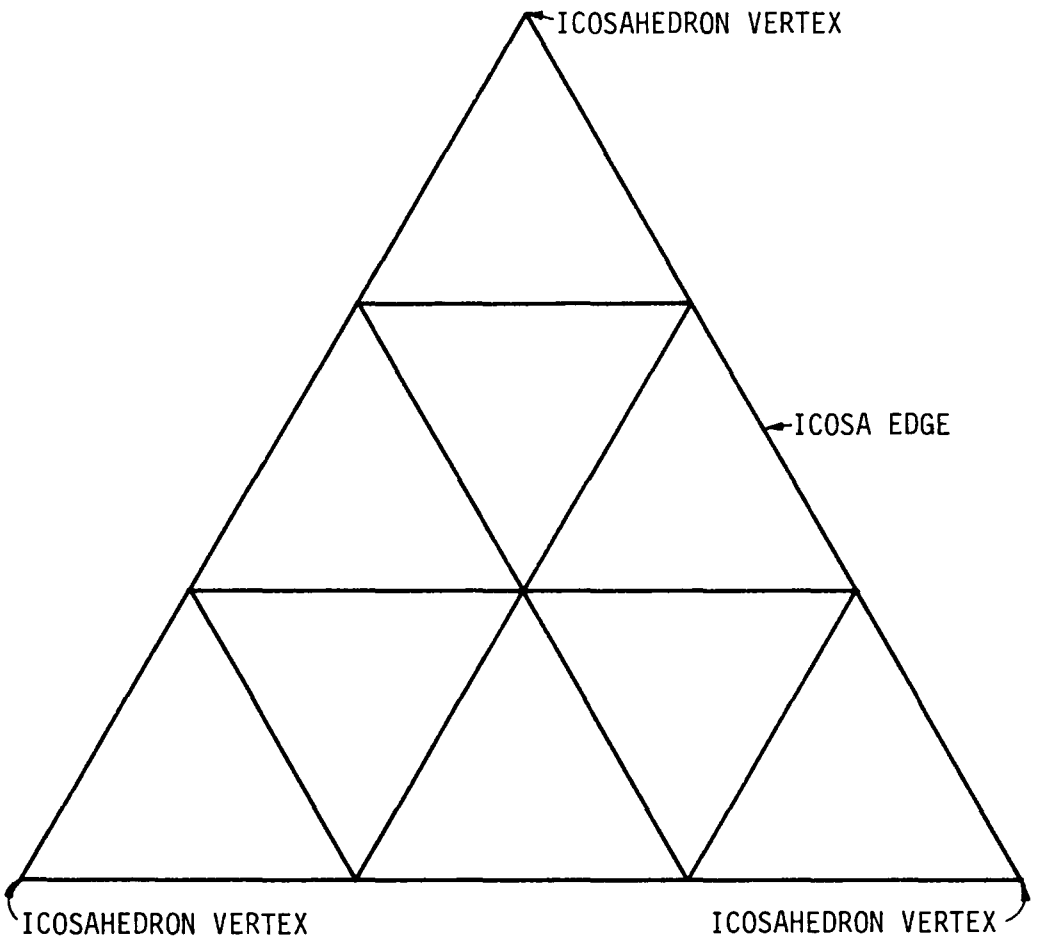

FIG. 4.4 - 3^V Alternate Breakdown

are, the larger the frequency (the degree to which the icosahedron has been subdivided) [24].

4.4.1 Frequency of Geodesic Domes

The frequency of a geodesic dome is graphically designated by the number of times the icosa edge has been segmented and a superscript v (i.e. 3^v). Referring to Fig. 4.4, the figure shown is a 3^v breakdown, the icosa edge being segmented three times.

Breakdown and frequency are of particular concern to the spherical designer from an erection and fabrication standpoint [24]. As the frequency increases, the number of members increases. The number of different member lengths increases as well, and triangles are produced which are no longer equilateral [24].

Every icosahedron vertex consists of the intersection of five icosa edges. The triangular faces which remain at the vertex during the subdivision process group together in the completed icosahedron to form a pentagon [7,18,24,30]. At points other than the icosahedron vertex, six triangles are joined to produce a hexagon (see Fig. 4.5). By locating any five-way or pentagonal vertex in the dome, the icosa vertices are found (see Fig. 4.5). Connecting any two adjacent five way vertices, an icosa edge is formed. The edge may or may not be an actual dome component. Where this icosa edge is coincidental with the structural pattern, the breakdown is Alternate [24,30]. When the triangular face lies across the icosa-edge, the breakdown is Triacon [24,30].

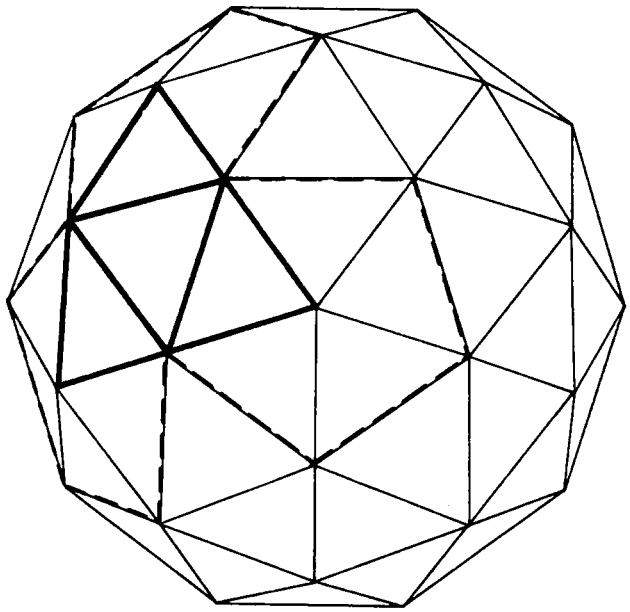

FIG. 4.5 - 2^V Alternate Breakdown - Icosahedron Face Breakdown with Pentagonal Vertex Cues Outlined

4.4.2 Base Truncations for Geodesic Domes

Domes are formed from truncated spheres. When considering the results of passing a horizontal datum plane normal to the north-south polar axis at various points, base truncations regulates the proportion of surface area, volumetric enclosure and horizontal floor area [24]. The least surface area and volume per unit gain of floor area exists in the first 1/3 sphere. As the datum plane approaches the equatorial truncations, surface area and volume contained rapidly increase while the rate of floor area gain decreases until maximum floor area is reached at the equator [24].

In terms of construction and maintenance of dome structures, base truncation can have economic consequences. The most economical range, surface and volume wise per floor area, is the 1/3 sphere icosa-cap or pent-cap truncation [24]. Beyond this point, the accumulation of structure and needless volume prohibit spherical use [24].

The Triacon and Alternate breakdown methods provide truncation limits. In the Triacon breakdown, no complete great circle is delineated naturally by the structural pattern and truncated base members are required [24,30]. In the Alternate breakdown, an equatorial line is delineated with members for even frequencies [24,30]. Since the icosa-edge remains a part of the final form of the dome in such a breakdown, the pent-cap truncations have a natural base ring [24,30].

CHAPTER 5

THE COMPUTER PROGRAMS

5.1 Introduction

In this chapter, a brief description of a WATFIV/FORTRAN computer program specifically assembled to analyze and design space trusses is presented. A similar program is assembled to analyze space frames using algorithms identical to those employed in the space truss program. The important aspects of the subroutines incorporated in these programs are reviewed in the following sections of this chapter. Several demonstration problems are described and numerical results obtained using the assembled computer programs are provided.

5.2 Program Description

The solution algorithms incorporated in the computer programs are based on the stiffness method of matrix strucutral analysis and the fully-stressed design procedure via the stress-ratio method. Comment cards have been used where appropriate to permit comprehension of the numerical operations which are performed. As an additional aid, a glossary of terms is included at the beginning of each subroutine. The liberal use of subroutines provides a more readable and organized program as well. A flowchart of the subroutines employed in the space truss computer code is presented in Figs. 5.1, 5.1a and 5.2 to permit inspection of the logic contained therein. It should be noticed that the space truss program is organized in a manner that provides the user with an option to perform structural analysis alone or structural

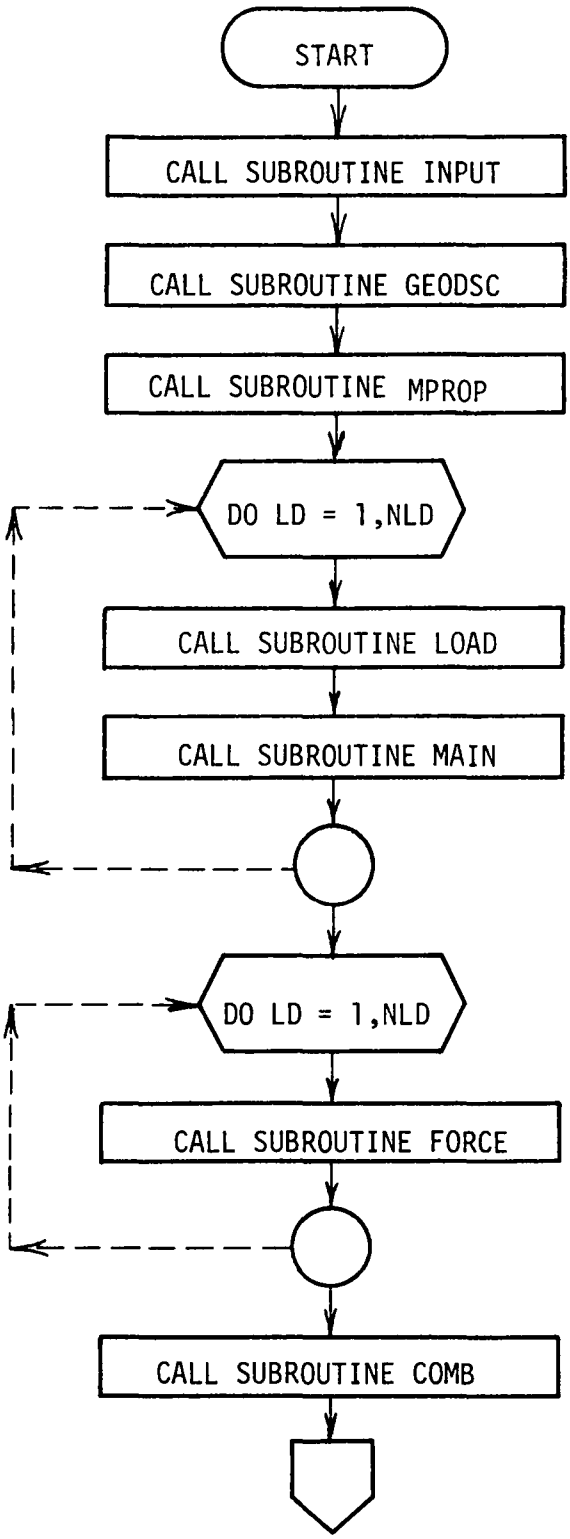

FIG. 5.1 - Computer Program Subroutine Flowchart

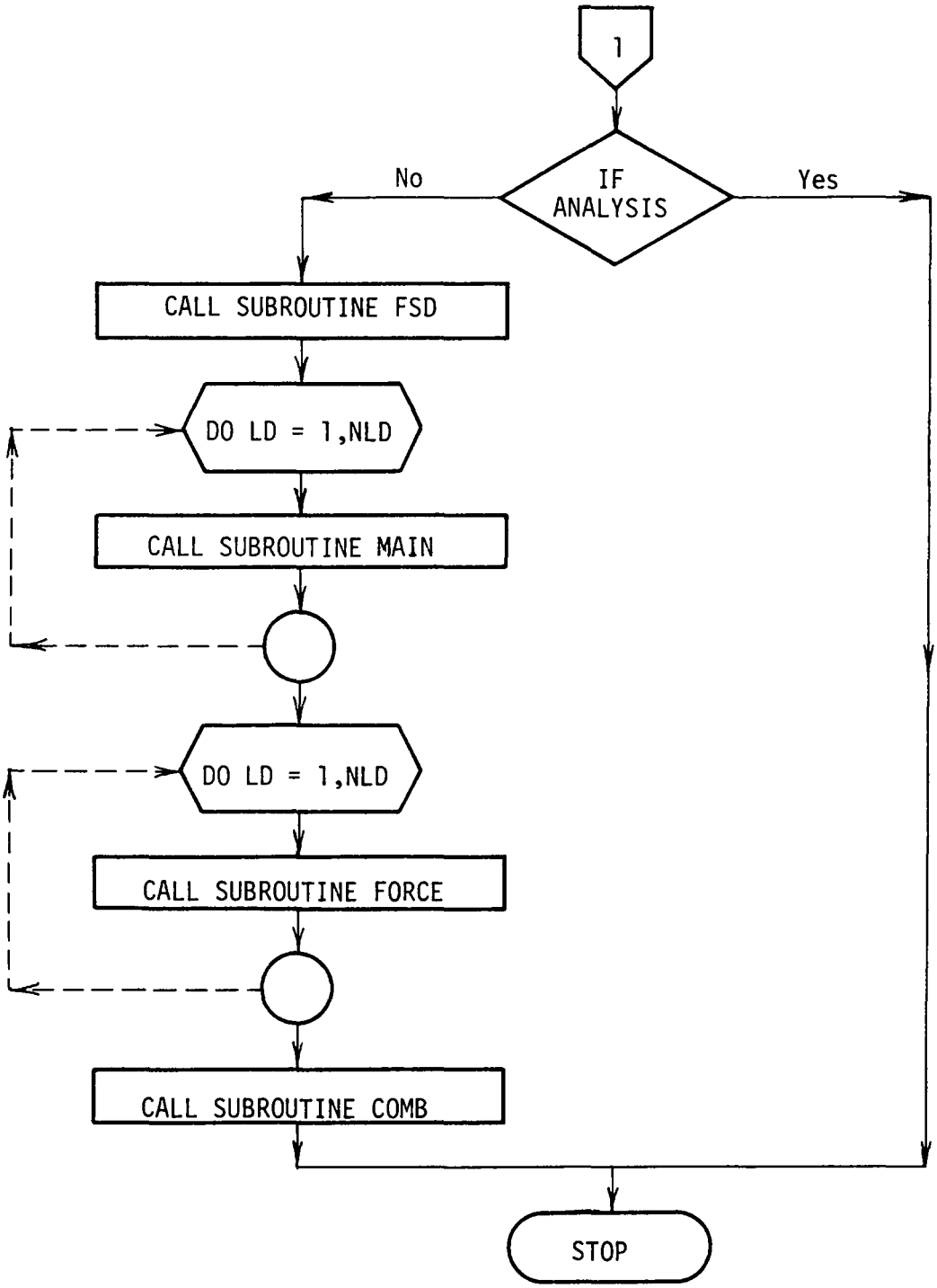

FIG. 5.1a - Computer Program Subroutine Flowchart

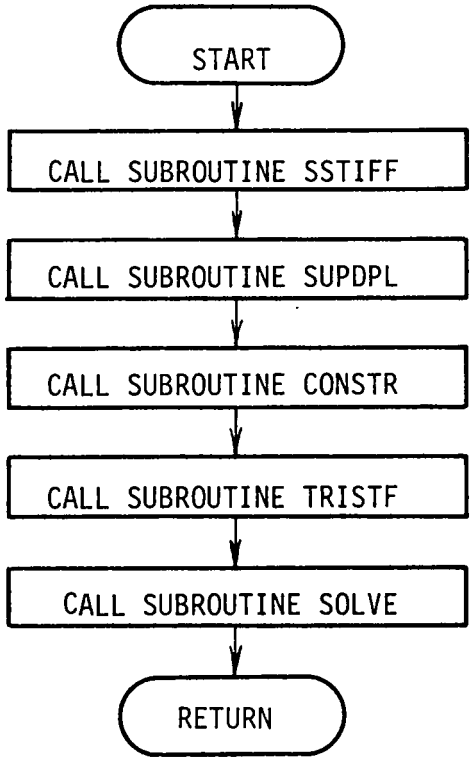

FIG. 5.2 - Flowchart of Subroutine Main

analysis and design. The space fram program is assembled to perform only structural analysis.

The computer code also utilizes a storage-saving technique known as "Dynamic Array Storage" [21]. In this concept, a "dummy" main program is employed to establish the amount of array storage available for the particular problem under consdieration. This permits an economical use of computer core storage, allowing access only to the required amount of core storage to perform the job. Thus, the dimensions of some arrays (e.g. BGK (NEQ, IBND) and P (NEQ)) used in the program will vary depending upon the required amount of computer core storage defined by the size of the problem under investigation.

The subroutines presented in Figs. 5.1, 5.1a and 5.2 have access to a common storage by using a COMMON STATEMENT [21]. This facilitates the transfer and storage of important data from one subroutine to another. It should be noted that the dimensions of the arrays of the COMMON STATEMENT will need to be altered when investigating a dome whose frequency is greater than 3^V or space trusses having more than 41 joints and 85 members.

The program performs all real number operations in DOUBLE PRECISION [21] which significantly lowers the chance for a buildup of round-off errors during the solution process.

The declared units shall be those of inches, kips and radians. Other units may not be used unless the program has been altered to accommodate these units. A brief description of the subroutines and their purpose will be presented in the following sections in the order

of their occurrence in the flowchart.

5.2.1 SUBROUTINE INPUT

SUBROUTINE INPUT is used to read numerical data pertaining to the number of members and joints the structure may possess. The total number of loadings to be considered in an individual problem are read along with the total number of critical load combinations which are defined in building codes [32,37]. All joints are automatically considered to be free joints until otherwise stated. The degrees of freedom at support joints are "fixed" only by providing the appropriate data. Cross-sectional area, modulus of elasticity, material density and coefficient of thermal expansion are read and printed for each member in an organized form to permit inspection for errors. All information is stored in the COMMON STATEMENT for use in the other subroutines.

5.2.2 SUBROUTINE GEODSC

SUBROUTINE GEODSC automatically defines the geometry of the geodesic dome. It employs an automatic joint generation scheme developed from the Alternate Method presented by Clinton [30]. In addition to establishing coordinates for each joint of the dome, member incidence values are defined internally to insure that the bandwidth of the stiffness matrix remains small.

5.2.3 SUBROUTINE MPROP

SUBROUTINE MPROP contains necessary WATFIV/FORTRAN commands to perform projection calculations of each member onto the global coordinate axes using Eqs. (A.1) through (A.10) presented in Appendix A.

In addition, the length of each member is computed and printed to allow inspection for errors. The member projections and lengths are stored in the COMMON STATEMENT for future use in a coordinate transformation process.

5.2.4 SUBROUTINE LOAD

SUBROUTINE LOAD is used to read the applied loadings which may include member loads, joint loads, and support settlements. The computer code computes "equivalent joint loads" for uniform temperature effects and fabrication errors as they occur in each number.

Joint loads are interpreted by the code as loads applied at the joints in the global reference frame. The applied joint loads due to the dead load of the truss are automatically generated by distributing half the total weight of each member to the end joints. These loads are applied in a downward direction in the global reference frame. Manual calculations are required to obtain the applied joint loads due to other loads such as snow load and wind load. Since the framework of the dome is visualized as being a truss, it is possible to use a computational method presented in certain references [20]. The manual calculation procedure is described in greater detail in Appendix B. Wind load calculations may be compared to the information presented by Maher [17] to insure overall correctness of results.

Support settlements are interpreted by the computer code as being a joint loading at the supports of a structure. A space truss joint possesses three translational degrees of freedom and a support

settlement may have components in all three directions. In a space frame, there are six degrees of freedom per joint, three translational and three rotational. Therefore, there are six possible components of support settlement per space frame joint.

5.2.5 SUBROUTINE SSTIFF

SUBROUTINE SSTIFF is coded to generate the unconstrained global stiffness matrix of a space truss by assembling the stiffness coefficient contributions of each member stiffness matrix into a banded matrix form. By doing this, a considerable amount of allocated matrix storage space is conserved. For large complex structures such as reticulated domes, the savings in computer core storage can be significant.

The computer code achieves the savings in core storage by storing only the banded non-zero coefficients of the upper triangular portion of the global stiffness matrix in a compact two-dimensional matrix [5]. The equation used to compute the half-bandwidth of the non-zero stiffness coefficients is written as

$$IBND = (MXDF + 1)\ DOF \tag{5.1}$$

where IBND = semi-bandwidth or half bandwidth, MXDF = the maximum member and joint difference; and DOF = the number of degrees of freedom per joint.

5.2.6 SUBROUTINE SUPDPL

In SUBROUTINE SUPDPL, the computer code computes the joint loads created by a support settlement. The algorithm employed is based on

the discussion presented by Desai and Abel [5] and class notes from Holzer [10].

5.2.7 SUBROUTINE CONSTR

SUBROUTINE CONSTR is used to constrain the unconstrained compact two-dimensional version of the banded global stiffness matrix. Zeros are placed in the compact two-dimensional version of the banded stiffness matrix and the global applied force matrix corresponding to each restricted degree of freedom. In addition, the leading element of each row corresponding to the restricted degree of freedom is set equal to unity.

5.2.8 SUBROUTINE TRISTF

In SUBROUTINE TRISTF, the compact two-dimensional version of the banded stiffness matrix is triangularized so that a Gaussian-elimination procedure may be used to solve for the values of the unknown displacements. The algorithm used is based on the WATFIV/FORTRAN coded version presented by Desai and Abel [5].

5.2.9 SUBROUTINE SOLVE

In SUBROUTINE SOLVE, a Gaussian-elimination procedure is used to obtain the unknown joint displacements. The algorithm employed is a forward reduction and backsubstitution scheme presented by Desai and Abel [5]. As the unknown displacements are computed for each loading condition, they are stored in the COMMON STATEMENT for access by other subroutines.

5.2.10 SUBROUTINE FORCE

SUBROUTINE FORCE contains WATFIV/FORTRAN computer code commands to compute the member end forces and support reactions from the joint displacements obtained in SUBROUTINE SOLVE.

The computer code converts the joint displacements in global coordinates to joint displacements in local coordinates using the coordinate transformation matrix. The member end forces are then obtained for each member individually. Member end forces in global coordinates are then summed at each joint and used as a joint equilibrium check as well as the computation of reactions at the supports.

5.2.11 SUBROUTINE COMB

SUBROUTINE COMB is used to combine loading conditions according to specified percentages established by building codes [32,37]. The computer code computes and stores in the COMMON STATEMENT the global joint displacements associated with each loading combination. No more than five loading combinations are allowed to be considered in a single problem. If more than five loading combinations are to considered, the array dimensions of the COMMON STATEMENT will require modification.

5.2.12 SUBROUTINE FSD

SUBROUTINE FSD is used to perform the design of any space truss problem. The design procedure employed is based on the fully-stressed design procedure via the stress-ratio method. The user is free to choose the yield stress and the maximum number of iterations for the

design process. Latest results for a particular iteration may be printed to permit monitoring of convergence to a fully-stressed design state. An f.s.d. is obtained for each load combination considered. The cross-sectional area results are stored for later retrieval and maximum size comparison to determine the cross-sectional areas to be used in the final design. The subroutine also contains commands which will perform a slenderness ratio check for each member according to the AISC specifications [31]. This aspect of the design process occurs after a fully-stressed design state has been obtained for all load combinations and final cross-sectional areas have been chosen for each member.

The approximate relationship between the radius of gyration and cross-sectional area of each member is assumed to be a straight line relationship of the graph of radii of gyrations and cross-sectional areas for various tubular sections. The radius of gyration and cross-sectional area for tubular members are provided in the AISC Manual of Steel Construction [32].

After the design process is finished, a minimum uniform size is used for all members based on the maximum cross-sectional area obtained from the slenderness-ratio criteria. A final analysis is automatically performed and results are printed.

5.3 Demonstration Problems and Numerical Results

In this section, several demonstration problems are defined and analyzed using the WATFIV/FORTRAN computer codes developed for the

analysis of space trusses and space frames. The numerical results obtained from the analyses accompany the general description of each demonstration problem.

The majority of the study concerns the space truss and space frame analyses of a 2^V and 3^V geodesic domes subjected to axisymmetric and asymmetric loads. In addition, some effort was directed towards investigating what effect shallowness would have on the space truss analysis results for the 2^V geodesic dome. Finally, the 3^V geodesic dome model was modified through the addition of several members and support joints to study the effect of fixing all joints on the base perimeter of the dome.

As a check, the analysis results were verified by using the frame analysis capabilities of the ICES STRUDL II computer program developed at the Massachusetts Institute of Technology [15].

5.3.1 General Description of Demonstration Problem No. 1

Demonstration Problem No. 1 is a 33 degree of freedom 2^V pent-cap geodesic dome whose elevation and plan views are shown in Figs. 5.3 and 5.4. The base diameter of the dome is 60'-0". The maximum height of the dome is given as 18'-6". The framework members are fabricated from steel tubing [31,36] having a modulus of elasticity of 30,000 ksi and cross-sectional area of 2.68 sq. in.

5.3.1.1 Space Truss Analysis Results for Demonstration Problem No. 1 Subjected to Axisymmetric and Asymmetric Loading

Axial load results are presented in Figs. 5.5 and 5.6 for the

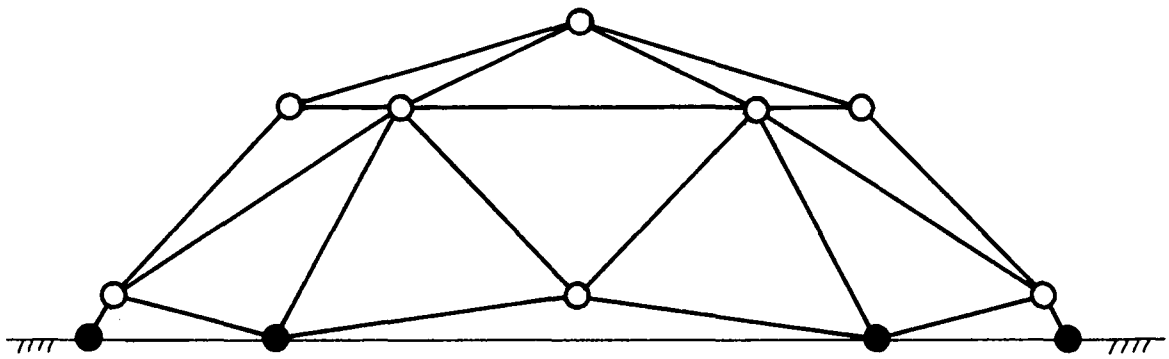

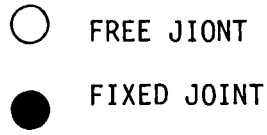

FIG. 5.3 - Elevation View of Demonstration Problems No. 1 and 2

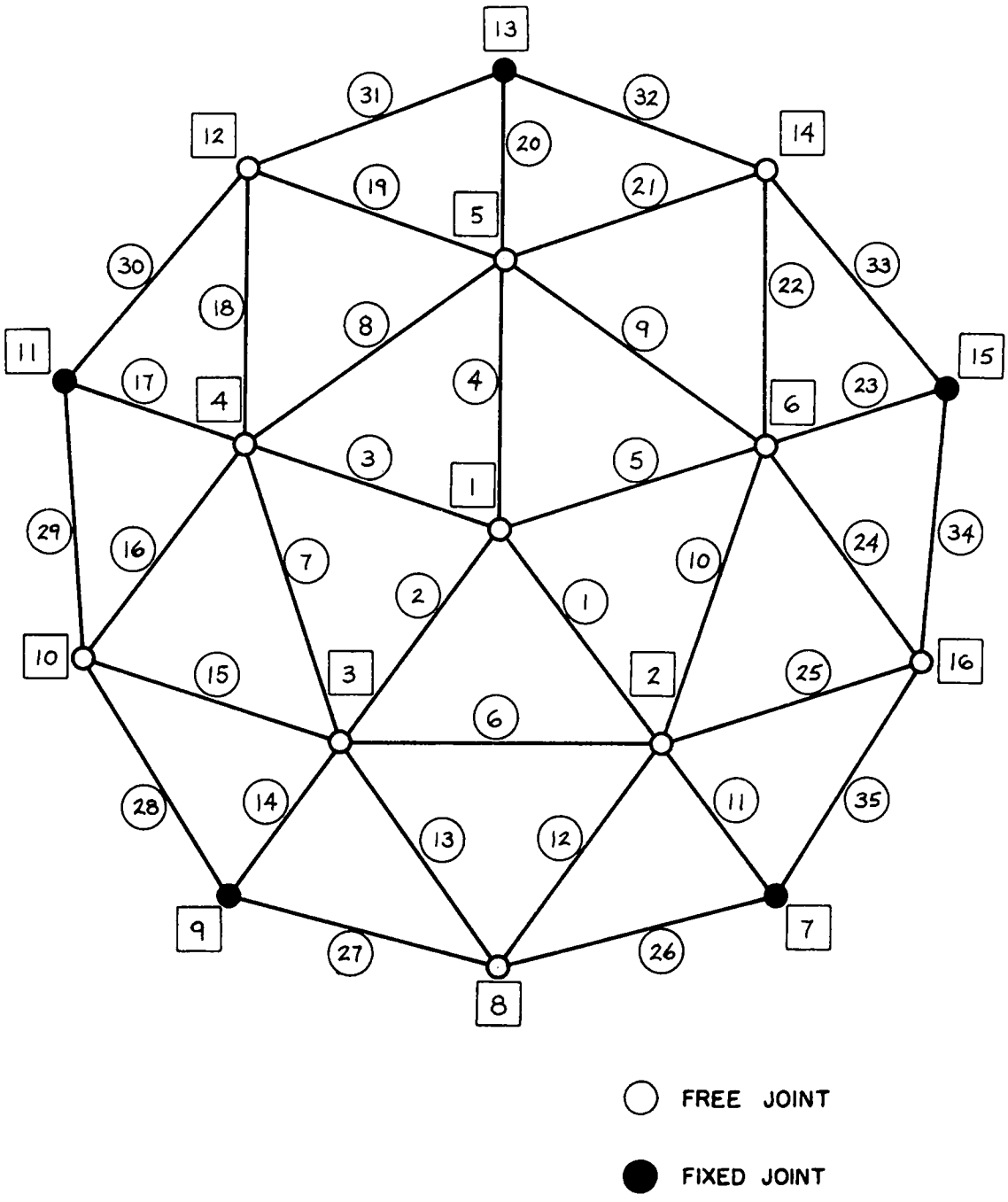

FIG. 5.4 - PLAN VIEW OF DEMONSTRATION PROBLEMS NO. 1 AND 2

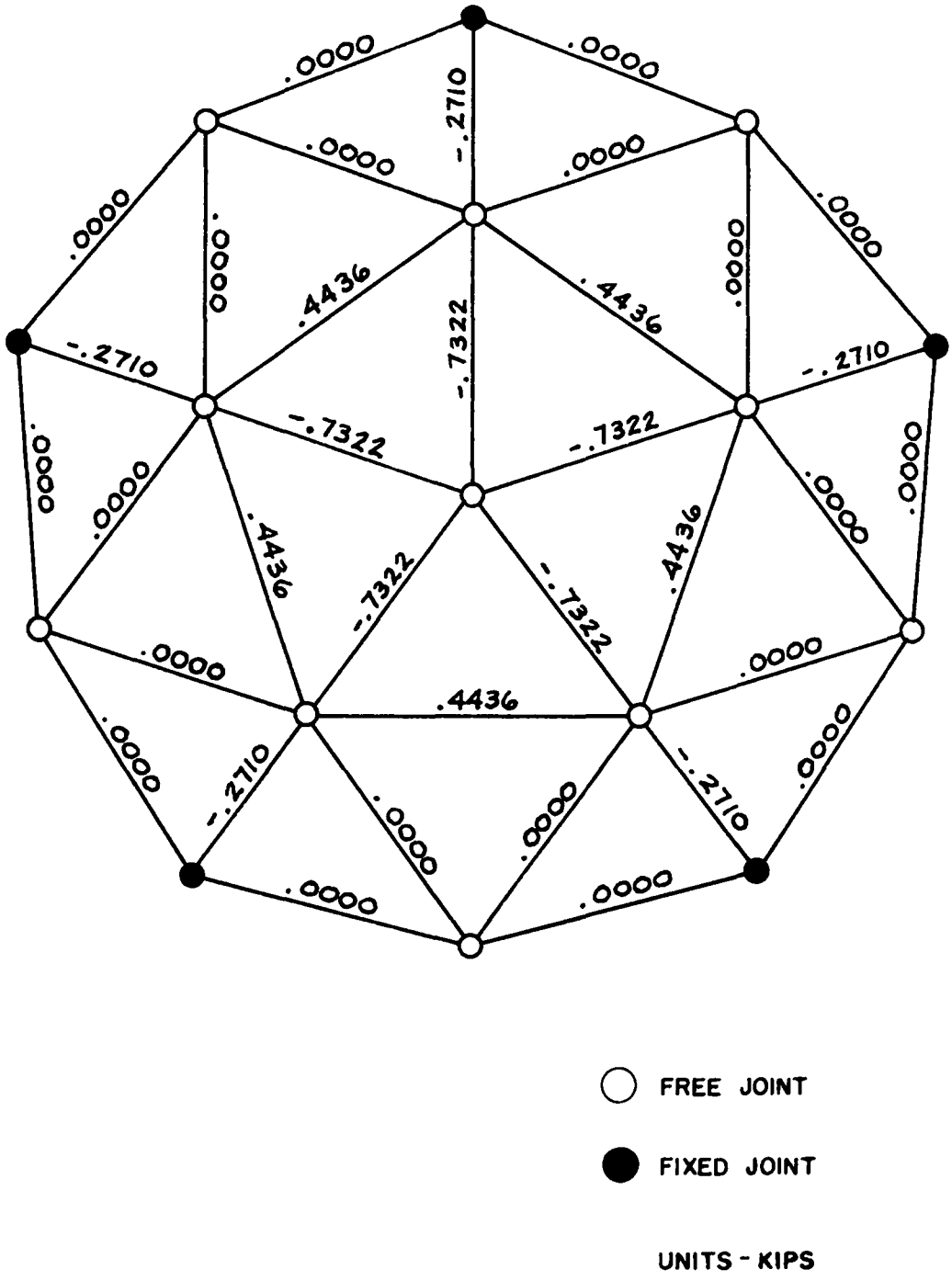

FIG. 5.5 - SPACE TRUSS ANALYSIS RESULTS FOR DEMONSTRATION PROBLEM NO. 1 SUBJECTED TO AN AXISYMMETRIC LOAD

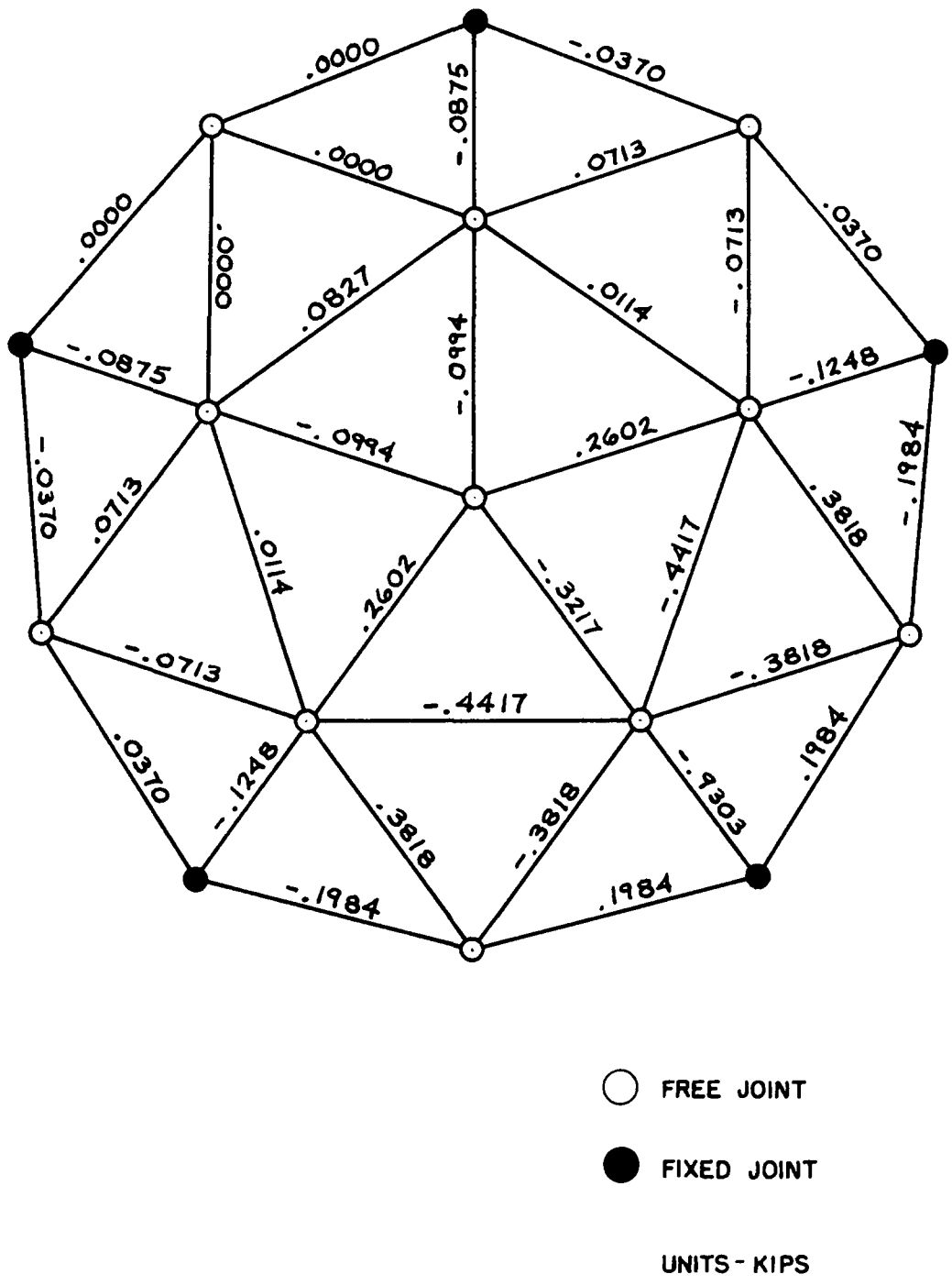

FIG. 5.6 - SPACE TRUSS ANALYSIS RESULTS FOR DEMONSTRATION PROBLEM NO. 1 SUBJECTED TO AN ASYMMETRIC LOAD

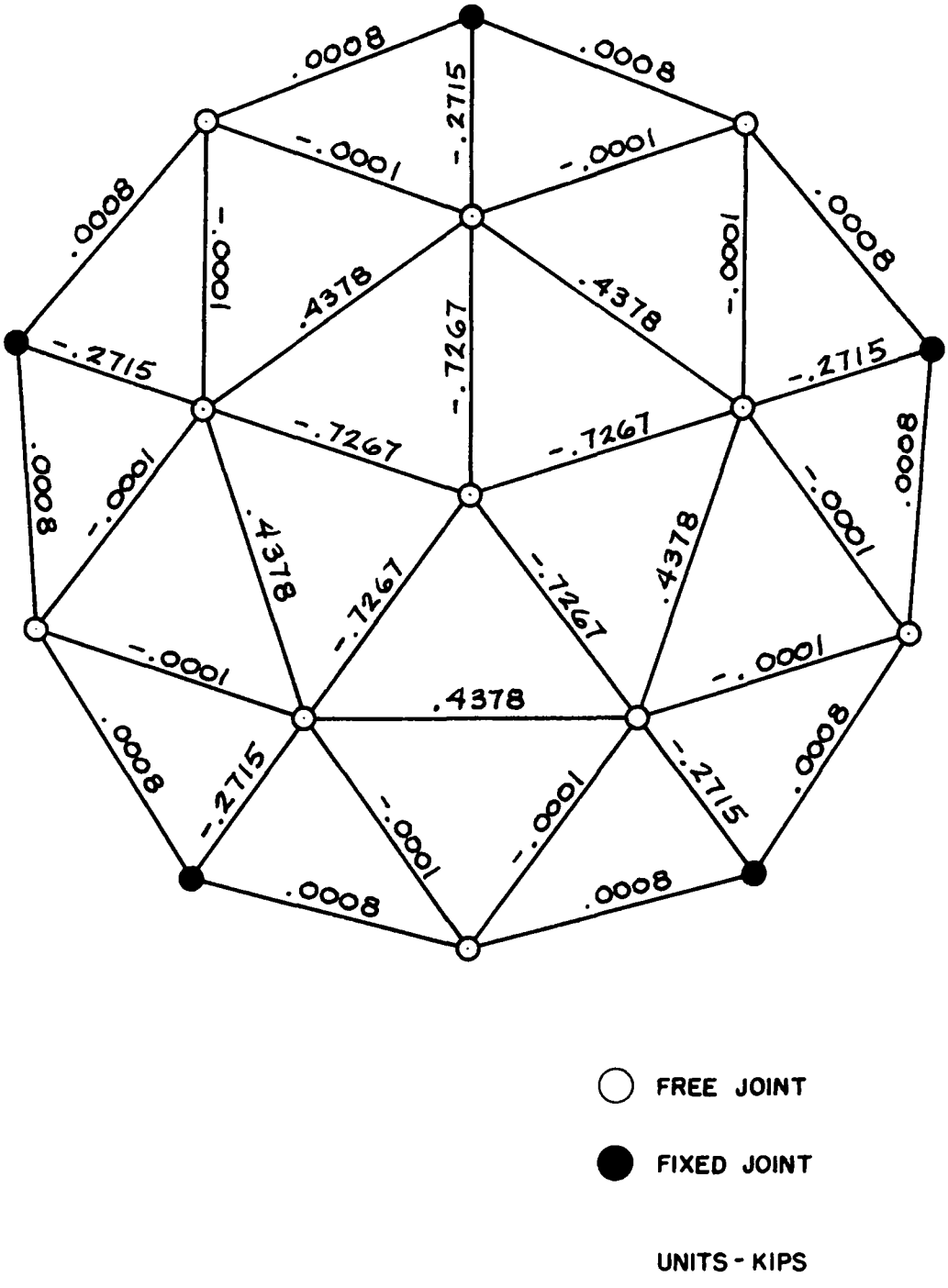

FIG. 5.7 - SPACE FRAME ANALYSIS RESULTS FOR DEMONSTRATION PROBLEM NO. 2 SUBJECTED TO AN AXISYMMETRIC LOAD

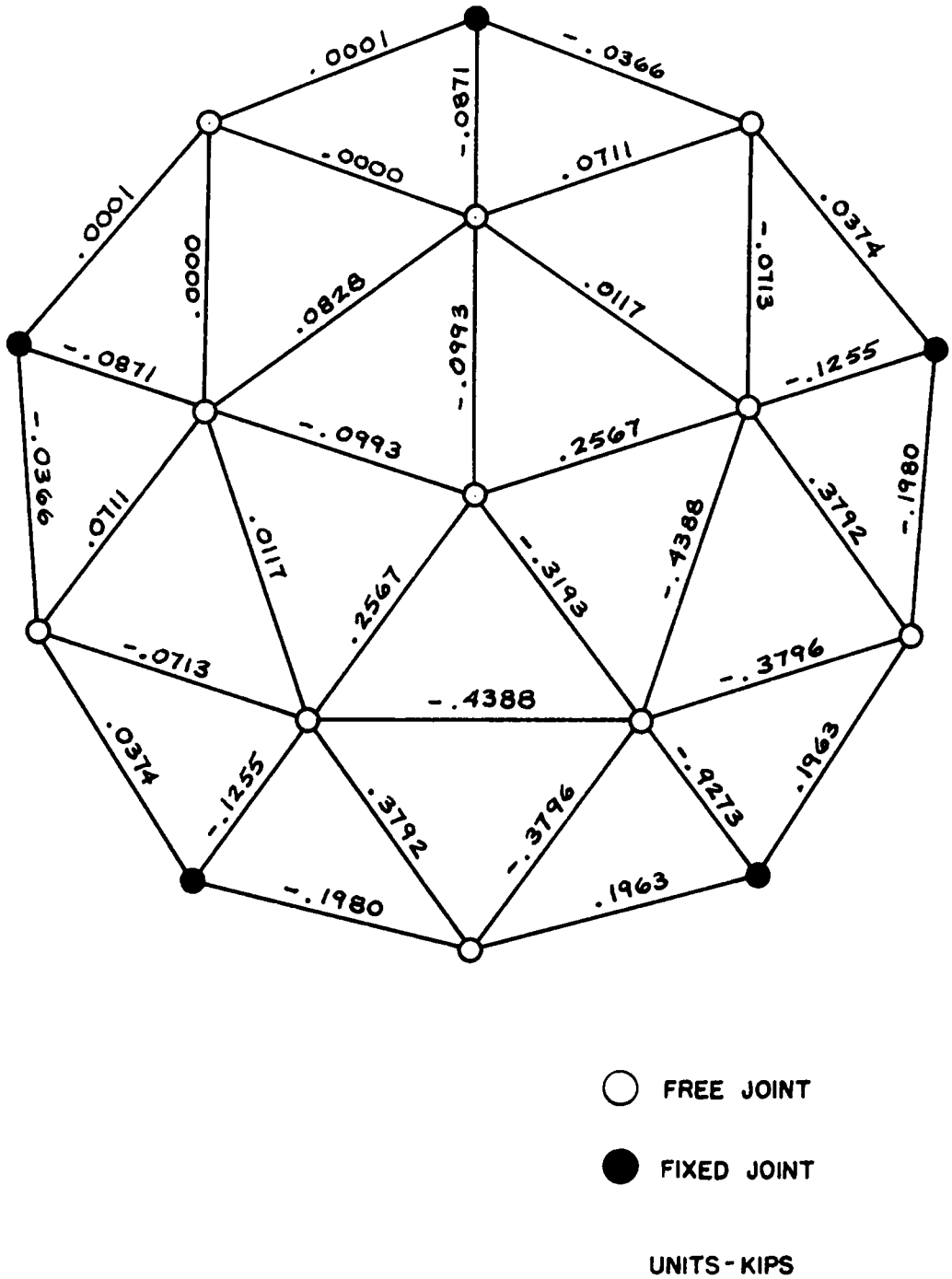

FIG. 5.8 - SPACE FRAME ANALYSIS RESULTS FOR DEMONSTRATION PROBLEM NO. 2 SUBJECTED TO AN ASYMMETRIC LOAD

space truss analysis of Demonstration Problem No. 1 subjected to an axisymmetric and asymmetric load of one kip applied in the vertical gravity direction at joint 1 and joint 2, respectively. The numbers next to each member in Figs. 5.5 and 5.6 indicate the magnitude of axial load carried by the member.

5.3.2 General Description of Demonstration Problem No. 2

Demonstration Problem No. 2 is a 66 degree of freedom 2^V pent-cap geodesic dome whose elevation and plan views are shown in Figs. 5.3 and 5.4. The structural dimensions and properties are identical to those for Demonstration Problem No. 1.

5.3.2.1 Space Frame Analysis Results for Demonstration Problem No. 2 Subjected to Axisymmetric Loading and Asymmetric Loading

Axial load results are provided in Figs. 5.7 and 5.8 for the space frame analysis of Demonstration Problem No. 2 subjected to an axisymmetric and asymmetric load of one kip applied in the vertical gravity direction at joint 1 and joint 2, respectively.

5.3.3 General Description of Demonstration Problem No. 3

Demonstration Problem No. 3 is a shallow 33 degree of freedom 2^V pent-cap geodesic dome whose elevation and plan views are shown in Figs. 5.9 and 5.10. The base diameter is approximately 70'-6" and maximum height is 10'-0". The framework is composed of steel tubing whose modulus of elasticity is 30,000 ksi. All members have the same cross-sectional area which is 2.68 sq. in.

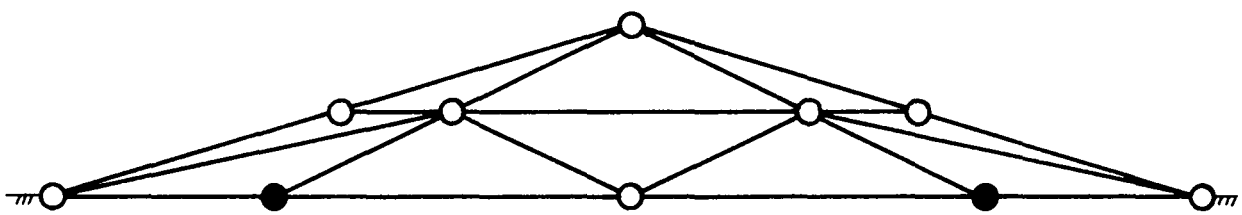

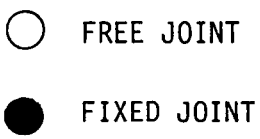

FIG. 5.9 - Elevation View of Demonstration Problem No. 3

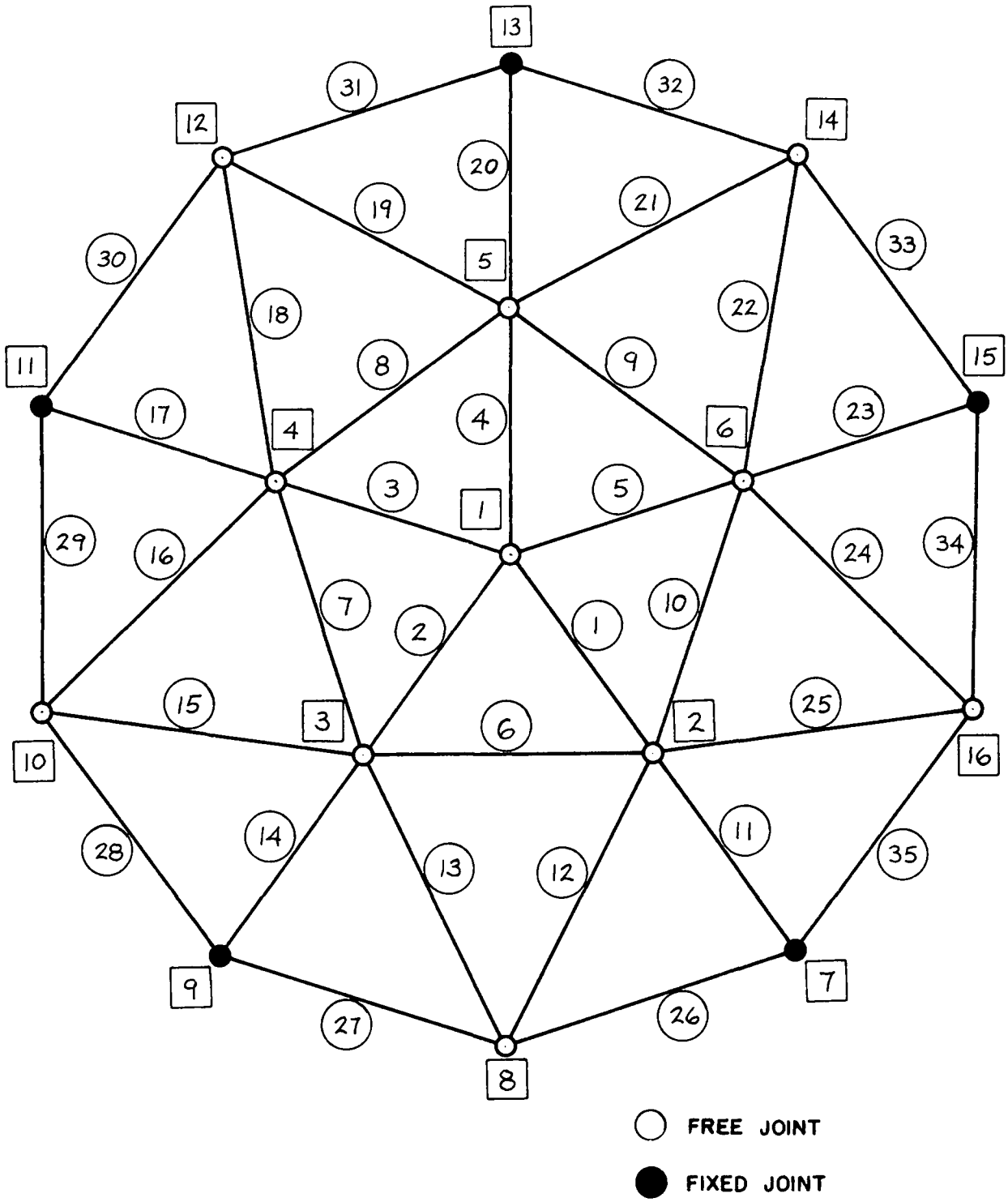

FIG. 5.10 - PLAN VIEW OF DEMONSTRATION PROBLEM NO. 3

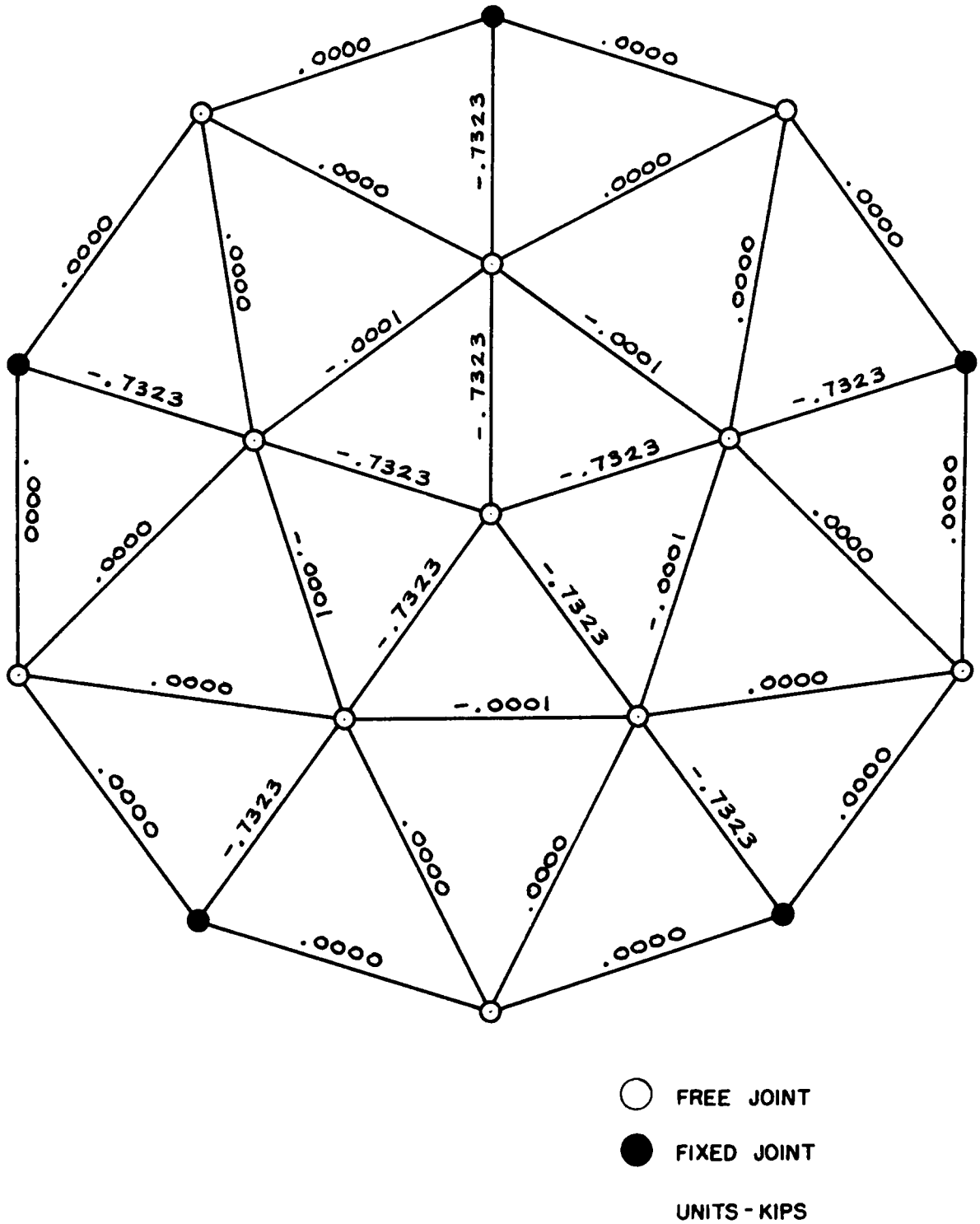

FIG. 5.11 - SPACE TRUSS ANALYSIS RESULTS FOR DEMONSTRATION PROBLEM NO. 3 SUBJECTED TO AN AXISYMMETRIC LOAD

5.3.3.1 Space Truss Analysis Results for Demonstration Problem No. 3 Subjected to Axisymmetric Loading

Axial load results are shown in Fig. 5.11 for the space truss analysis of Demonstration Problem No. 3 subjected to an axisymmetric load of one kip applied in the vertical gravity direction at joint 1.

5.3.4 General Description of Demonstration Problem No. 4

Demonstration Problem No. 4 is a 78 degree of freedom 3^V pent-cap geodesic dome whose elevation and plan views are shown in Fig. 5.12 and 5.13. The base diameter is 60'-0". The maximum height is 18'-6". All members are steel tubes possessing a modulus of elasticity of 30,000 ksi and cross-sectional area of 2.68 sq. in.

5.3.4.1 Space Truss Analysis Results for Demonstration Problem No. 4 Subjected to Axisymmetric and Asymmetric Loading

In Figs. 5.14 and 5.15 are shown the axial load results for Demonstration Problem No. 4 subjected to an axisymmetric and asymmetric load of one kip applied in the vertical gravity direction at joint 1 and joint 2, respectively.

5.3.5 General Description of Demonstration Problem No. 5

Demonstration Problem No. 5 is a 156 degree of freedom 3^V pent-cap geodesic dome whose elevation and plan views are shown in Figs. 5.12 and 5.13. The structural geometry and properties are the same as Demonstration Problem No. 4.

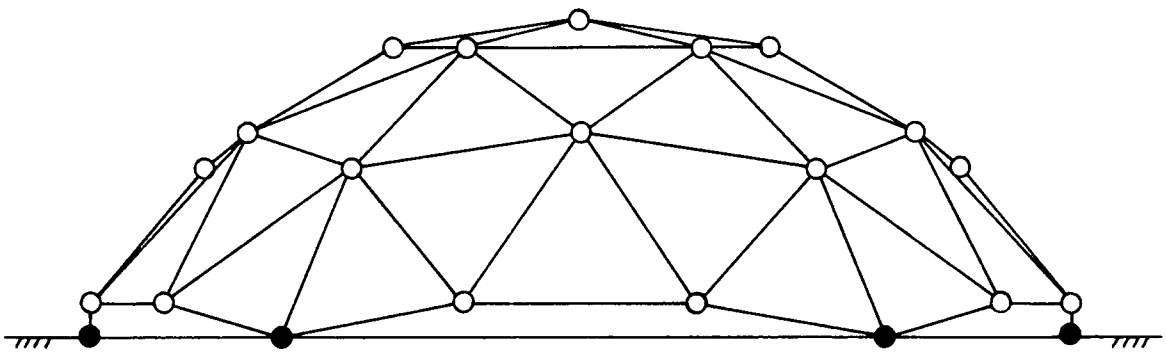

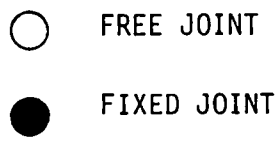

FIG. 5.12 - Elevation View of Demonstration Problems No. 4 and 5

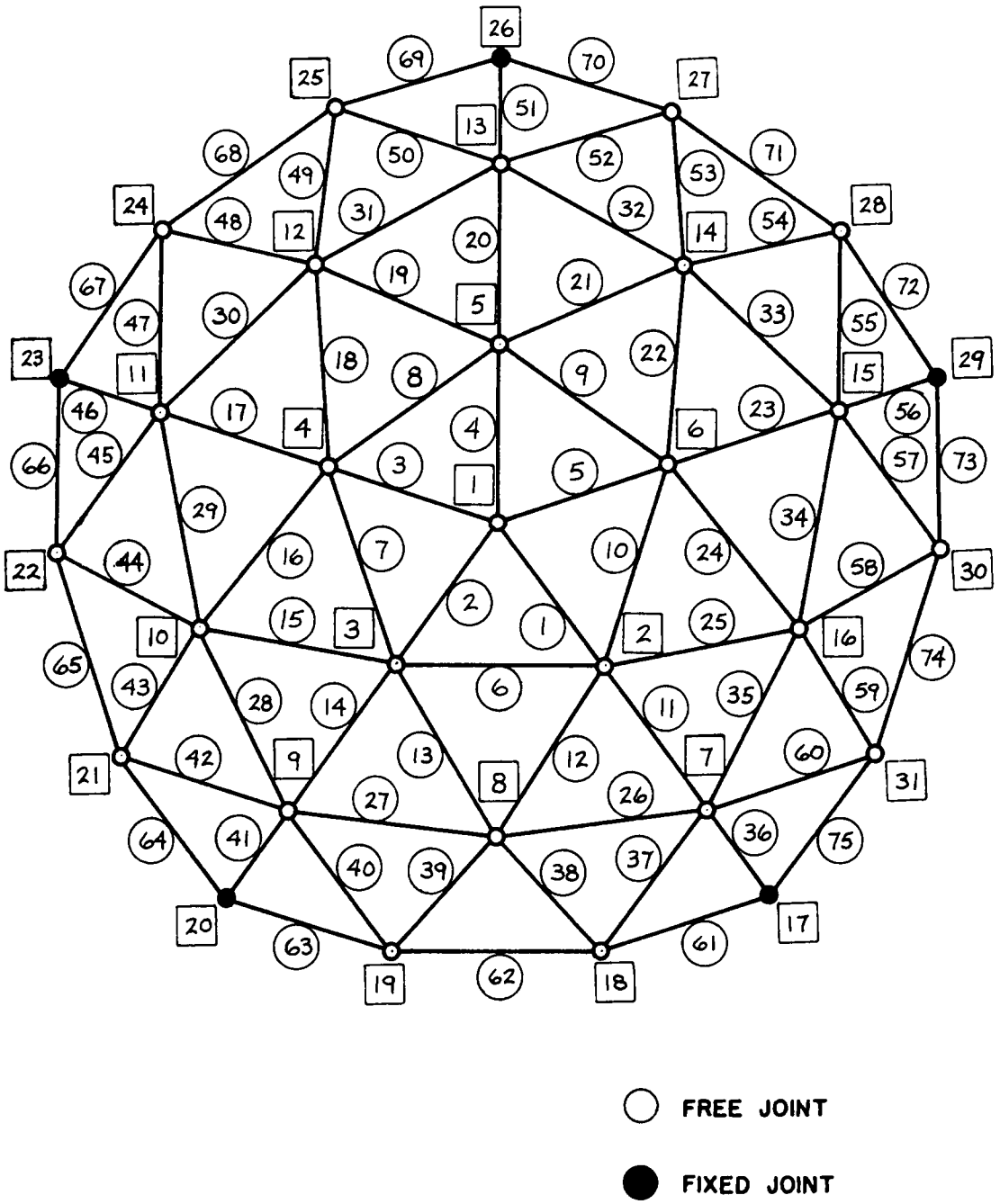

FIG. 5.13 - PLAN VIEW OF DEMONSTRATION PROBLEMS NO. 4 AND 5

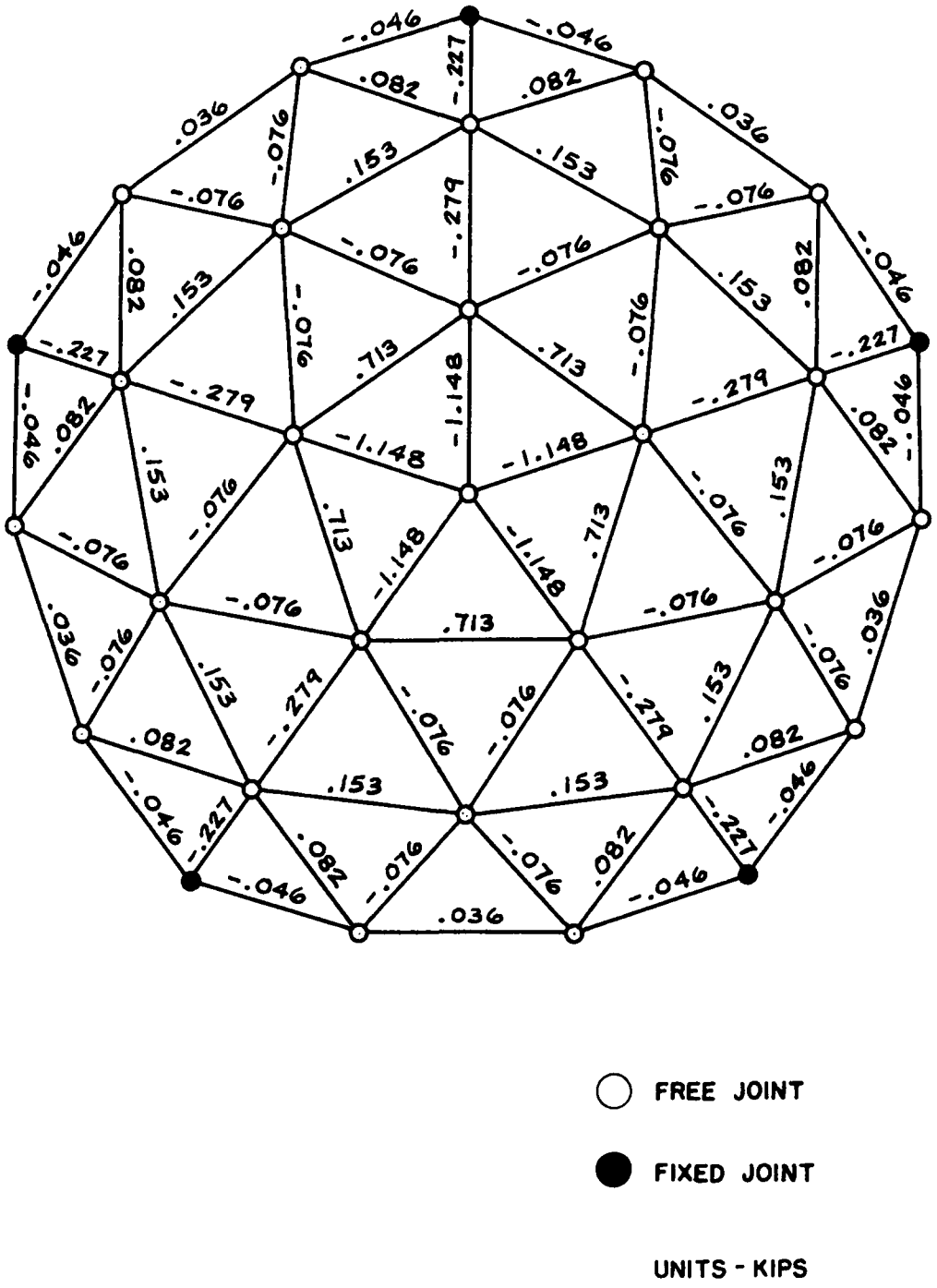

FIG. 5.14 - SPACE TRUSS ANALYSIS RESULTS FOR DEMONSTRATION PROBLEM NO. 4 SUBJECTED TO AN AXISYMMETRIC LOAD

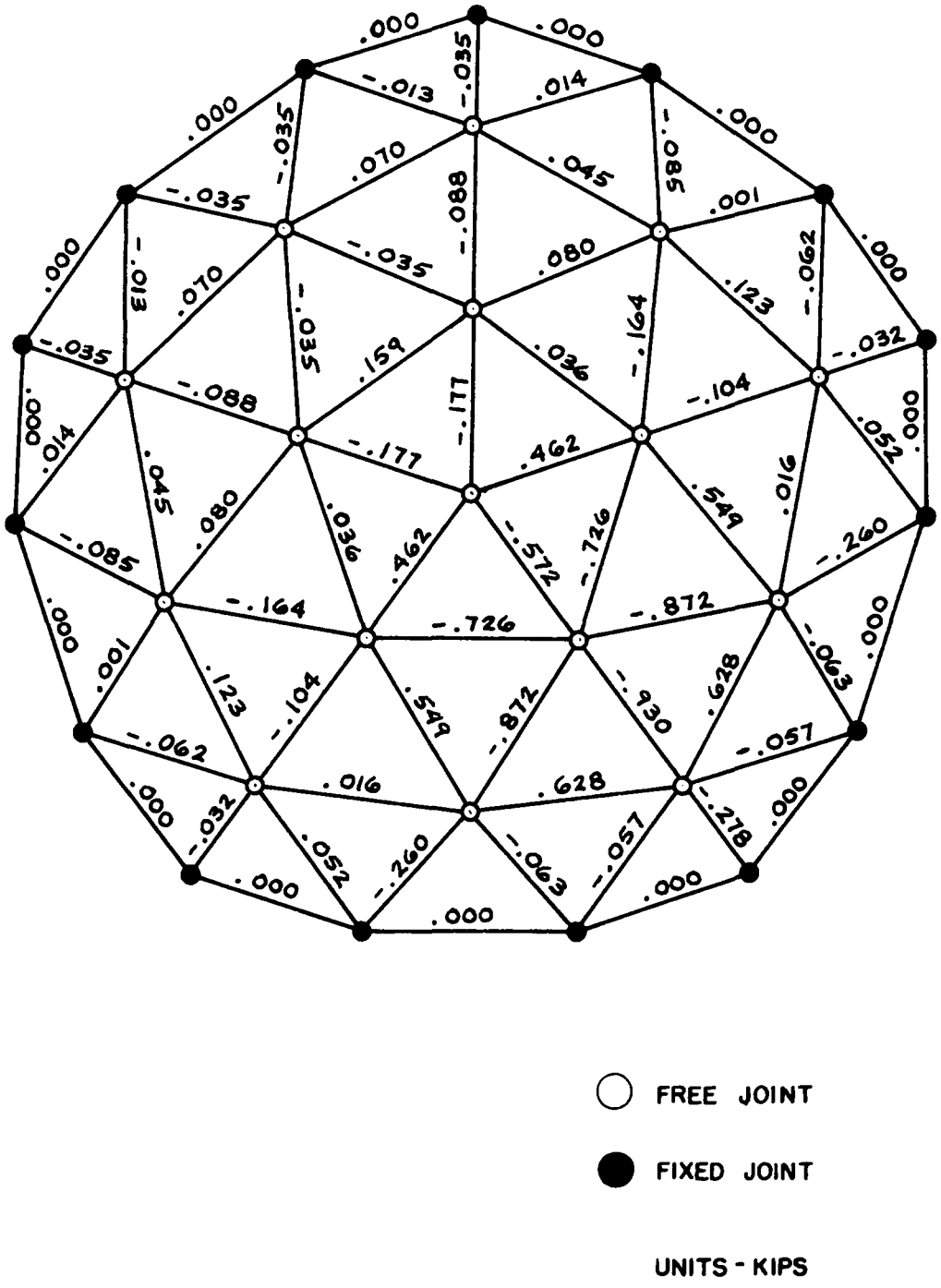

FIG. 5.15 - SPACE TRUSS ANALYSIS RESULTS FOR MODIFIED DEMONSTRATION PROBLEM NO. 4 SUBJECTED TO AN ASYMMETRIC LOAD

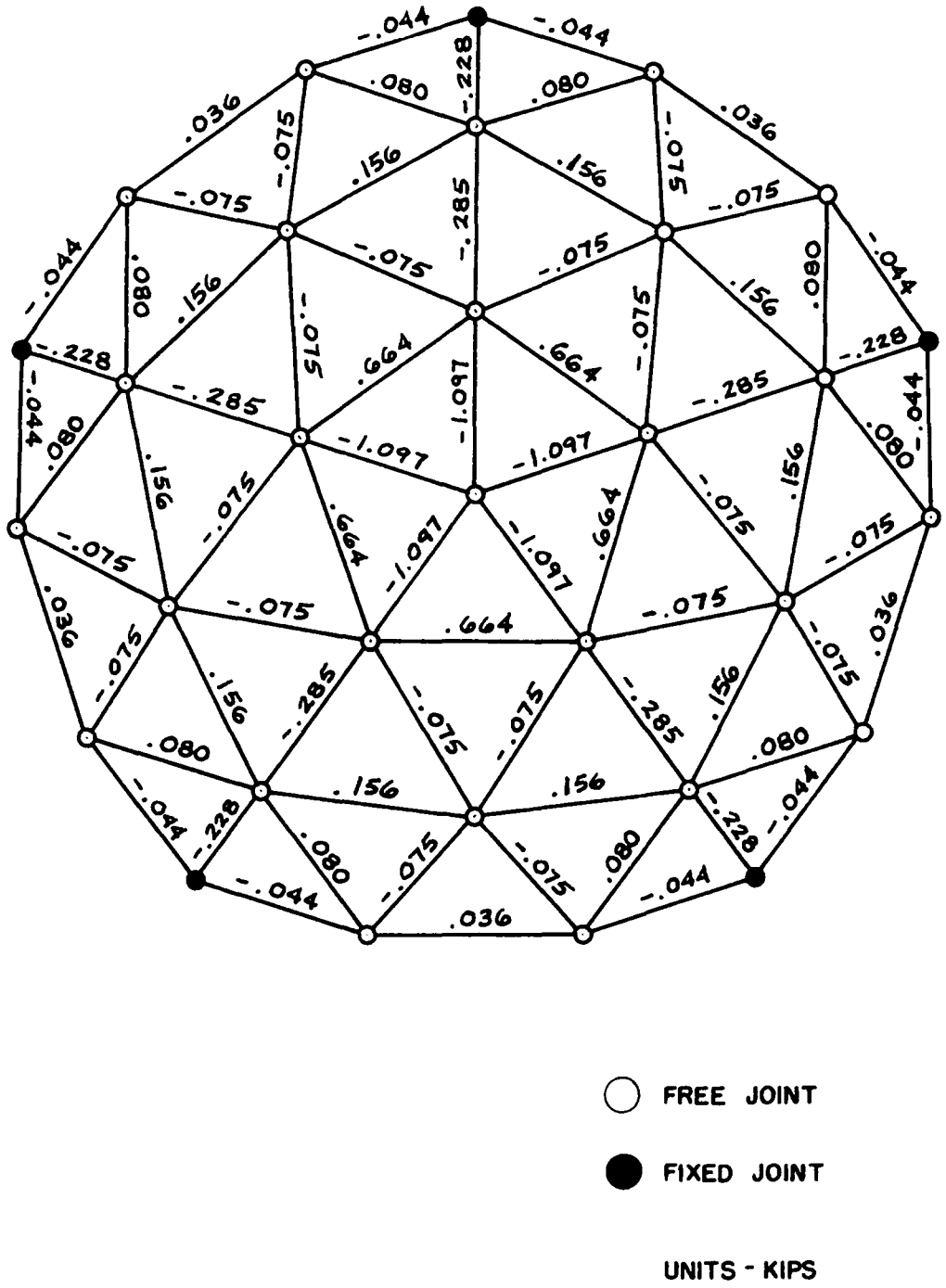

FIG. 5.16 - SPACE FRAME ANALYSIS RESULTS FOR DEMONSTRATION PROBLEM NO. 5 SUBJECTED TO AN AXISYMMETRIC LOAD

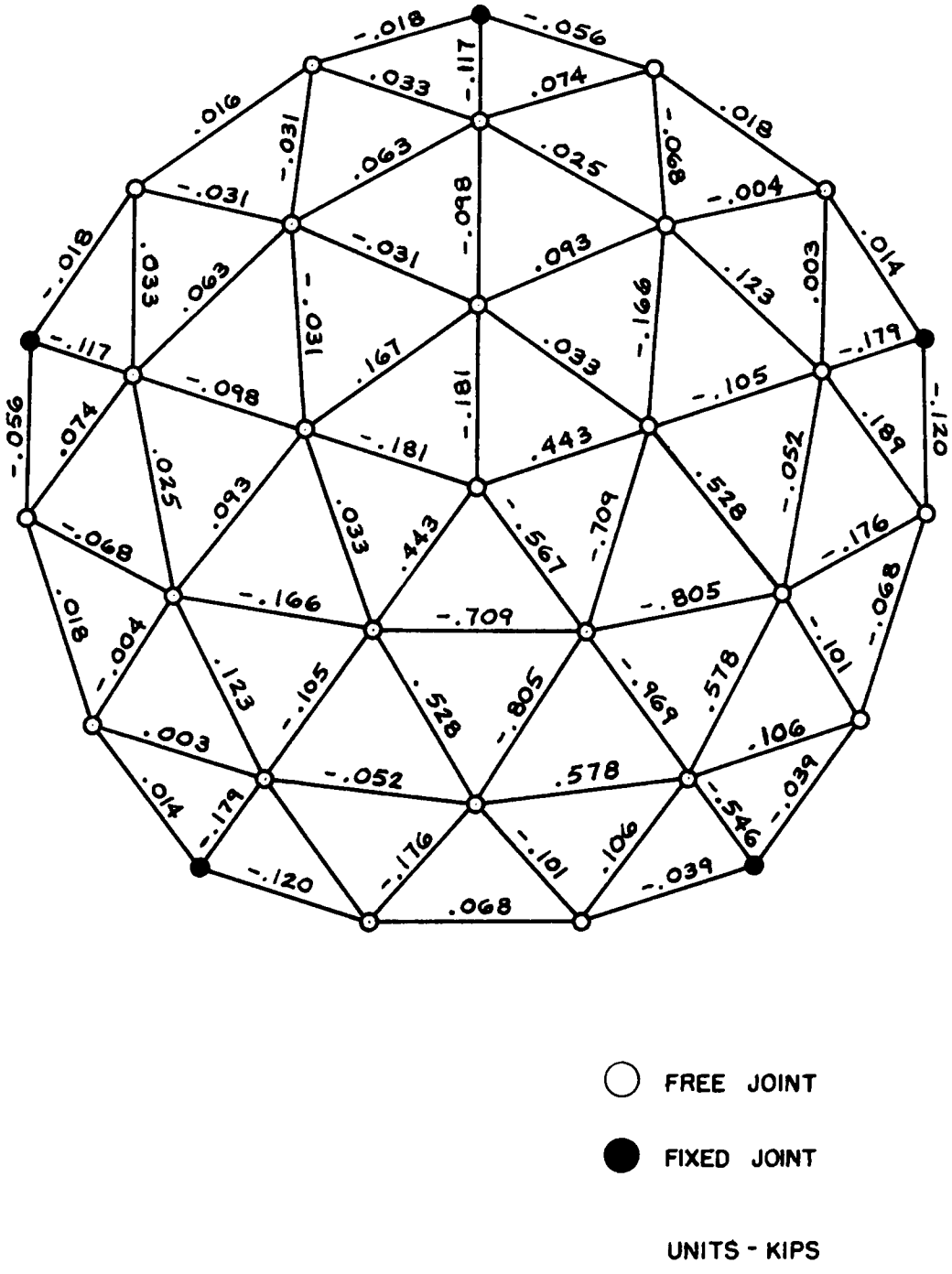

FIG. 5.17 - SPACE FRAME ANALYSIS RESULTS FOR DEMONSTRATION PROBLEM NO. 5 SUBJECTED TO AN ASYMMETRIC LOAD

5.3.5.1 Space Frame Results of Demonstration Problem No. 5 Subjected to Axisymmetric and Asymmetric Loading

Axial load results are presented in Figs. 5.16 and 5.17 for the space frame analysis of Demonstration Problem No. 5 subjected to an axisymmetric and asymmetric load of one kip applied in the vertical gravity direction at joint 1 and joint 2, respectively.

5.3.6 General Description of Demonstration Problem No. 6

Demonstration Problem No. 6 is a 78 degree of freedom 3^V pent-cap geodesic dome whose elevation and plan views are shown in Figs. 5.18 and 5.19. The structural geometry and properties are identical to Demonstration Problem No. 4. Several new members have been added at the periphery of the dome such that all joints on the horizontal base ring form the support for the structure.

5.3.6.1 Space Truss Analysis Results for Demonstration Problem No. 6 Subjected to Axisymmetric Loading

Fig. 5.20 contains the axial load results for the space truss analysis of Demonstration Problem No. 6 subjected to an axisymmetric load of one kip applied in the vertical gravity direction at joint 1.

5.3.7 Fully-Stressed Design of Demonstration Problem No. 1 Subjected to Design Loads

Results of the fully-stressed design of Demonstration Problem No. 1 subjected to design loads could not be obtained because the number of members and the number of degrees of freedom of the structure require a minimum of two load conditions ($p = \frac{n}{e} = \frac{35}{33} = 1.06$). Thus, for a

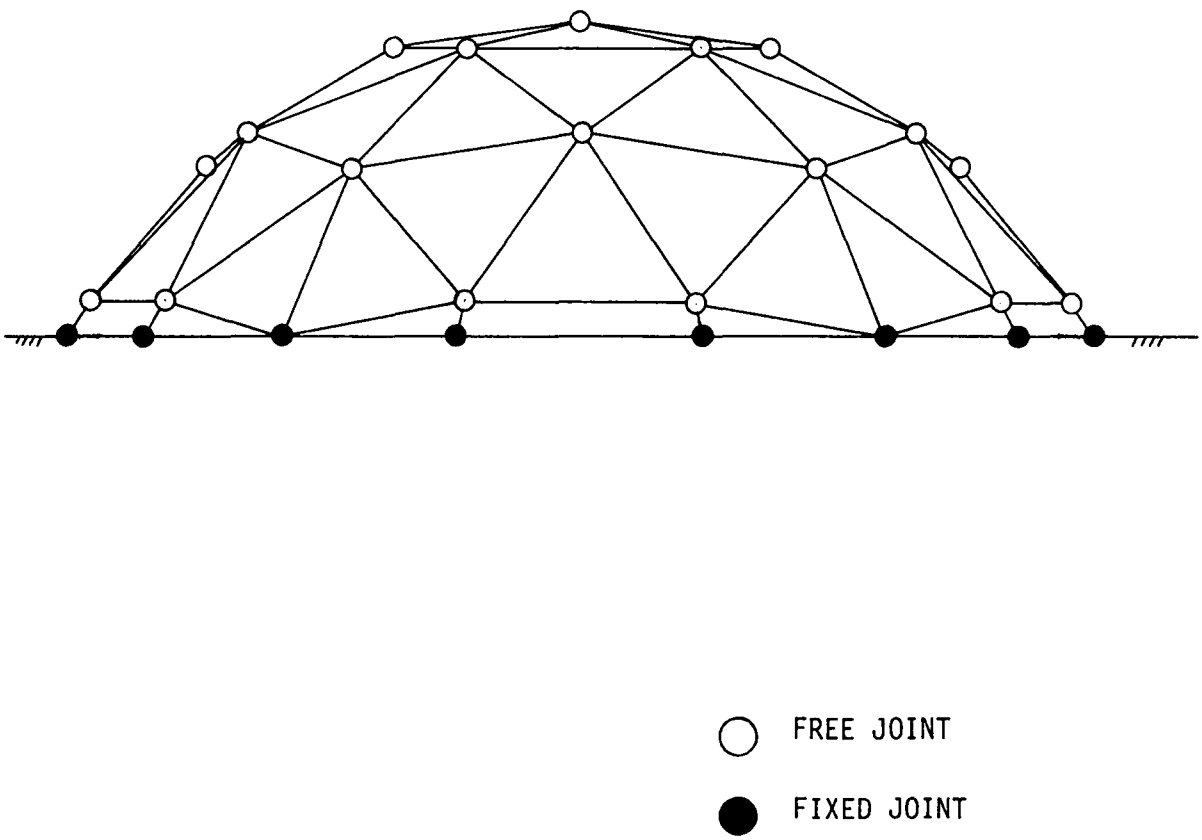

FIG. 5.18 - Elevation View of Demonstration Problem No. 6

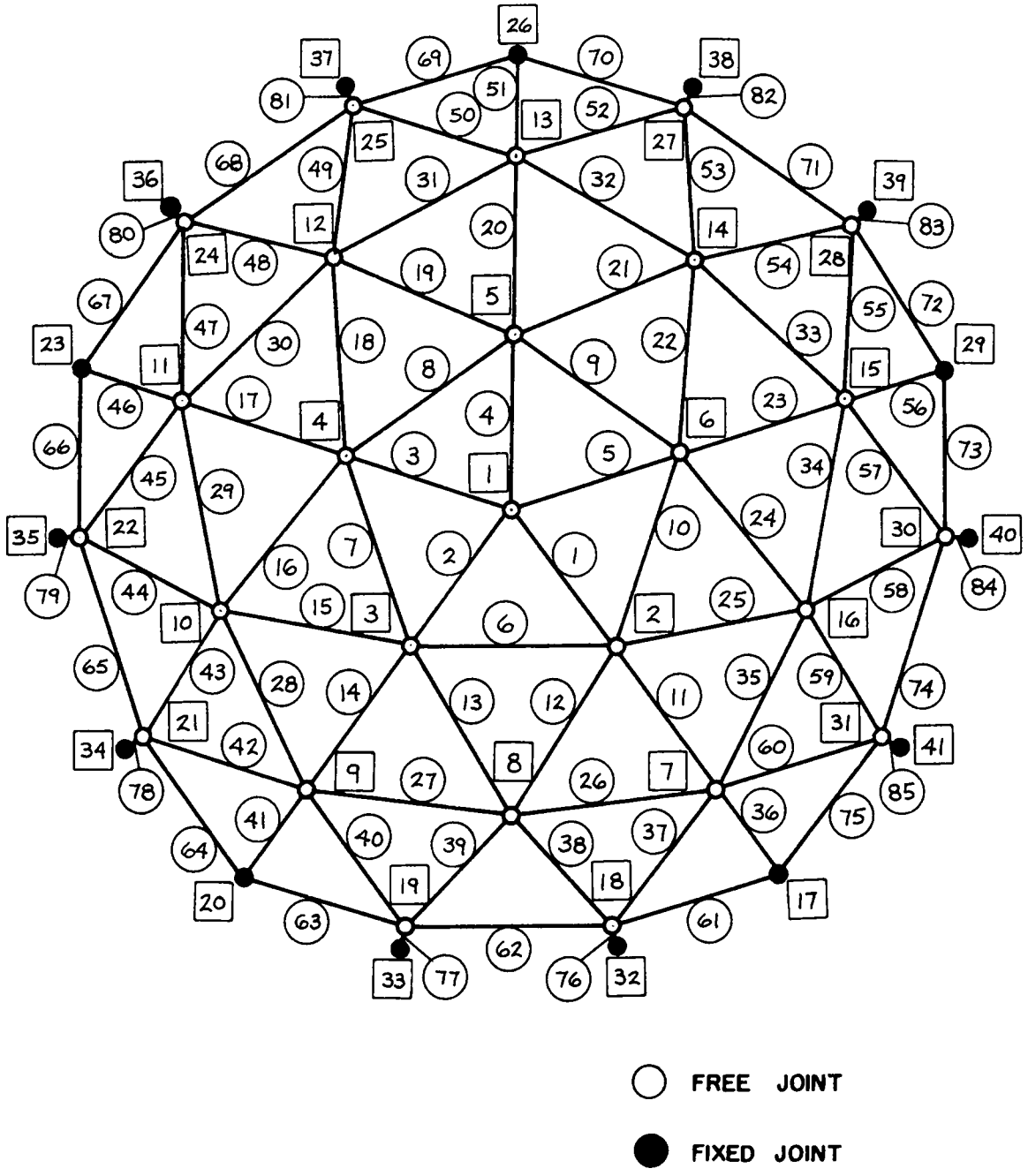

FIG. 5.19 - PLAN VIEW OF DEMONSTRATION PROBLEM NO. 6

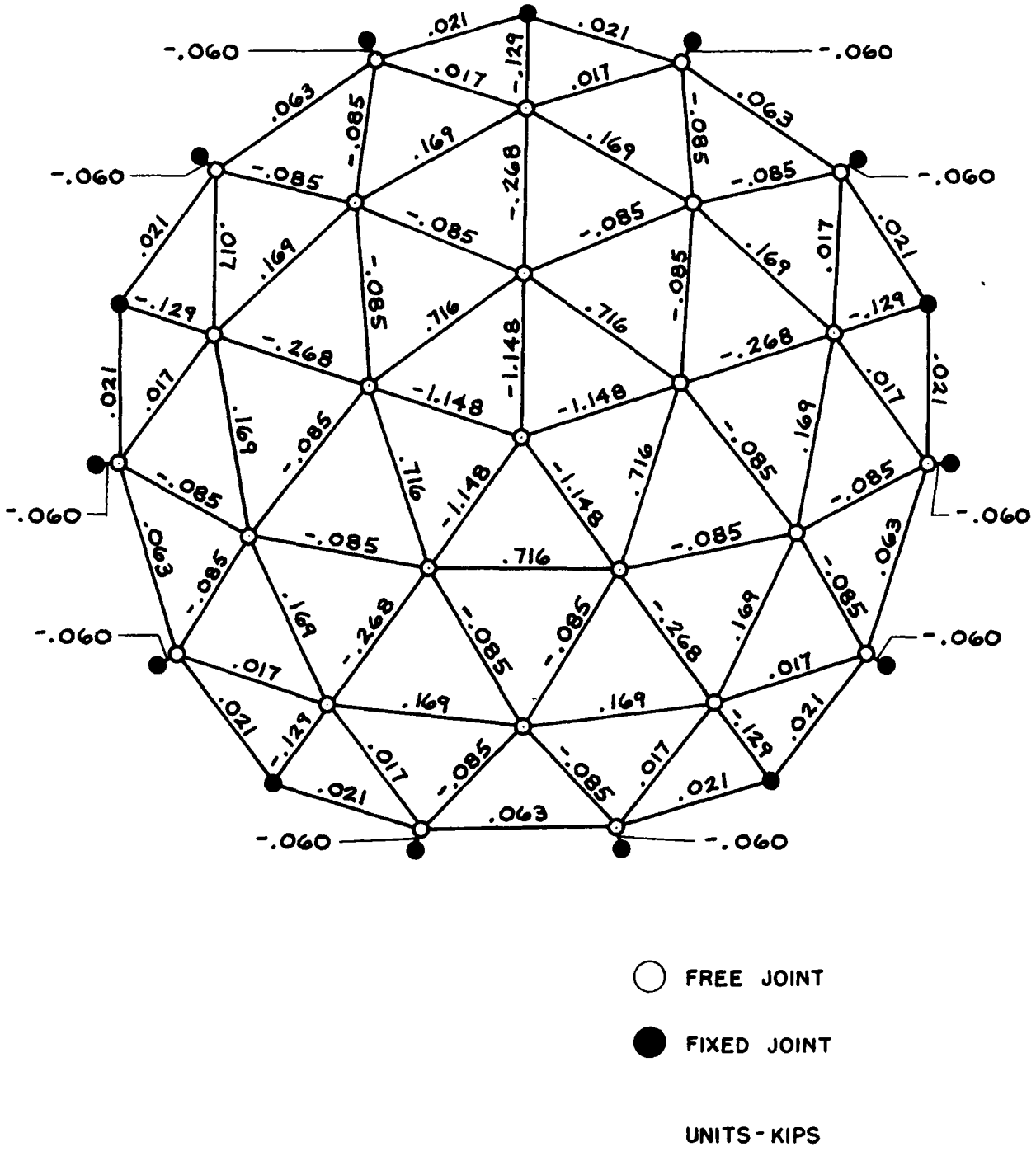

FIG. 5.20 - SPACE TRUSS ANALYSIS RESULTS FOR DEMONSTRATION PROBLEM NO. 6 SUBJECTED TO AN AXISYMMETRIC LOAD

single load combination a fully-stressed design is infeasible (see Section 3.4 of text).

Thus, the automated design procedure of the WATFIV/FORTRAN computer program could not be used to size the members of the framework of the dome as the final design, in practice, utilizes cross-sectional areas obtained from an evaluation of analysis results of the framework subjected to each load combination. Nevertheless, the initial cross-sectional areas of the members are shown in Fig. C.6. These were obtained using Eqs. (3.17) through (3.20).

The framework of the dome is fabricated from steel tubing whose modulus of elasticity is 30,000 ksi. The tensile yield strength of the steel is 36 ksi.

Several different design loads were imposed on the structure, representing as realistically as possible the effect of dead weight, snow, wind and unbalanced snow. The actual design of the dome is based on critical combinations of these loads which can be found in building codes [32,37] and steel specifications [31]. Axial load results due to these load combinations are presented in Figs. C.1 through C.5.

The dead load consists of the actual weight of the structural steel framework whose material density is given in the steel manual by AISC [31] as 490 lb/cu.ft.

Snow load is 30 lb/sq.ft. on horizontal projection [32]. A general description of the procedure used for obtaining the applied joint forces due to the snow load is given in Appendix B.

The wind load varies for each triangular face of the geodesic dome and the calculation of the applied joint loads due to wind effects is based on the information presented in several references [16,17]. A description of the calculation procedure is given in Appendix B.

The effect of an unbalanced snow load is considered by reducing the snow load by 50% over one-half of the dome's surface (the north side of Fig. C.5) [26,32,37].

CHAPTER 6

SUMMARY AND CONCLUSIONS

The space truss and space frame analysis results presented in Figs. 5.5 through 5.20 clearly demonstrate that the triangulated framework of a geodesic dome is very effective in distributing the stresses induced in the members by externally applied loads. In all cases involving the axisymmetric loading of the dome, the internal stress was uniformly distributed in all directions from the point of applications of the load. However, the distribution of stress in the framework is not uniform in the sense that all members are subjected to the same magnitude of axial load. Instead, some members are more heavily stressed than others. For example, in Fig. 5.6, it is quite evident that the members near the point of application of the load at joint 1 are subjected to higher axial loads than the members located on the periphery of the dome. It is also apparent that the members forming the shortest path between the point of application of the load and the support joints carry larger axial loads than members which are not a part of this path.

In the axisymmetric loading case, tension rings can be clearly identified at each level of the framework of the dome as shown in Figs. 5.14 and 5.16. The tension rings occur due to the outward thrust of the joints located on each level as a result of the applied axisymmetric vertical gravity loading at joint 1. This action causes the members on each level of the dome to be subjected to tensile forces.

The tensile force carried in each tension ring diminishes for each successive level of the dome (see Fig. 5.14 and 5.16).

For the aymmetric loading case, the distribution of stress in the framework of the dome is symmetrical about a vertical plane passing through the point of application of the load and the vertex of the dome. As in the axisymmetric loading case, the distribution of stress is not in a manner which evenly apportions the stress to each member. Those members nearest the point of application of the external load sustain higher axial stresses than those members on the side of the dome opposite the applied loading. In addition, the majority of the load is carried to the foundation supports through those members located on the shortest path between the externally applied load and the supports (see Fig. 5.17).

In the asymmetric loading case, several members in the tension ring on the side of the dome subjected to the externally applied load carry compressive axial loads. There is also sufficient data presented in Figs. 5.6 and 5.8 which would indicate that the web members (which are located between the five main radials emanating from the dome's vertex when viewed in plan) act most effectively in resisting asymmetric loads.

Comparing the space truss analysis results to the space frame analysis results for the 2^V and 3^V geodesic domes presented in chapter 5, it becomes evident that the members in a space frame model near the point of application of the externally applied load are subjected to smaller axial stresses than the same members in a space truss model. In

a space frame model, the joints are visualized as being rigid and the frame members are allowed to carry axial as well as shear forces. The shear forces act in such a manner as to reduce the axial forces in those members nearest the point of application of the external load. In a space truss model, the joints are visualized as ball and socket type joints which are free to rotate and the truss members are allowed to carry only axial loads. Accordingly, the axial load in the truss member nearest the point of application of the external load will be slightly greater than that in a frame member.

Although the amount of axial stress is reduced for those members near the point of application of the external load in a space frame model, the axial loads in members on the periphery of the dome are increased. This is a result of the transfer of shear and axial load from those members near the point of application of the external load (see Figs. 5.7 and 5.16). In the space truss model, only axial loads are transmitted from member to member and the magnitude of the axial load is less in the peripherial members (see Figs. 5.5 and 5.14). However, the reactions at the supports for the space truss and space frame model are nearly identical.

One advantage to be gained in making the joints as rigid as possible in the construction of the dome is the decrease in likelihood and in some cases the elimination of "local instability" or "snap-through" problems associated with the joints in single layer lattice domes. The rigid joints in the framework will not deflect as much as ball and socket type joints when subjected to an applied load.

Shallowness in a geodesic dome affects the amount of load carried by each of the members in the dome's framework. Comparing the axial load results of Figs. 5.5 and 5.11, it is seen that the members in a shallow dome are subjected to larger axial loads than the same members in a dome which isn't quite as shallow. As the angle between the centroidal axis of the member and a horizontal plane increases, the amount of load sustained by the member will decrease. As this angle decreases, the axial load in the member will increase, accordingly. The steeper the angle of inclination of the member in relationship to the horizontal plane, the less the amount of axial load transmitted through the member. Therefore, the more shallow the dome, the greater the amount of stress induced in the members by an externally applied load. This, in turn, results in larger reactions at the supports of the dome. In the design of geodesic domes supported at only five points on the periphery of the dome (as shown in Fig. 5.5), it would therefore seem prudent to prevent the dome from becoming too shallow. This will eliminate the high construction costs for heavy foundations to resist the outward horizontal thrusts at the base of the dome. However, if the dome possesses a natural horizontal base ring, the need for a foundation per se may be eliminated completely, as the tension ring at the base will act to resist the outward thrusts of the dome.

Upon study of the space truss analysis results for 2^V and 3^V geodesic domes subjected to axisymmetric and asymmetric loadings, it is evident that externally applied loads are more uniformly distributed

throughout the complex framework of the higher frequency dome (see Figs. 5.5, 5.6, 5.14 and 5.15). The greater the number of members in the framework, the more uniform the distribution of internal stresses. For example, the web members of the 3^V dome in Fig. 5.14 aid in transmitting the externally applied load to supports of the dome. In addition, the analysis results for the 2^V and 3^V geodesic domes of Figs. 5.5 and 5.15 indicate that the magnitudes of horizontal restraining forces at the supports of the 3^V dome are slightly less than those for the 2^V dome. It appears that the more complex framework of the 3^V dome is more effective in reducing the outward thrusts at the base of the dome.

Upon close examination of Fig. 5.15, it may be noticed that all joints on the periphery of the dome are fixed. This has been done since the space truss analysis results of Demonstration Problem No. 4 subjected to an asymmetric load reveal that the structure is geometrically unstable. This problem is remedied when all joints on the base ring of the dome are fixed. Thus, the space truss analysis results of Fig. 5.15 are provided for the modified version of Demonstration Problem No. 4. It is interesting to note that a space frame analysis of a 3^V dome subjected to an asymmetric load reveals no such geometric instability (see results for Demonstration Problem No. 5 shown in Fig. 5.17). It is apparent that the rigid joints of a space frame model supply the required geometric stability that ball and socket joints are unable to provide in the space truss model of the 3^V dome supported at only five points (as shown in Fig. 5.14).

The addition of supports at the base ring of the 3^V dome (whose

elevation and plane views are depicted in Figs. 5.18 and 5.19) results in a more efficient distribution of axial forces in the framework of the dome. The axial loads in the members near support joint 17 of Fig. 5.14, for example, are somewhat reduced when additional supports are provided (see Fig. 5.20). This might be expected, as there are more supports to which the induced stresses in the framework can be distributed. In addition, the magnitudes of the horizontal restraining forces at each of the supports will also be less than those for a dome with fewer supports.

The results of the fully-stressed design of the 2^V geodesic dome geometrically defined in Figs. 5.3 and 5.4 are found in Appendix C. They are placed in Appendix C because during the development and solution of the problem, it became evident that an automated procedure for obtaining a fully-stressed design of the dome was not practical. It became impractical because of certain types of loading conditions such as wind which would require a separate design for each direction of application. This would, in turn, necessitate the requirement that all members be of the same size. For such a case, a fully-stressed design cannot be obtained if the same material is used throughout the framework. A fully-stressed design for the framework of the dome would also be impractical from the viewpoint that all members should be of the same size for economic reasons of fabrication and erection.

The rate of convergence to the fully-stressed design state for this particular problem was very slow. After 40 cycles of iterative analysis, only 10 members of a total of 35 were fully-stressed (see Table 6.1).

Table 6.1 Number of Members Fully-Stressed after 40 cycles of Iterative Analysis

Loading Combination	Number of members fully-stressed after 40 cycles of iterative analysis
Dead Load + Snow Load	10
3/4 (Dead Load + Wind Load)	10
3/4 (Dead Load + Snow Load + Wind Load/3)	10
3/4 (Dead Load + Snow Load/2 + Wind Load)	10
3/4 (Unbalanced Snow Load + Wind Load)	22

The remaining 25 members were still either highly overstressed (700%-1300% fully-stressed) or understressed (9%). This occurred because convergence to a fully-stressed design state for Demonstration Problem No. 1 was infeasible for the application of a single load combination. The number of members and the number of degrees of freedom of the structure require a minimum of two load combinations for a fully-stressed design to be feasible. Thus, the automated design procedure of the WATFIV/FORTRAN computer program can not provide a fully-stressed design for Demonstration Problem No. 1

Even so, the assembled WATFIV/FORTRAN computer code is capable of providing a fully-stressed design via the stress-ratio method for problems in which the feasibility criteria of Section 3.4 is satisfied.

After a fully-stressed design is obtained, a slenderness ratio check is performed for all members to satisfy the buckling requirements of the AISC Specifications [31]. All members are equally sized based on the largest required cross-sectional area obtained after the slenderness ratio check. Although the automated procedure for the fully-stressed design of a geodesic dome cannot be used directly in sizing members for the dome, it can provide a basis for the selection of uniformly sized members considering the applied load conditions and the economic factors of fabrication and erection.

Although this parametric study accomplished much in investigating the three-dimensional load distribution characteristics of geodesic domes, there is still room for further study. It would be interesting to observe and compare the load distribution characteristics in the

framework of higher frequency domes such as 4^V, 5^V, and 6^V. Axisymmetric and asymmetric load studies of these domes can be easily performed using either the assembled WATFIV/FORTRAN computer program or ICES STRUDL II [15], although the array dimensions of the WATFIV/FORTRAN program would require alteration to provide enough storage space for the more complex frameworks. The automatic joint coordinate generator routine in the WATFIV/FORTRAN computer code would be particularly helpful in generating the geometry for these domes. The analysis could then be performed using ICES STRUDL II.

Using either of these computer programs, a more thorough study of the effects of shallowness can be conducted. Space truss and space frame analysis results can be obtained for shallow 3^V, 4^V, 5^V, and 6^V geodesic domes subjected to axisymmetric as well as asymmetric loadings.

The stress effects induced in the framework by releasing various degrees of freedom at the support joints could also be studied for axisymmetric and asymmetric loadings.

Consideration can be given to studying the effects of temperature changes and fabrication errors in the members as well as support settlement, using either the WATFIV/FORTRAN program or ICES STRUDL II.

A parametric study can be conducted by varying the diameter of the 2^V and 3^V geodesic dome and comparing the analysis results obtained. In addition, analysis results may be compared for frameworks using different cross-sectional areas for the members. Also, the use of different shaped members such as square tubular members may be investigated in lieu of circular tubular members. Different types of material

such as aluminum, wood and high strengh alloys can be investigated to determine the most efficient load carrying material for the framework.

Finally, different framework configurations can be studied to ascertain which type of framework is most efficient in distributing externally applied loads. There are many types of lattice or "steel-braced" frameworks which may be investigated. Examples may be found in many available references on the subject of lattice domes and related structures [18,24,30,36].

In conclusion, the parametric study of a 2^v and 3^v geodesic dome subjected to axisymmetric and asymmetric loading reveals that these structures are very efficient in distributing externally applied loads. But as pointed out earlier in the discussion, there is still room for additional study. The automated design procedure of the WATFIV/FORTRAN computer program can produce satisfactory numerical results, if the feasibility criteria for a fully-stressed design is satisfied. Practical considerations of the economics of fabrication and erection as well as the application of external loadings will also dictate the usefulness of the information provided.

In the process of performing the study, the value of automated matrix methods of structural analysis became quite apparent. Without the services of a computer and the automated procedures developed for the analysis of skeletal structures, the task of structurally analyzing lattice domes becomes overwhelming merely because of the size of the problem. For example, a space truss and space frame analysis of the 3^v geodesic dome involves 78 and 156 degrees of freedom, respectively.

To solve such a problem by hand would be too much to ask. The high speed computer can obtain results in seconds even though large amounts of computer core storage space are required (see Table 6.2 for computer run times).

A close examination of the charges presented in Table 6.2 for using the assembled WATFIV/FORTRAN computer codes and ICES STRUDL II reveals that the use of the latter is somewhat cheaper. However, the majority of the charges for the WATFIV/FORTRAN computer program result from the reading of the source deck and input data cards. The cost is about the same for both programs if these charges are removed. Thus, it might be cheaper to use the geodesic dome joint coordinate and member incidence generator portion of the WATFIV/FORTRAN program to establish the geometry of the dome and use ICES STRUDL II to perform the actual analysis.

The cost for a space truss computer solution of a 2^V and 3^V geodesic dome subjected to the same type of loading (axisymmetric or asymmetric) is nearly equal. On the other hand, the space frame analysis of the two structures reveals a substantial increase in cost (on the order of $7.00). This is a result of the tremendous increase in the size of the problem investigated, as discussed previously.

The cost of using the automated design portion of the WATFIV/FORTRAN program is not too great for the 2^V dome problem containing 35 members and 16 joints. Several iterations of analysis may be performed and incur very little additional computer cost (about $3.00). But the computer costs will vary depending upon the size of the problem under investiga-

Table 6.2 Comparison of Computer Costs and Execution Times for Demonstration Problems

Problem No.	General Description	Type of Loading	WATFIV/FORTRAN Program		ICES STRUDL II Program	
			Cost ($)	Time (sec)	Cost ($)	Time (sec)
1	2^V space truss	axisymm	2.49	6	1.02	8
1	2^V space truss	asymm	2.55	6	1.54	8
2	2^V space frame	axisymm	2.78	25	1.21	12
2	2^V space frame	asymm	2.82	26	1.71	12
3	2^V space truss	axisymm	3.86	7	-	-
4	3^V space truss	axisymm	3.21	23	-	-
4	3^V space truss	asymm	3.32	23	1.95	15
5	3^V space frame	axisymm	9.58	151	-	-
5	3^V space frame	asymm	9.53	149	-	-
6	3^V space truss	axisymm	3.98	35	-	-

tion as well as the symmetry of the applied loading and the availability of good initial design variables.

REFERENCES

1. Banhem, R., "Climatron St. Louis Missouri," Age of the Masters, Icon Editions, Harper & Row Rublishers, New York, 1975.

2. Bartholomew, P. and Morris, A. J., "A Unified Approach to Fully-Stressed Design," Engineering Optimization, Vol. 2, 1976, pp. 3-15.

3. Boell, D., "Summer Performance in Winter with Polyframe Domes," Water and Sewage Works, Scranton Gillette Publication, July, 1974.

4. Dayaratnam, P. and Patnaik, S., "Feasibility of Full Stress Design," Journal of the American Institute of Aeronautics and Astronautics, Vol. 7, No. 4, April, 1969.

5. Desai, C. S. and Abel, J. F., Introduction to the Finite Element Method, Van Nostrand Reinhold Company, New York, 1972.

6. Fuller, R. B., "The age of the dome," Build International, Vol. 2, No. 6, July/August, 1969.

7. Fuller, R. B., Building Construction, United States Patent No. 2,682,235, June, 1954.

8. Gallagher, R. H. and Zienkiewicz, O C., eds., Optimum Structural Design-Theory and Applications, John Wiley & Sons, New York, 1973.

9. Gere, J. M. and Weaver, Jr., W., Analysis of Framed Structures, D. Van Nostrand Company, Princeton, New Jersey, 1965.

10. Holzer, S. M., "Lecture Notes on CE 4001, 4002 - Matrix Structural Analysis," V.P.I. & S.U., Blacksburg, Va., Fall & Winter Quarters, 1975-76.

11. Holzer, S. M., "Lecture Notes on CE 5980 - Special Study (Introduction to Structural Optimization Design)," V.P.I. & S.U., Blacksburg, Va., 1st Summer Session, 1977.

12. Holzer, S. M., "Static and Dynamic Stability of Reticulated Shells," Proceedings of the International Colloquium on Stability of Steel Structures, Washington, D. C., May 17-19, 1977, pp. 27-39.

13. Holzer, S. M., Somers, A. E., and White, III, W. S., "Stability of Lattice Structures Under Combined Loading," ASCE Nat. Conv. Preprint 2975, San Francisco, CA., October 17-21, 1977.

14. Livesly, R. K., Matrix Methods of Structural Analysis, Pergamon Press, New York, 1964.

15. Logcher, R. D., et al., "ICES STRUDL-II, Frame Analysis," 1st ed., Massachusetts Institute of Technology, Vol. 1, 1968.

16. Lothers, J. E., Design in Structural Steel, Prentice-Hall, Englewood Cliffs, New Jersey, 1972, pp. 310-312.

17. Maher, F. J., "Wind Loads on Basic Dome Shapes," Journal of the Structural Division, ASCE, Vol. 91, No. ST3, Proc. Paper 4383, June, 1965, pp. 219-228.

18. Makowski, Z. S., Steel Space Structures, Michael Joseph Ltd., London, England, 1965.

19. McNeil, W. A., "Structural weight minimization using necessary and sufficient conditions," Journal of Optimization and Applications, Vol. 8, No. 6, 1971, pp. 454-466.

20. Merritt, F. S., ed., Standard Handbook for Civil Engineers, McGraw-Hill Book Company, New York, 1968, pp. 6-92 - 6-95.

21. Moore, J. B., WATFIV: FORTRAN Programming with the WATFIV Compiler, Reston Publishing Co., Reston, Va., 1975.

22. Norris, C. H., Wilbur, J. B., and Utku, S., "Approximate Analysis of Statically Indeterminate Structures," Elementary Structural Analysis, 3rd ed., McGraw-Hill Book Co., 1976, pp. 192-212.

23. Parikh, K. S., "Analysis of Shells Using Framework Analogy," thesis presented to the Massachusetts Institute of Technology, at Cambridge, Mass., in 1962, in partial fulfillment of the requirements for the degree of Doctor of Philosophy.

24. Popko, E., Geodesics, University of Detroit Press, Detroit, Michigan, 1968.

25. Razini, R., "The Behavior of Fully-Stressed Design of Structures and its Relationship to Minimum Weight Design," Journal of the American Institute of Aeronautics and Astronautics, Vol. 3, 1965, pp. 2262-2268.

26. Richter, D. L., "Design of a Geodesic Dome South Pole," presented at the October 17-21, 1977, ASCE, Fall Convention and Exhibit, held at San Francisco, CA. (Preprint 3060).

27. Schnobrich, W. C. and Mohraz, B., "Analysis of Latticed Structures as Equivalent Continua," presented at the October 13-17, 1969 ASCE Annual and Environmental Engineering Meeting, held at Chicago, Ill.

28. Turner, M. R., "Timber Dome Roof Over Stadium Spans Record 502 Ft.," Civil Engineering - ASCE Magazine, August, 1977, pp. 69-72.

29. White, R. N., Gergely, P. and Sexsmith, R. G., Structural Engineering, Vol. 2, John Wiley & Sons, New York, 1972.

30. Domebook 2, 2nd ed., Shelter Publications Bolinas, CA., October, 1972.

31. Manual of Steel Construction, 7th ed., American Institute of Steel Construction, 1973.

32. The Boca Basic Building Code/1970, 5th ed., Building Officials and Code Administrators, International, Inc., 1969.

33. "Home Sweet Dome," Time Magazine, March, 1977, pp. 34-35.

34. "Polyframe Dome," Temcor, Torrance, CA.

35. "Aluminum domes protect city's water," The American City Magazine, Butterhiem Publishing Co., September, 1974.

36. "Latticed Structures: State-of-the-Art Report," Journal of the Structural Division, ASCE, Vol. 102, No. ST11, November, 1976, pp. 2197-2230.

37. American National Standard Building Code Requirements for Determining Design Loads in Building and Other Structures, A58.1-1972, American National Standards Institute, 1972.

APPENDIX A

DERIVATION OF THE COORDINATE TRANSFORMATION MATRIX

Appendix A is concerned with the derivation of the coordinate transformation matrix, λ. This matrix is used in the transformation process from local to global coordinates [9,10,14].

The derivation begins by considering an element arbitrarily located in space as shown in Fig. A.1 [10]. In Fig. A.1, the space element i has a direction from joint j to joint k. X_{mn} = coordinate of joint m in the n direction. ℓ = length of projection of element in onto the 1-2 plane. L = actual length of the space element i. The rotation angles Φ_2 and Φ_3 are shown in the positive sense. The roll angle Φ_1 (shown in Fig. A.1a) is obtained from engineering drawings [10].

The coefficeints of the coordinate transformation matrix may be identified in Figs. A.1 and A.1a.

Letting

$$c_k = \cos \Phi_k \tag{A.1}$$

$$s_k = \sin \Phi_k \tag{A.2}$$

where $k = 1,2,3$

then

$$c_1 = \cos \Phi_1 \tag{A.3}$$

$$s_1 = \sin \Phi_1 \tag{A.4}$$

But, c_2, s_2, c_3, s_3 may be obtained directly from Fig. A.1 by letting

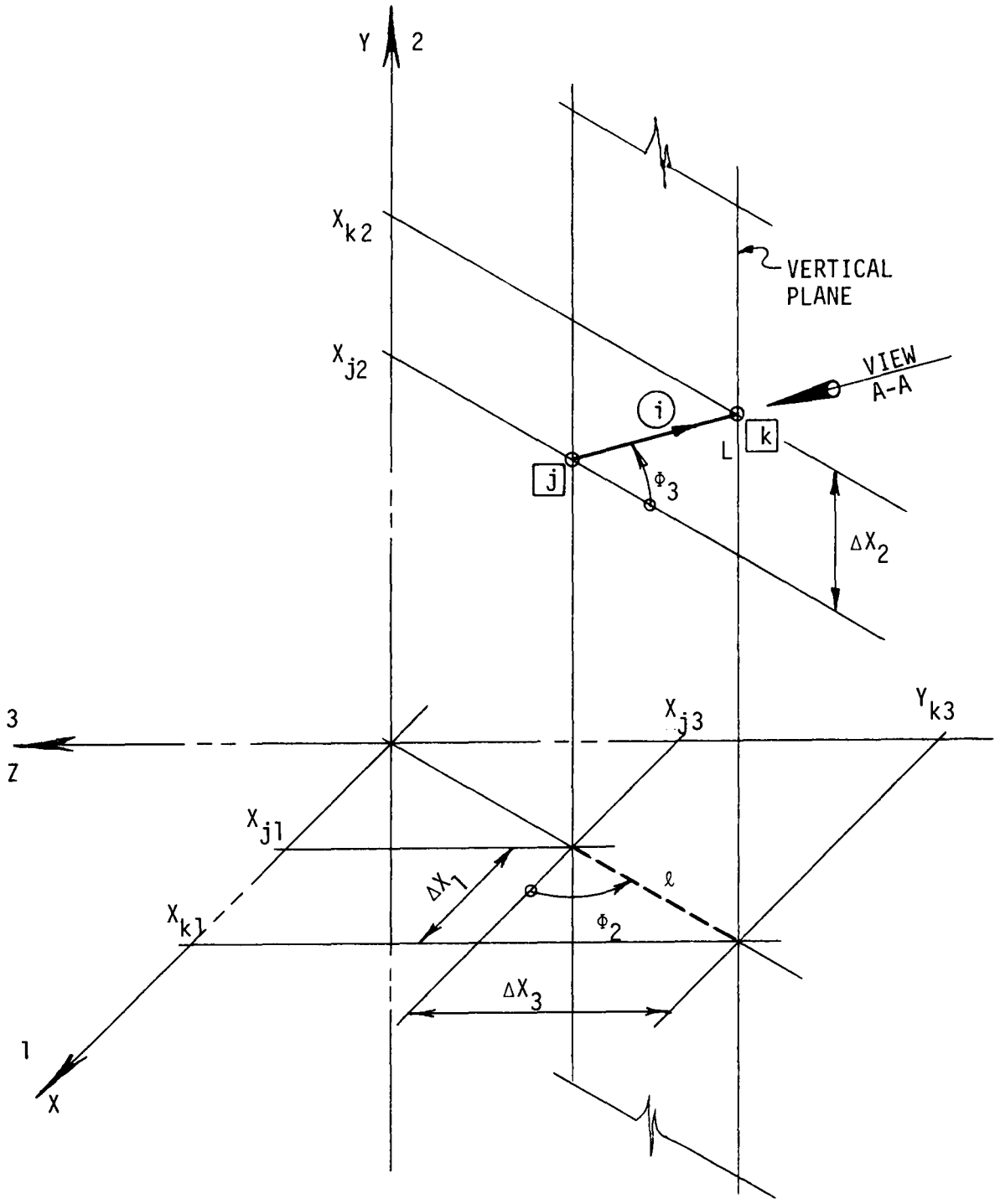

FIG. A.1 - Frame Element i Arbitrarily Located in Space

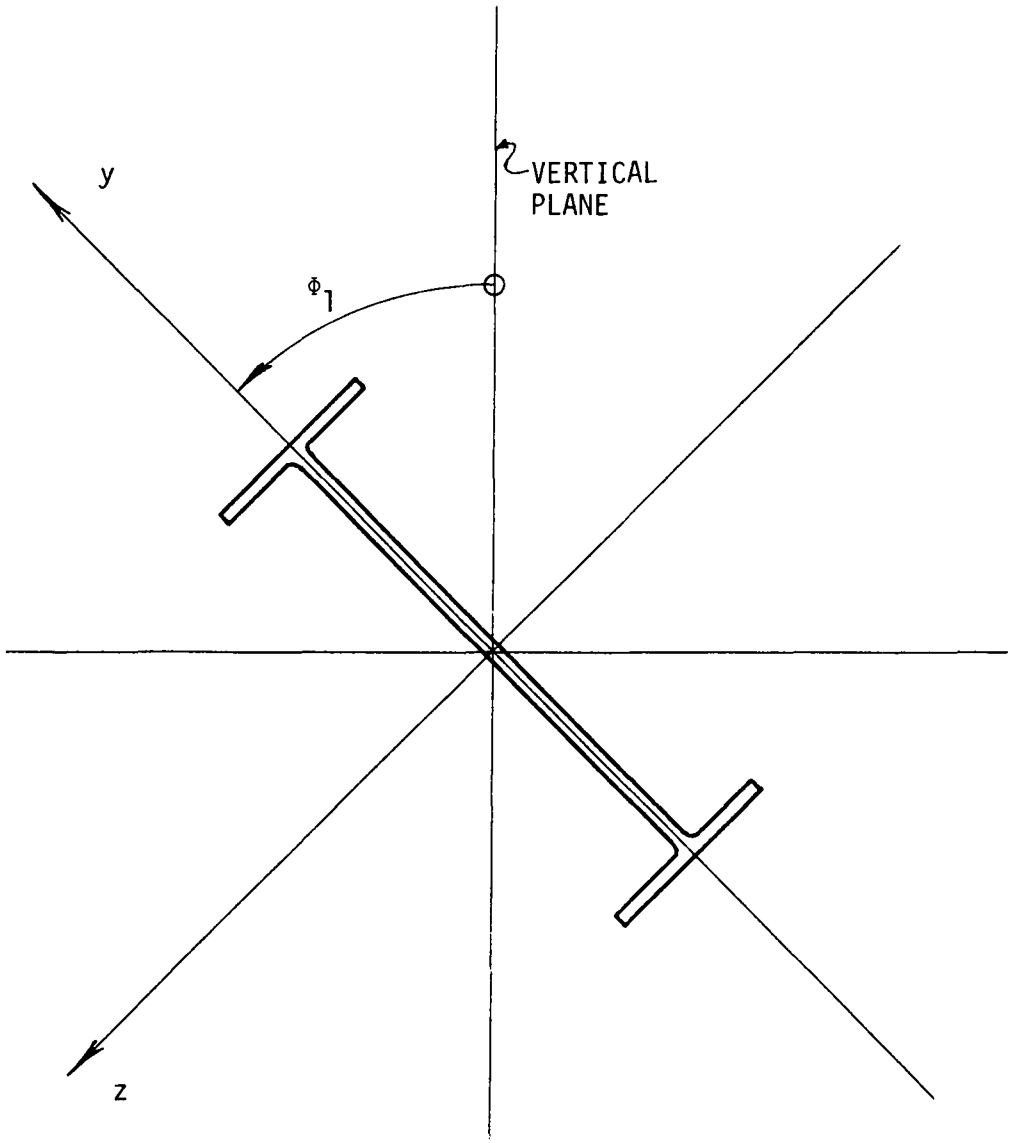

VIEW A-A

FIG. A.1a - Rotation Angle, Φ_1

$$\ell = (\Delta X_1^2 + \Delta X_3^2)^{\frac{1}{2}} \tag{A.5}$$

and

$$L = (\ell^2 + \Delta X_2^2)^{\frac{1}{2}} \tag{A.6}$$

then

$$c_2 = \frac{\Delta X_1}{\ell} \tag{A.7}$$

$$s_2 = -\frac{\Delta X_3}{\ell} \tag{A.8}$$

$$c_3 = \frac{\ell}{L} \tag{A.9}$$

$$s_3 = \frac{\Delta X_2}{L} \tag{A.10}$$

These expressions can be easily incorporated into a computer code.

Consider the matrix equation associated with Fig. A.2:

$$X = \lambda x \tag{A.11}$$

where X = the vector in global coordinates; and x = the vector in local coordinates. The λ matrix has the property such that it may be expressed in partitioned form as

$$\lambda = [i_1 \; i_2 \; i_3] \tag{A.12}$$

where i_j = the unit vector on the j-local axis (j=1,2,3) defined relative to the global coordinate reference frame (i.e. the components of i_j are the projections of a unit length vector from j-local onto the global axes [10].) The property of the λ matrix expressed in Eq. (A.12) is useful in computing the elements of the matrix. The

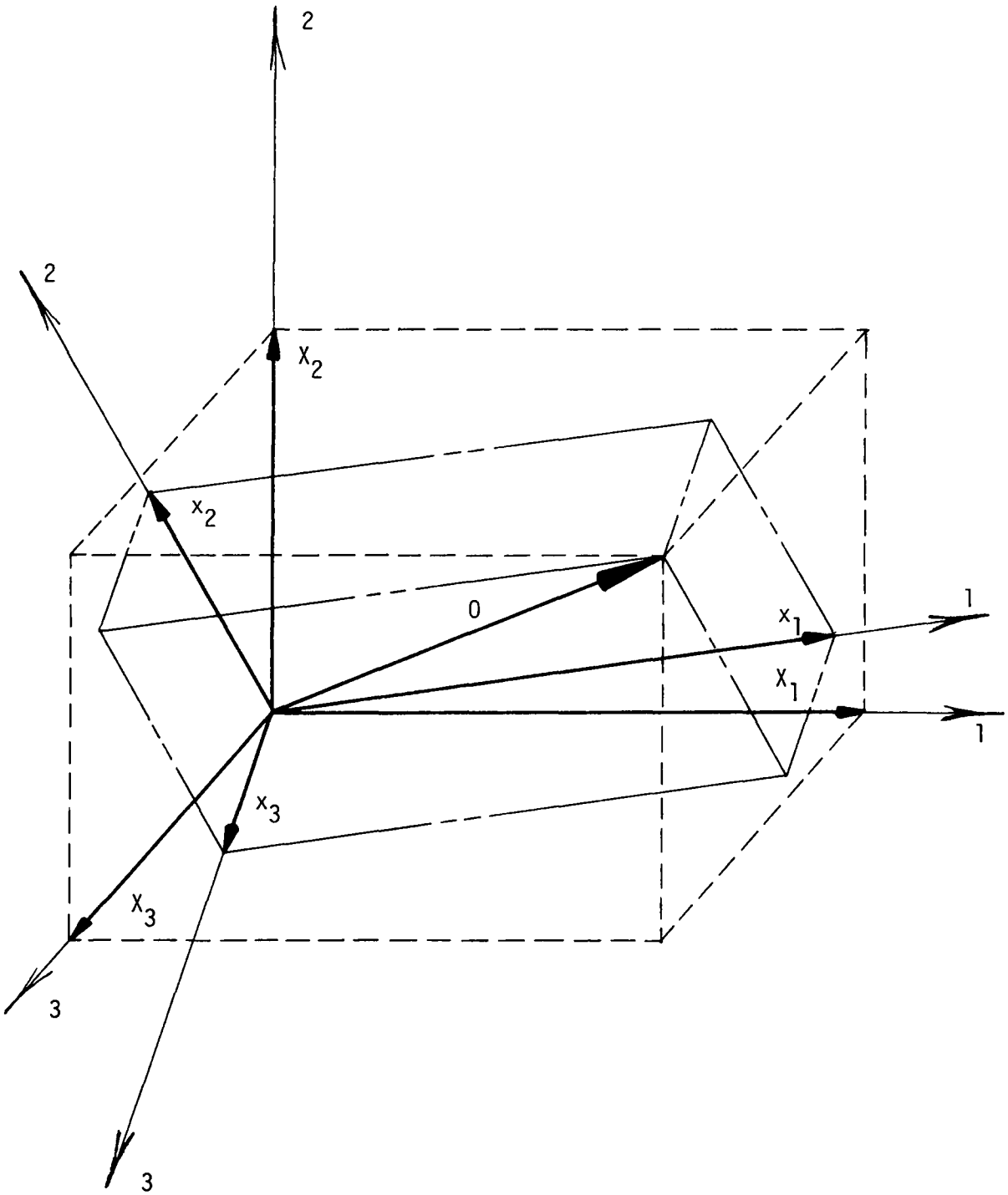

FIG. A.2 - Components of General Vector, 0, in Two Different Coordinate Systems

coefficients of the matrix are found from the rotational transformations depicted in Figs. A.3 and A.3a. From Fig. A.3

$$X = \lambda_2 a \tag{A.13}$$

$$a = \lambda_3 b \tag{A.14}$$

$$b = \lambda_1 x \tag{A.15}$$

Eq. (A.14) into Eq. (A.13) yields

$$X = \lambda_2(\lambda_3 b) \tag{A.16}$$

Eq. (A.15) into Eq. (A.16) gives

$$X = \lambda_2\lambda_3(\lambda_1 x) \tag{A.17}$$

or

$$X = \lambda x \tag{A.11}$$

where

$$\lambda = \lambda_2\lambda_3\lambda_1 \tag{A.18}$$

Letting

$$c_i = \cos \Phi_i$$

$$s_i = \sin \Phi_i$$

where $i = 1,2,3$

the coefficients of λ_2 can be defined as shown in Fig. A.4:

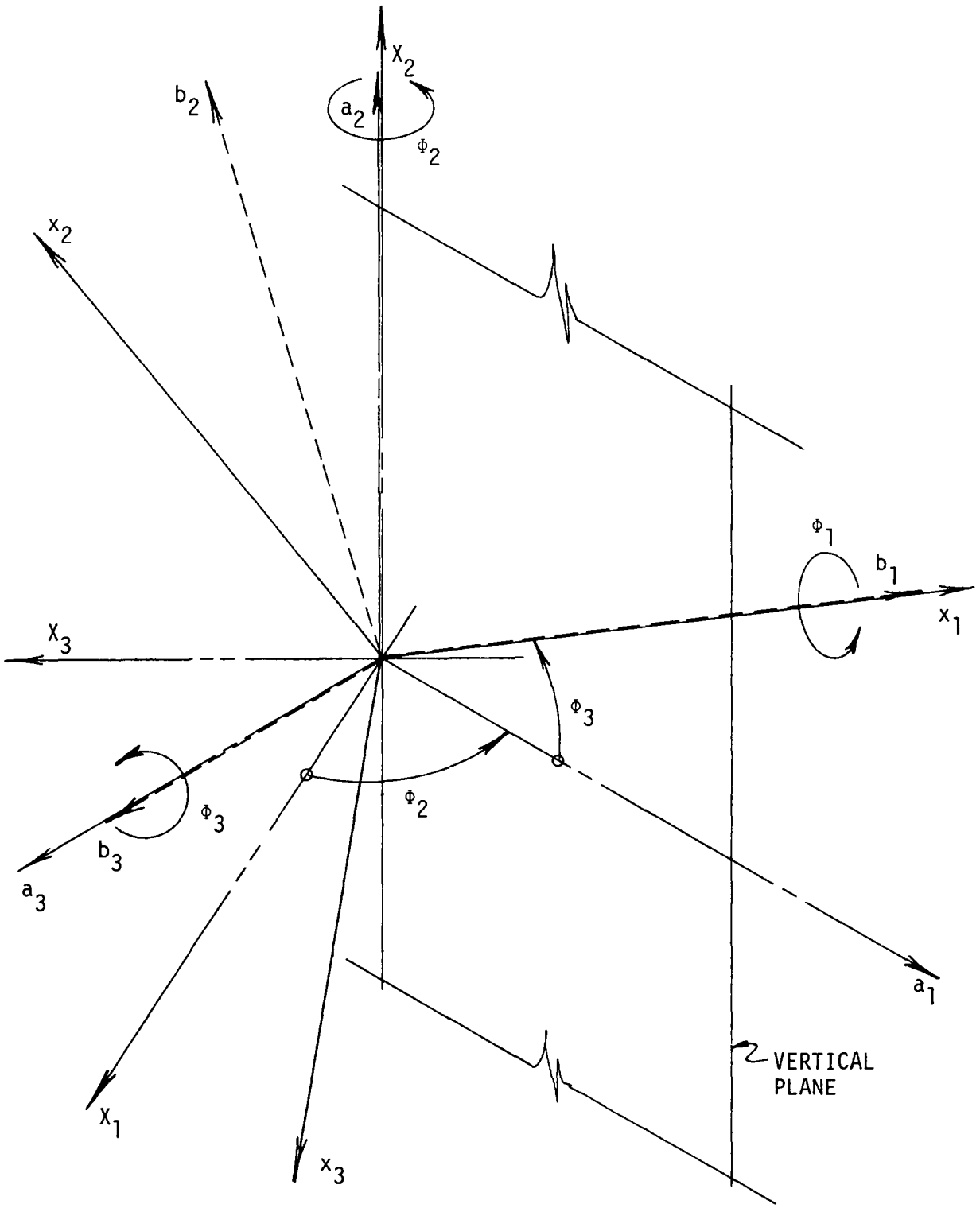

FIG. A.3 - Rotational Transformations, Φ_1, Φ_2, Φ_3

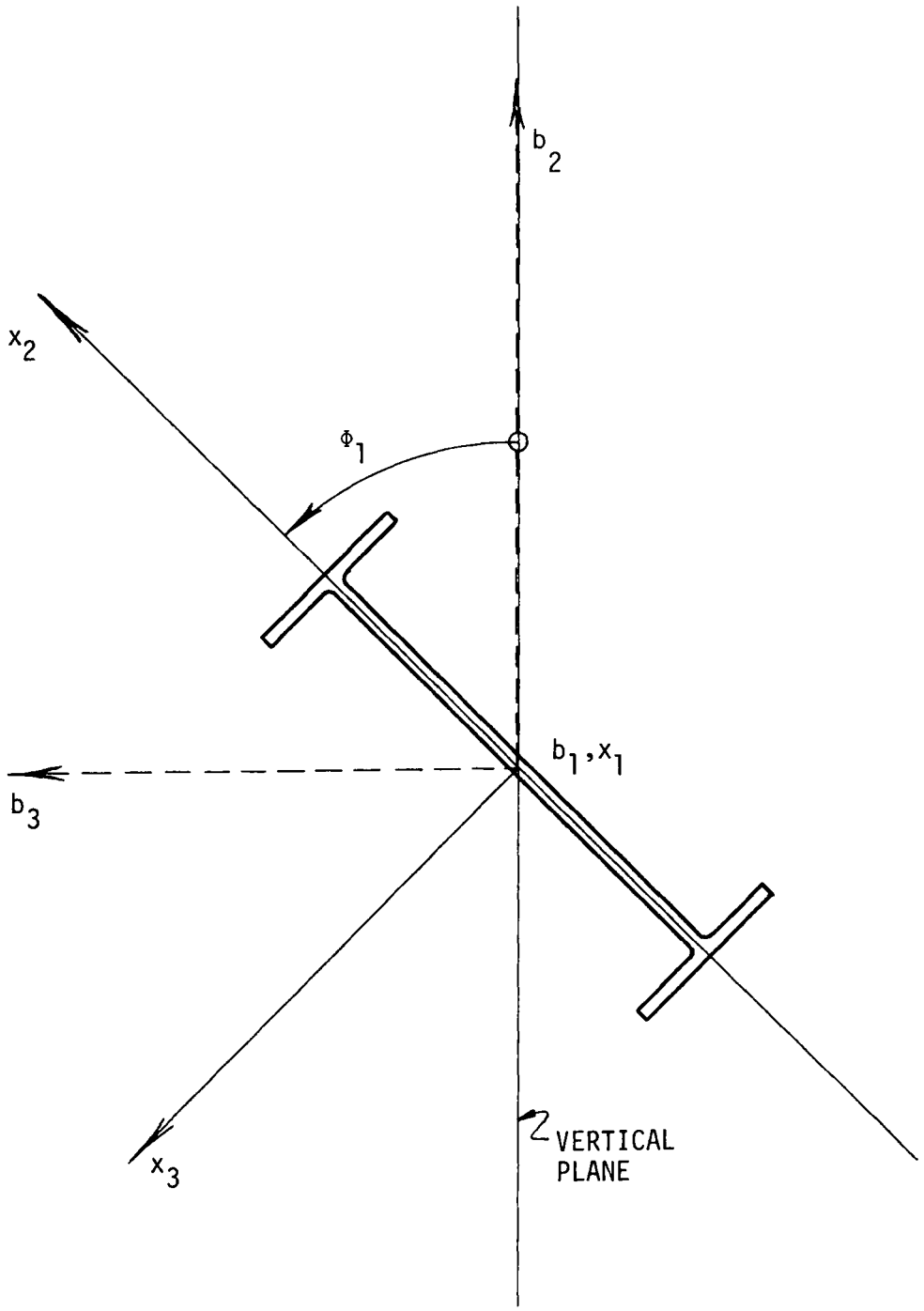

FIG. A.3a - Rotation Angle, Φ_1

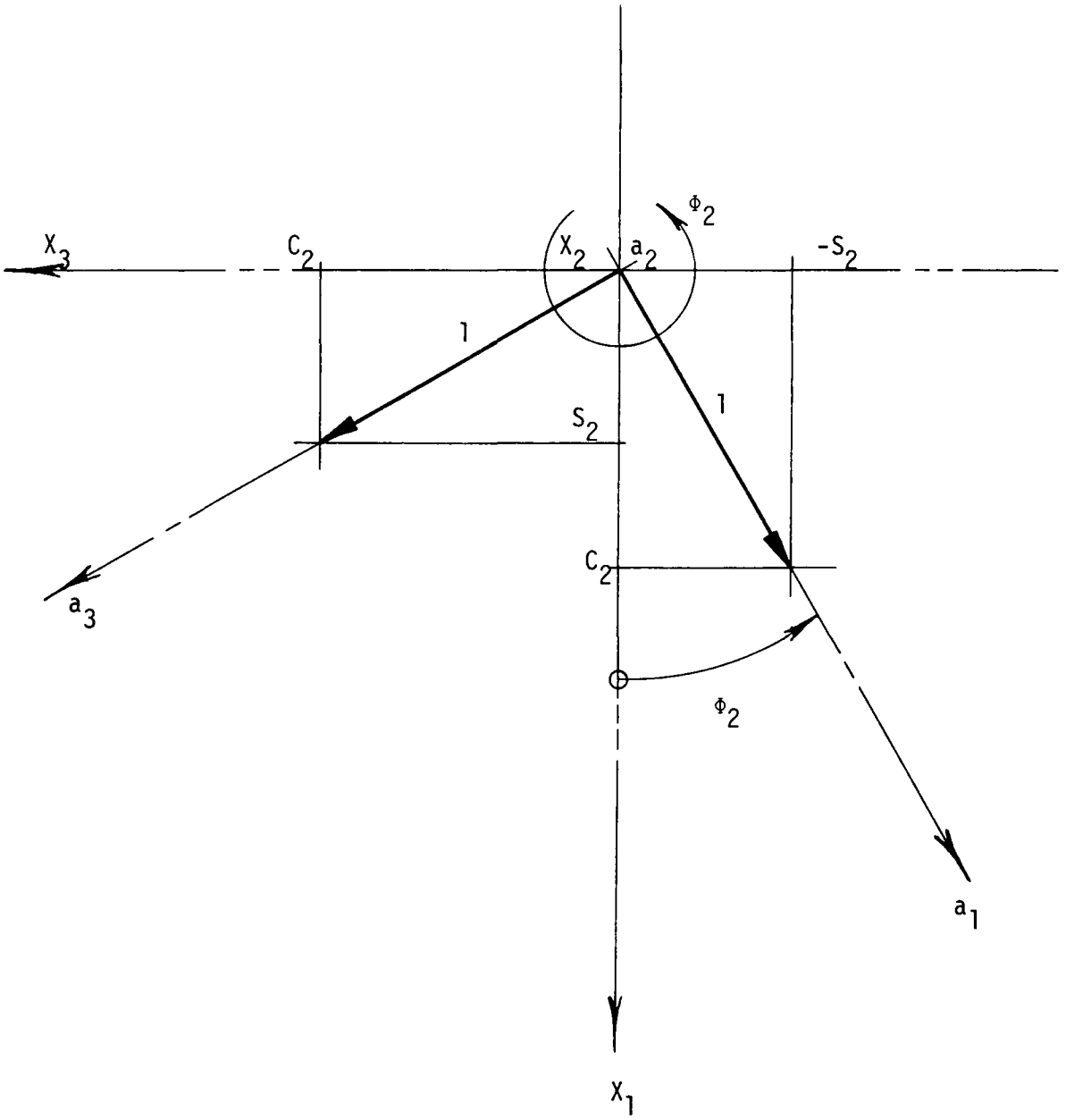

FIG. A.4 - Rotational Transformation, Φ_2

$$X_1 = c_2 a_1 + s_2 a_3 \tag{A.19}$$

$$X_2 = a_2 \tag{A.20}$$

$$X_3 = -s_2 a_1 + c_2 a_1 \tag{A.21}$$

Writing Eqs. (A.19), (A.20) and (A.21) in matrix form,

$$\begin{bmatrix} X_1 \\ X_2 \\ X_3 \end{bmatrix} = \begin{bmatrix} c_2 & 0 & s_2 \\ 0 & 1 & 0 \\ -s_2 & 0 & c_2 \end{bmatrix} \begin{bmatrix} a_1 \\ a_2 \\ a_3 \end{bmatrix} \tag{A.22}$$

or

$$\underset{(3,1)}{X} = \underset{(3,3)}{\lambda_2} \; \underset{(3,1)}{a} \tag{A.23}$$

where

$$\underset{(3,3)}{\lambda_2} = \begin{bmatrix} c_2 & 0 & s_2 \\ 0 & 1 & 0 \\ -s_2 & 0 & c_2 \end{bmatrix} \tag{A.24}$$

It follows from Fig. A.5 that

$$\underset{(3,3)}{\lambda_3} = \begin{bmatrix} c_3 & -s_3 & 0 \\ s_3 & c_3 & 0 \\ 0 & 0 & 1 \end{bmatrix} \tag{A.25}$$

where

$$a = \lambda_3 b \tag{A.26}$$

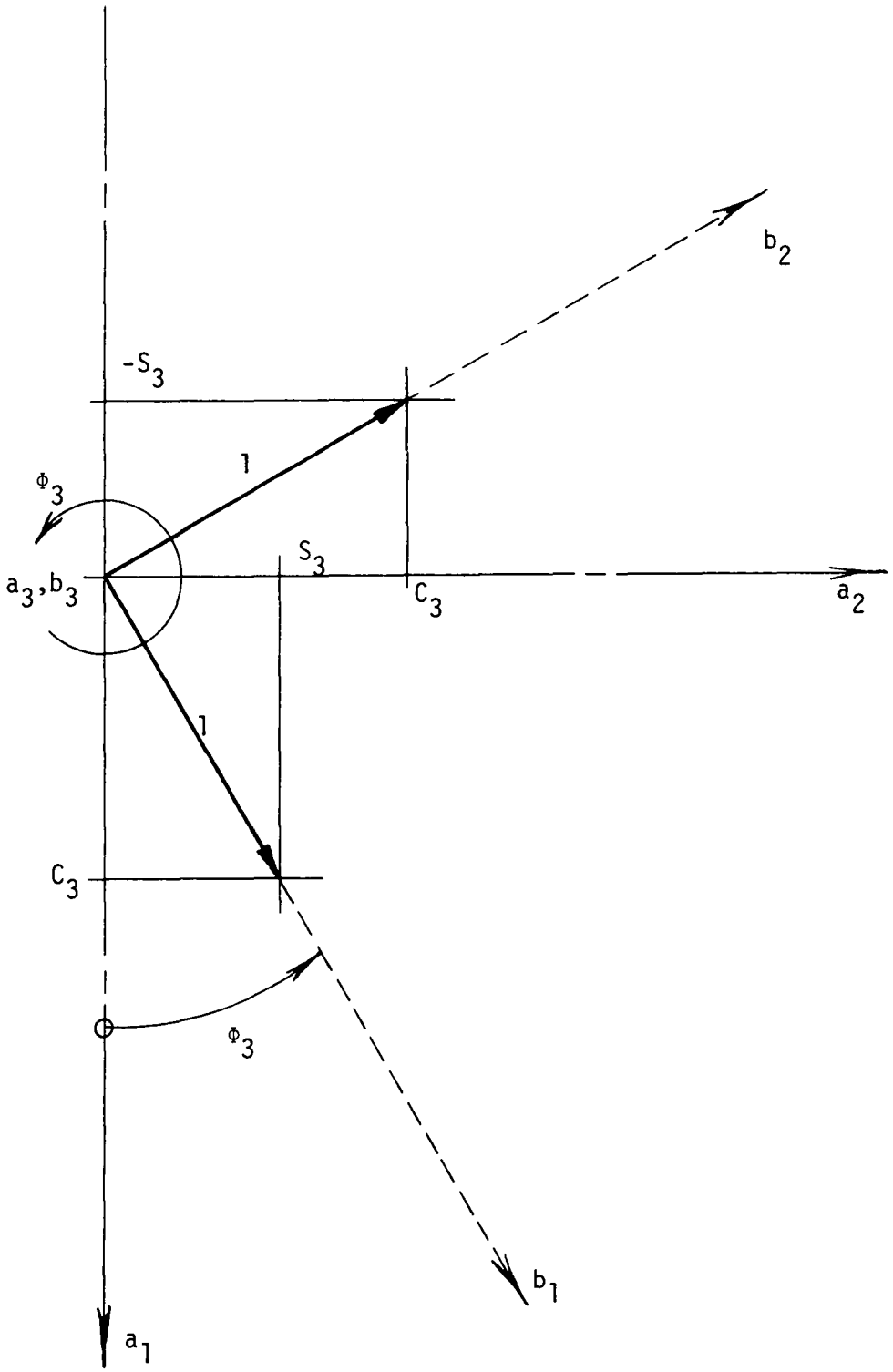

FIG. A.5 - Rotational Transformation, Φ_3

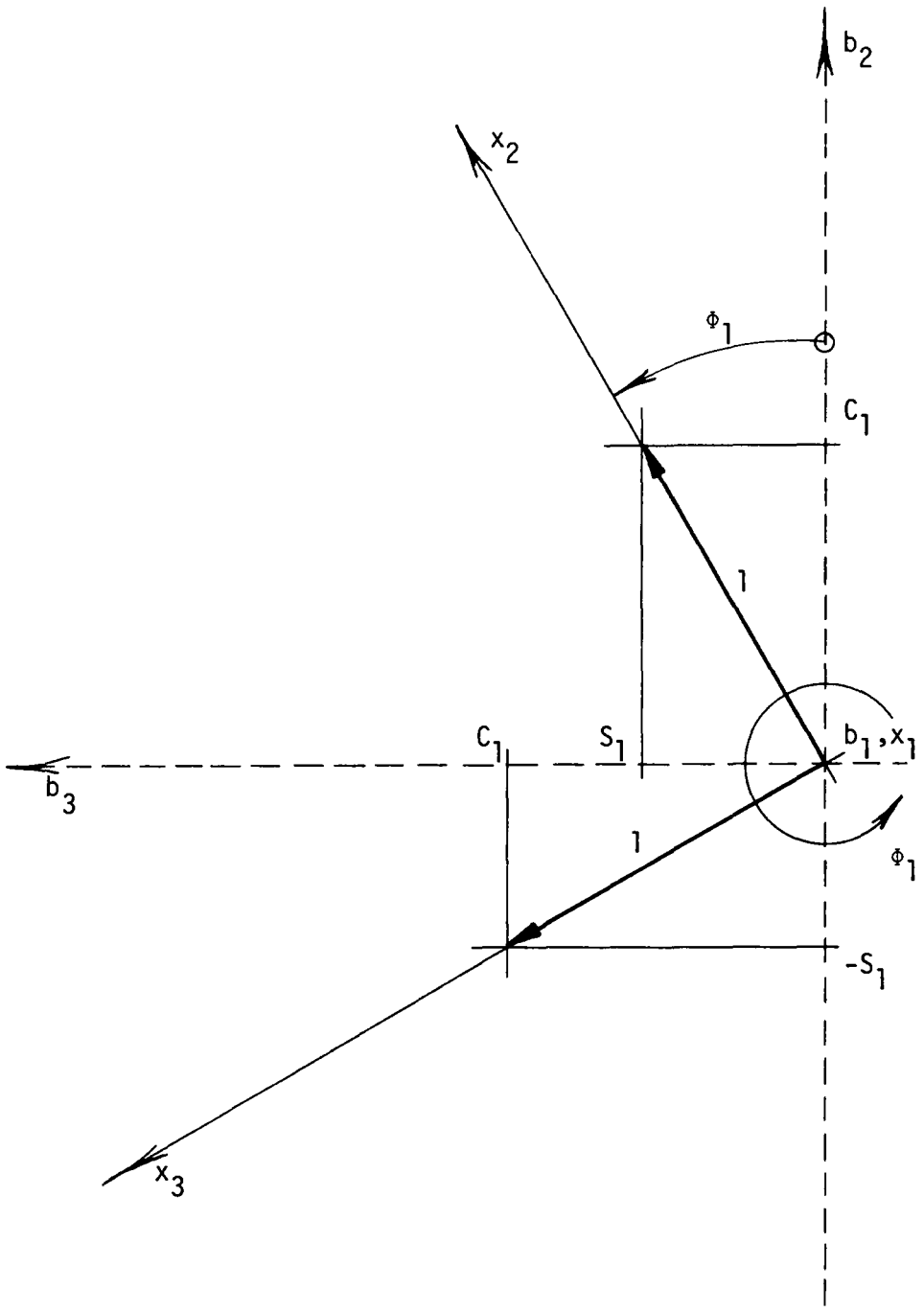

FIG. A.6 - Rotational Transformation, Φ_1

Similarly from Fig. A.6

$$\underset{(3,3)}{\lambda_1} = \begin{bmatrix} 1 & 0 & 0 \\ 0 & c_1 & -s_1 \\ 0 & s_1 & c_1 \end{bmatrix} \tag{A.27}$$

where

$$b = \lambda_1 x \tag{A.28}$$

Substituting Eqs. (A.24), (A.25) and (A.27) into Eq. (A.18) yields

$$\lambda = \begin{bmatrix} c_2 & 0 & s_2 \\ 0 & 1 & 0 \\ -s_2 & 0 & c_2 \end{bmatrix} \begin{bmatrix} c_3 & -s_3 & 0 \\ s_3 & c_3 & 0 \\ 0 & 0 & 1 \end{bmatrix} \begin{bmatrix} 1 & 0 & 0 \\ 0 & c_1 & -s_1 \\ 0 & s_1 & c_1 \end{bmatrix} \tag{A.29}$$

or

$$\underset{(3.3)}{\lambda_{FRAME}} = \begin{bmatrix} c_2c_3 & s_1s_2-c_1c_2s_3 & c_1s_2+s_1c_2s_3 \\ s_3 & c_1c_3 & -s_1c_3 \\ -c_3s_2 & c_2s_1+c_1s_2s_3 & c_1c_2-s_1s_2s_3 \end{bmatrix} \tag{A.30}$$

Eq. (A.30) is the coordinate transformation matrix for a frame element arbitrarily located in space.

In the case of vertical space frame elements such as the element i shown in Fig. A.7, the coordinate transformation matrix is altered by the fact that there is no need to rotate the element through the angle Φ_2. Φ_2 is used to locate the vertical plane containing the element

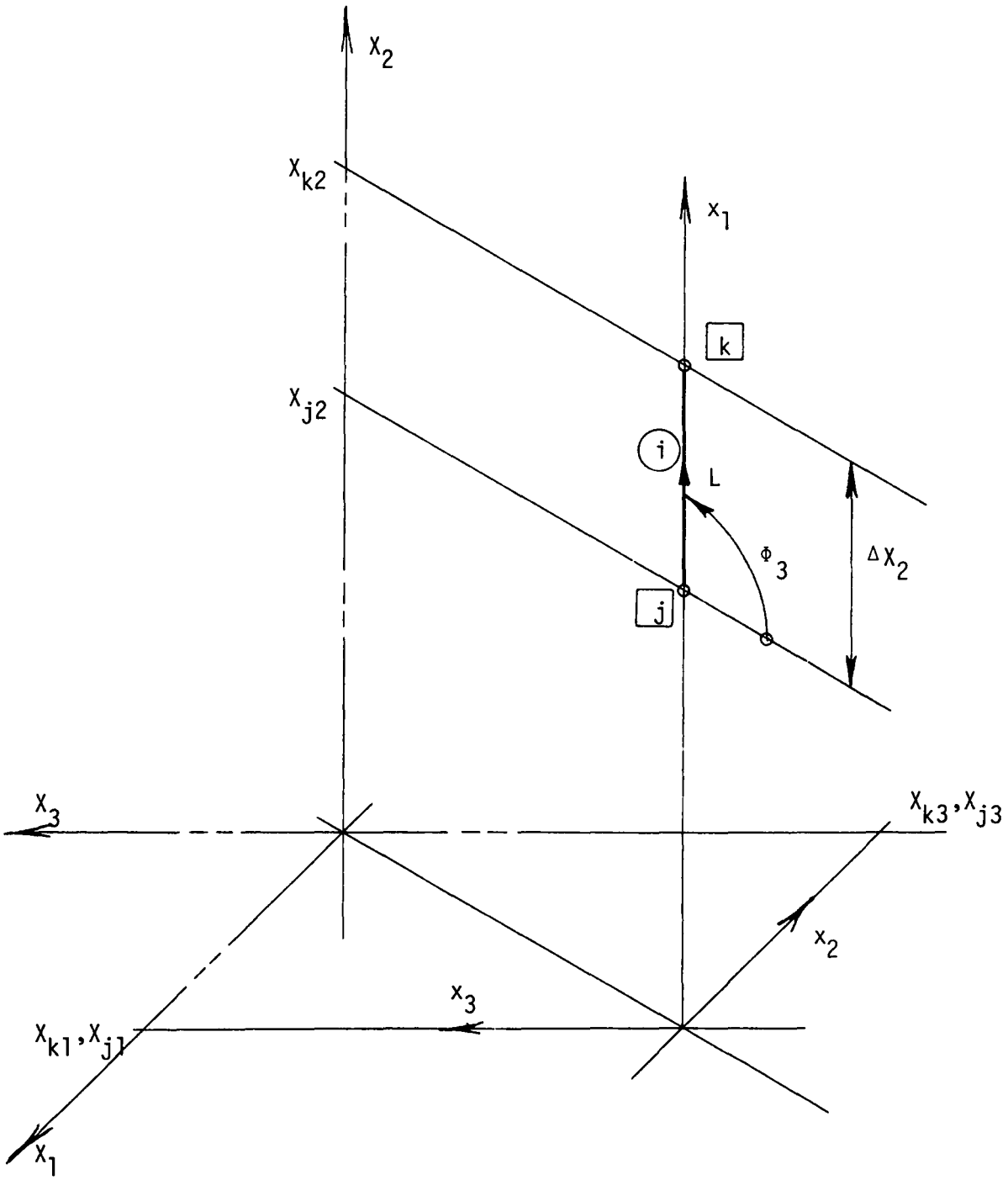

FIG. A.7 - Vertical Frame Element i Arbitrarily Located in Space

relative to the X_2-X_1 plane of Fig. A.3. Since a vertical element is contained in all vertical planes passing through the element i, it is logical to require that the angle Φ_2 be zero [10]. If Φ_2 is zero, then Φ_1 is measured from the X_2-X_1 plane as shown in Fig. A.8.

If

$$\Phi_2 = 0 \tag{A.31}$$

then

$$c_2 = \cos \Phi_2 = 1 \tag{A.32}$$

$$s_2 = \sin \Phi_2 = 0 \tag{A.33}$$

Substitution of Eqs. (A.32) and (A.33) into Eq. (A.30) yields

$$\lambda_{\substack{\text{VERTICAL} \\ (3,3)}} = \begin{bmatrix} c_3 & -s_3c_1 & s_1s_3 \\ s_3 & c_1c_3 & -s_1c_3 \\ 0 & s_1 & c_1 \end{bmatrix} \tag{A.34}$$

Eq. (A.34) is the coordinate transformation matrix for a vertical space frame element as presented by Gere and Weaver [9].

The coordinate transformation matrix for a space truss can be obtained by extracting the first column of Eq. (A.30) since a truss element is assumed to carry only axial loads. Thus

$$\lambda_{\substack{\text{TRUSS} \\ (3,1)}} = \begin{bmatrix} c_2c_3 \\ s_3 \\ -c_3s_2 \end{bmatrix} \tag{A.35}$$

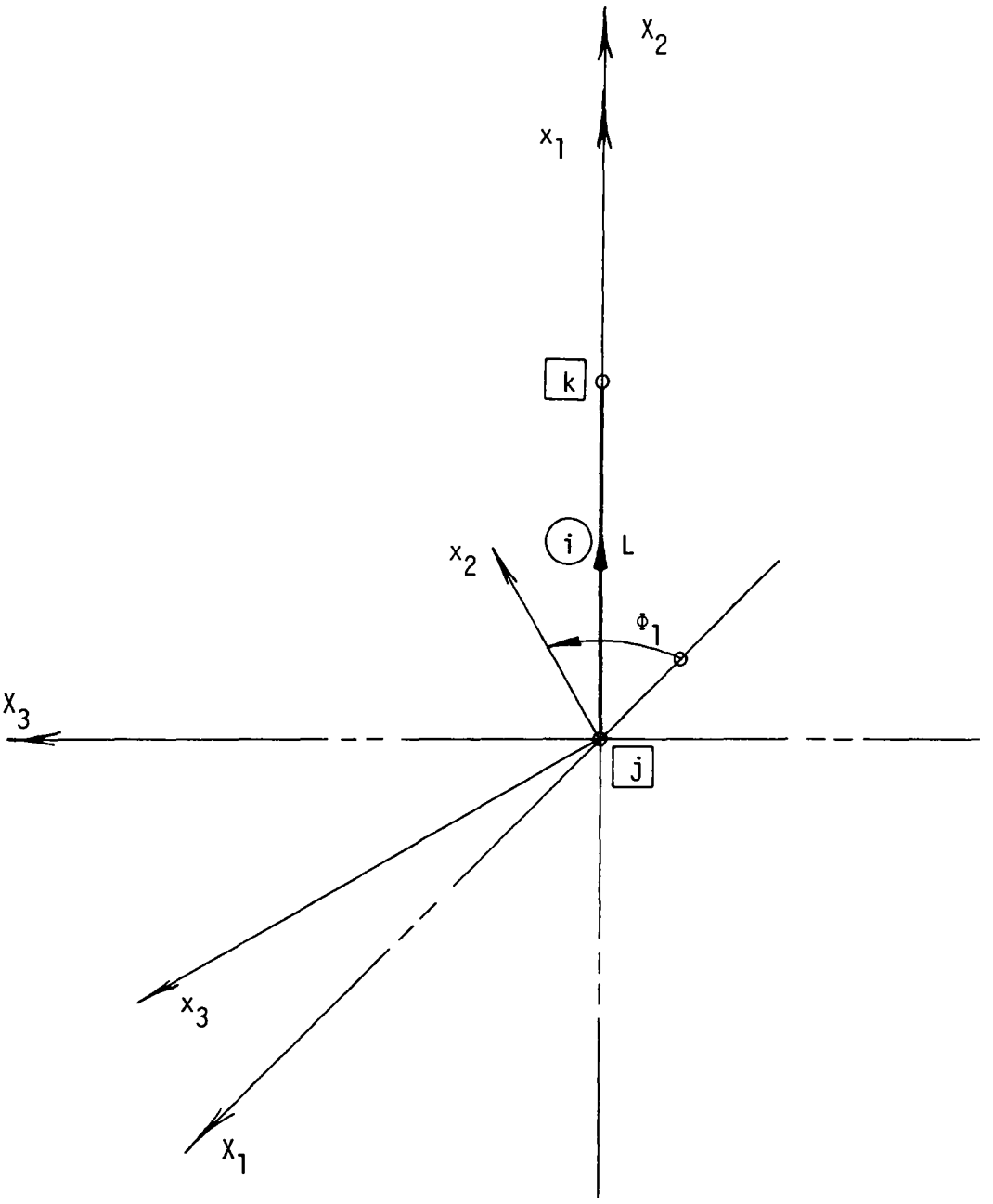

FIG. A.8 - Vertical Frame Element i Rotated Through Angle Φ_1

APPENDIX B

PRELIMINARY CALCULATIONS FOR THE FULLY-STRESSED DESIGN OF DEMONSTRATION PROBLEM NO. 1

B.1 Introduction

The method employed in calculating the applied joint loads due to snow and wind effects is explained in this appendix. The method described is similar to a procedure presented in reference [16].

B.1.1 Procedure for Computing Applied Snow Loading

The first step in the method is to consider each triangular face of the geodesic dome isolated from the other faces in the dome. The angle of inclination of the face with respect to the horizontal plane is then calculated and used to determine the magnitude of an equivalent distributed snow load.

Next, the area of the triangular face is used to obtain the total load on the face. From equations of static equilibriu, the reactions at the three joints of the face are determined. The total load due to the distributed snow load is removed and the direction of application of the reactive forces at the joints are reversed to produce an equivalent snow loadings consisting only of joint loads. This process is continued until all faces of the dome have been considered. The joint load contributions from each face are then summed at each joint to obtain the total applied load on the dome.

To illustrate the process in greater detail, a step by step sample procedure is performed for one of the triangular faces of the dome

using Figs. B.1 through B.3.

STEP 1. Consider the triangular face subjected to an equivalent distributed snow load as shown in Fig. B.1. Isolate the face from all other faces of the dome.

STEP 2. Determine the magnitude of the equivalent distributed snow load on the surface of the inclined face, using the angle of inclination, θ, between the plane of the face and the horizontal plane as shown in Fig. B.2:

$$q' = q \cos\theta \tag{B.1}$$

STEP 3. Compute the area of the face:

$$A = (1/2)b\ h \tag{B.2}$$

where b = base length of triangular face and h = height of triangular face.

STEP 4. Determine the value of an equivalent concentrated load, P:

$$P = q'\ A \tag{B.3}$$

STEP 5. Locate the centroid of the triangular face and apply force P at this point.

STEP 6. Compute the reactions R_1, R_2, R_3 of Fig. B.1 using equations of static equilibrium.

STEP 7. Remove the equivalent concentrated force, P, and reverse the

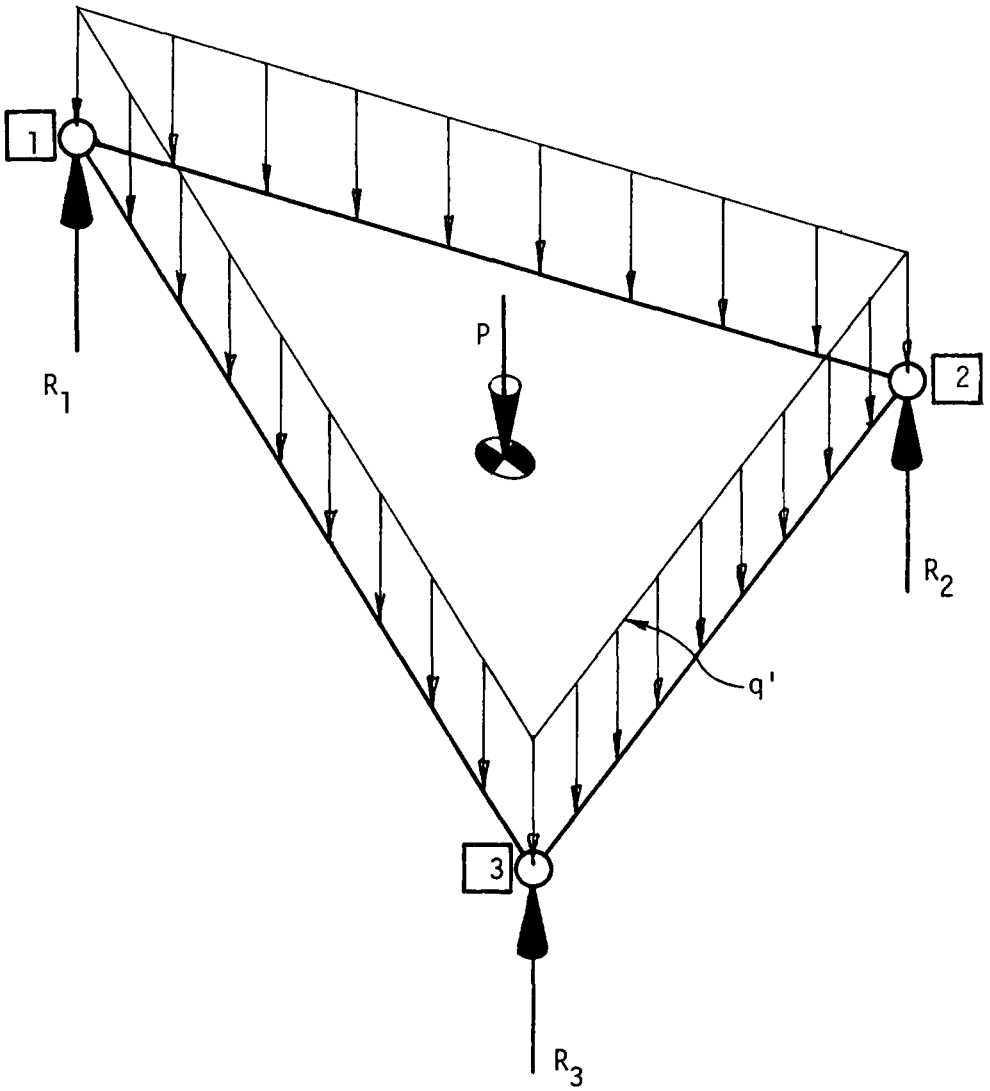

FIG. B.1 - Triangular Face Subjected to Distributed Load q'

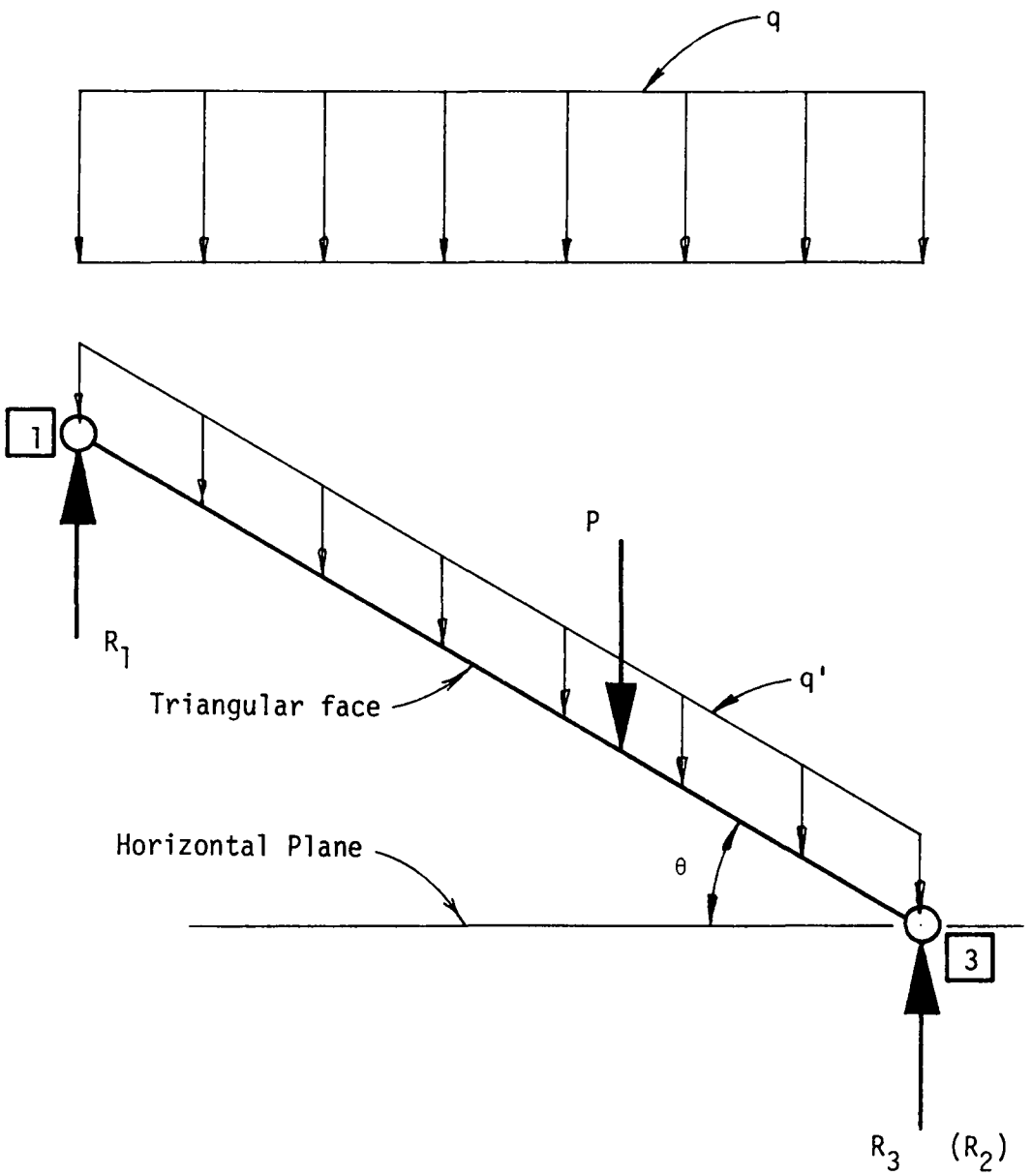

FIG. B.2 - Side View of Triangular Face Subjected to an Equivalent Distributed Load q'

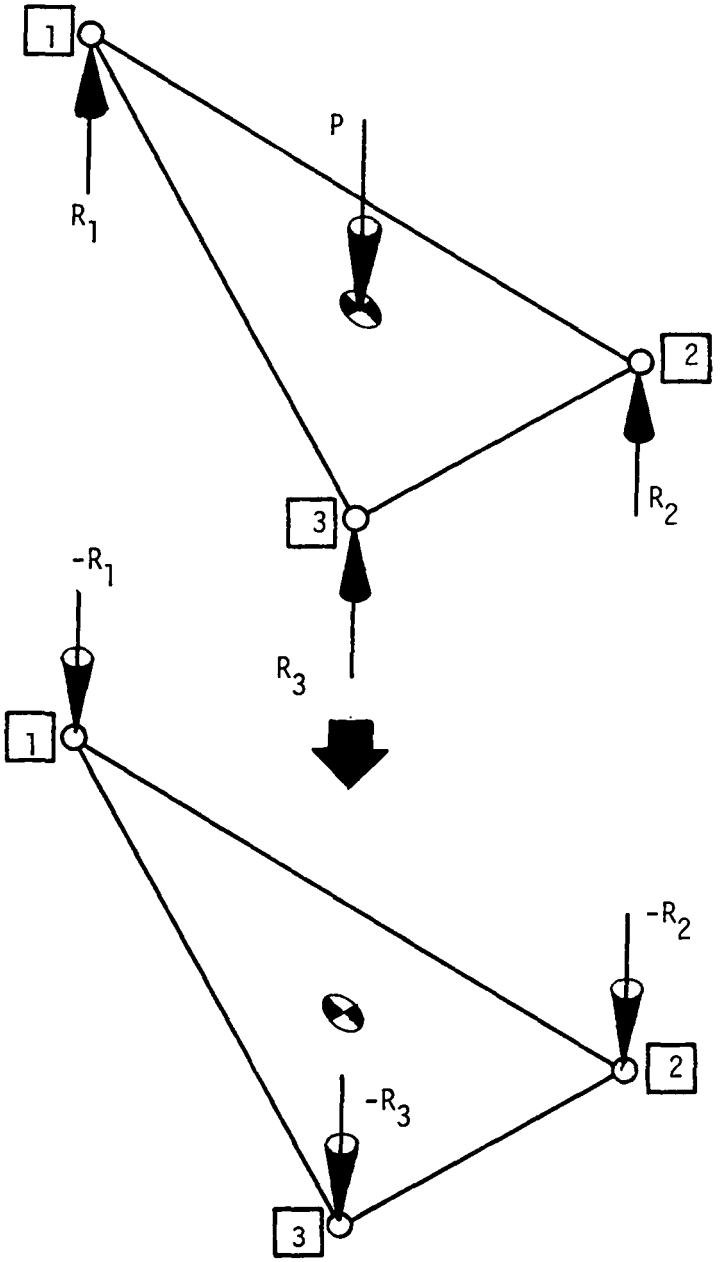

FIG. B.3 - Computation of Equivalent Joint Loading

direction of application of the reaction forces R_1, R_2 and R_3 as shown in Fig. B.3. These forces represent an equivalent joint loading for the actual distributed snow load on the triangular face.

STEP 8. Tabulate and sum the joint loads for all faces at each joint of the dome to obtain the total equivalent joint loading on the dome due to the applied distributed snow load, q.

B.1.2 Procedure for Computing Applied Wind Loading

The procedure for calculating the applied joint loads due to wind is identical to the procedure used for snow. However, joint forces are summed in the vertical as well as horizontal directions. This is due to the nature of the application of the loading.

To illustrate the procedure, a step by step explanation of the calculations is provided.

STEP 1. Consider each triangular face of the dome isolated from the rest of the structure and subjected to a distributed wind load, q, as shown in Fig. B.4.

STEP 2. Determine the magnitude of the distributed load, q, on the triangular face utilizing the information provided by the ASCE Sub-Committee No. 31 [16]. The procedure involves computing the angle between the face and a vertical plane which is perpendicular to the wind direction. Comparing the value of this angle to the information cited above, a wind pressure is selected. This pressure is applied normal to the surface of the face in the form of a distributed load as shown in

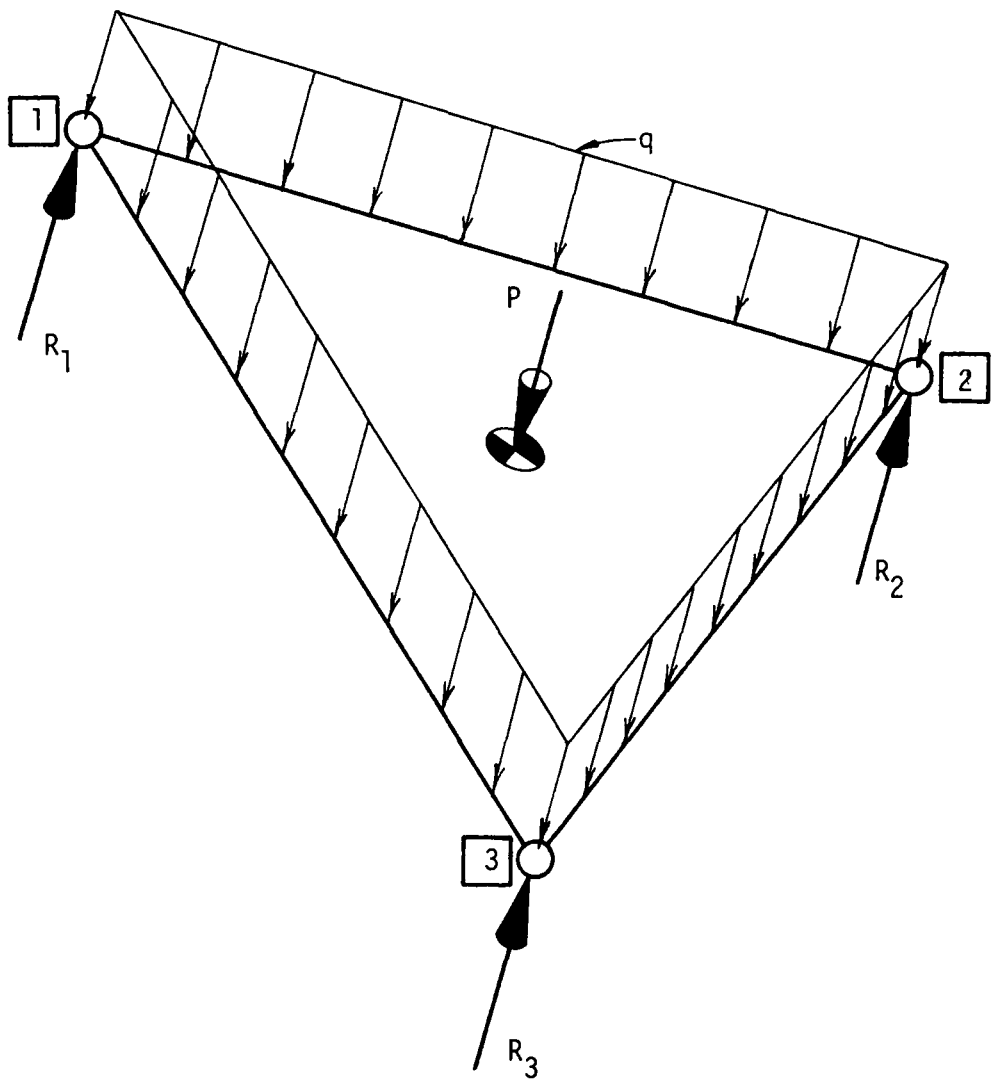

FIG. B.4 - Triangular Face Subjected to Distributed Wind Load q

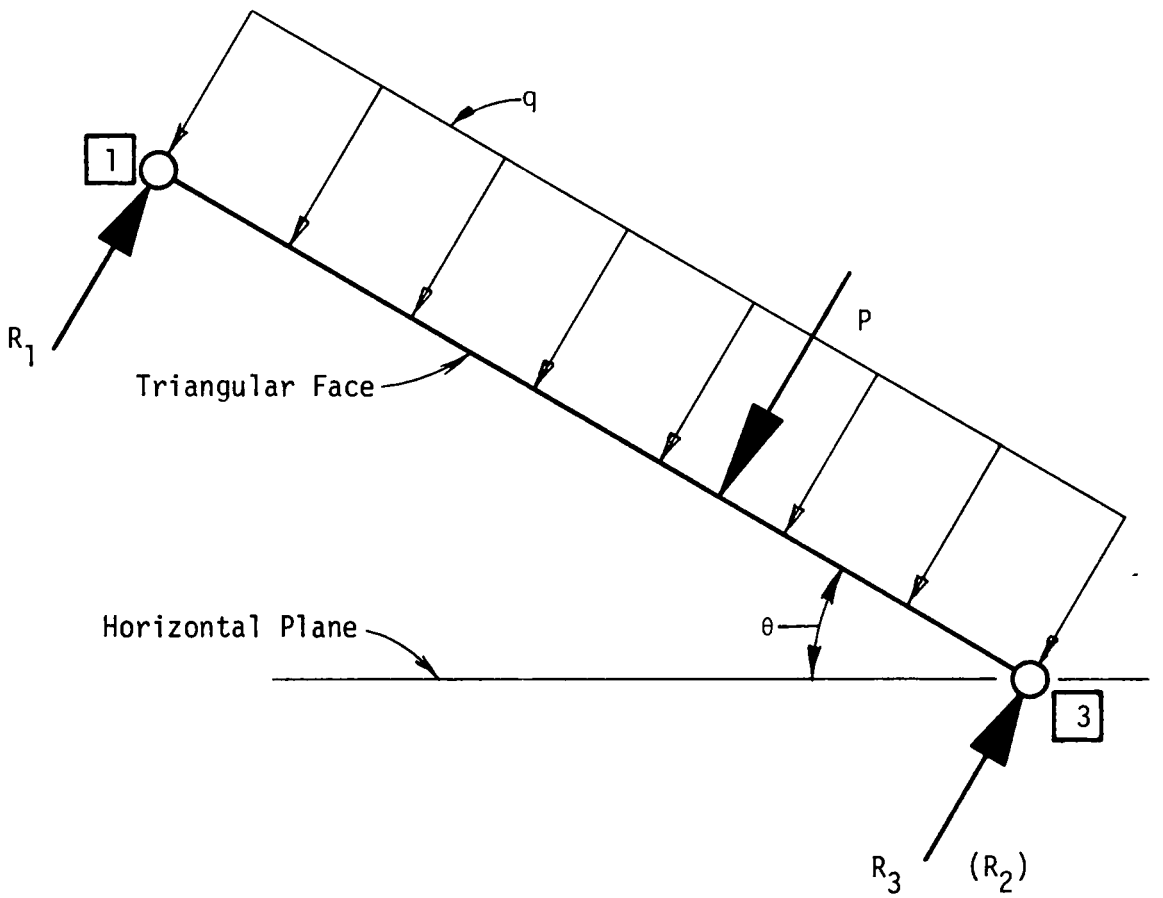

FIG. B.5 - Side View of Triangular Face Subjected to Distributed Load q

Fig. B.5.

STEP 3. Compute the area of the face using Eq. (B.2).

STEP 4. Determine the value of an equivalent concentrated force, P:

$$P = q\ A \tag{B.4}$$

STEP 5. Locate the centroid of the triangular face and apply force P at this point.

STEP 6. Compute the reactions R_1, R_2, R_3 of Fig. B.6 using equations of static equilibrium.

STEP 7. Remove the equivalent concentrated force, P, and reverse the direction of application of the reaction forces R_1, R_2 and R_3 in a similar manner as described in Fig. B.6. These forces represent an equivalent joint loading for the actual distributed wind load acting normal to the surface of the triangular face.

STEP 8. Determine vertical and horizontal components of each "reversed" reaction force using the angle of inclination, θ, shown in Fig. B.5.

STEP 9. Resolve the horizontal components into components applied in the global X and Z directions using the horizontal plane angle, β, shown in Fig. B.7.

STEP 10. Tabulate and sum force components in the global X, Y, Z directions at each joint for all faces to obtain an equivalent joint loading for the applied distributed wind load, q.

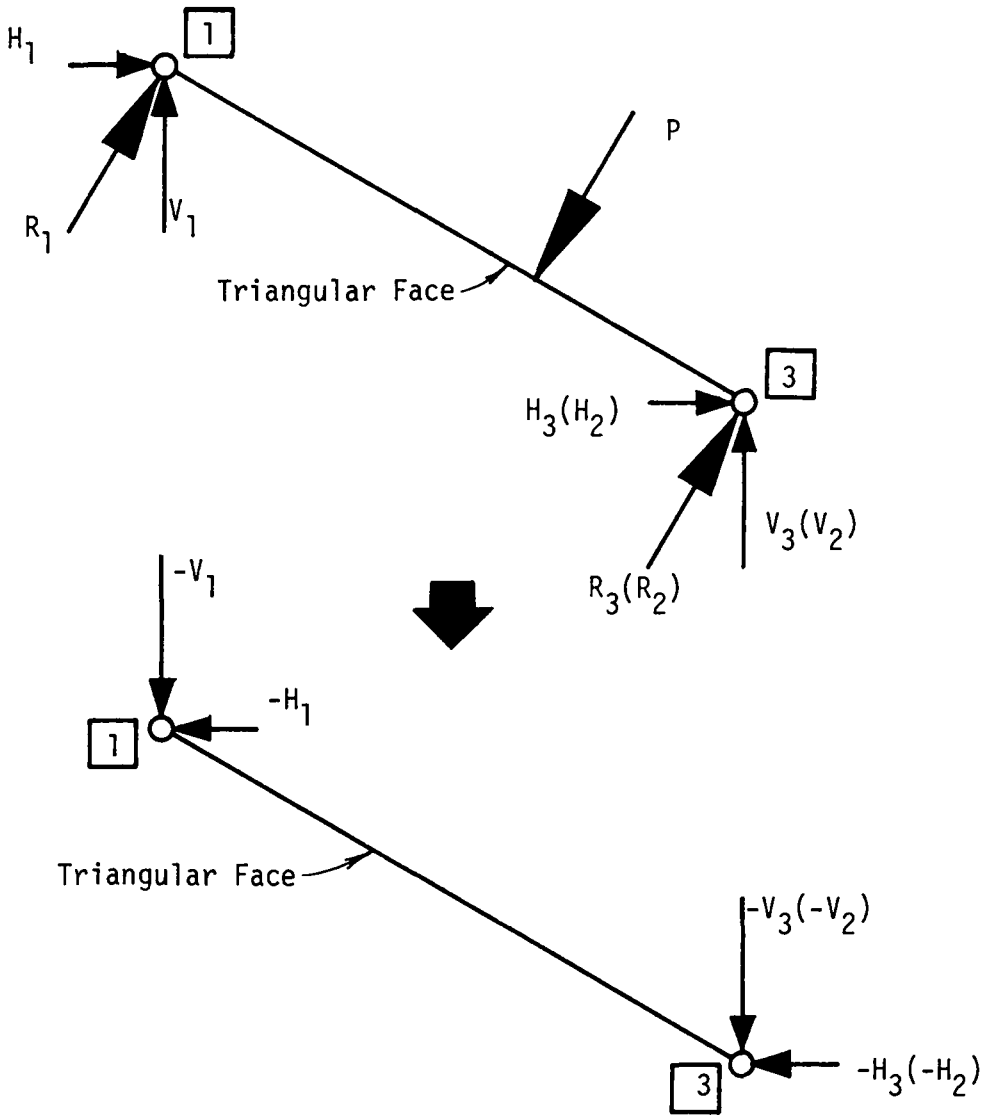

FIG. B.6 - Side View of Triangular Face Subjected to Equivalent Joint Loads

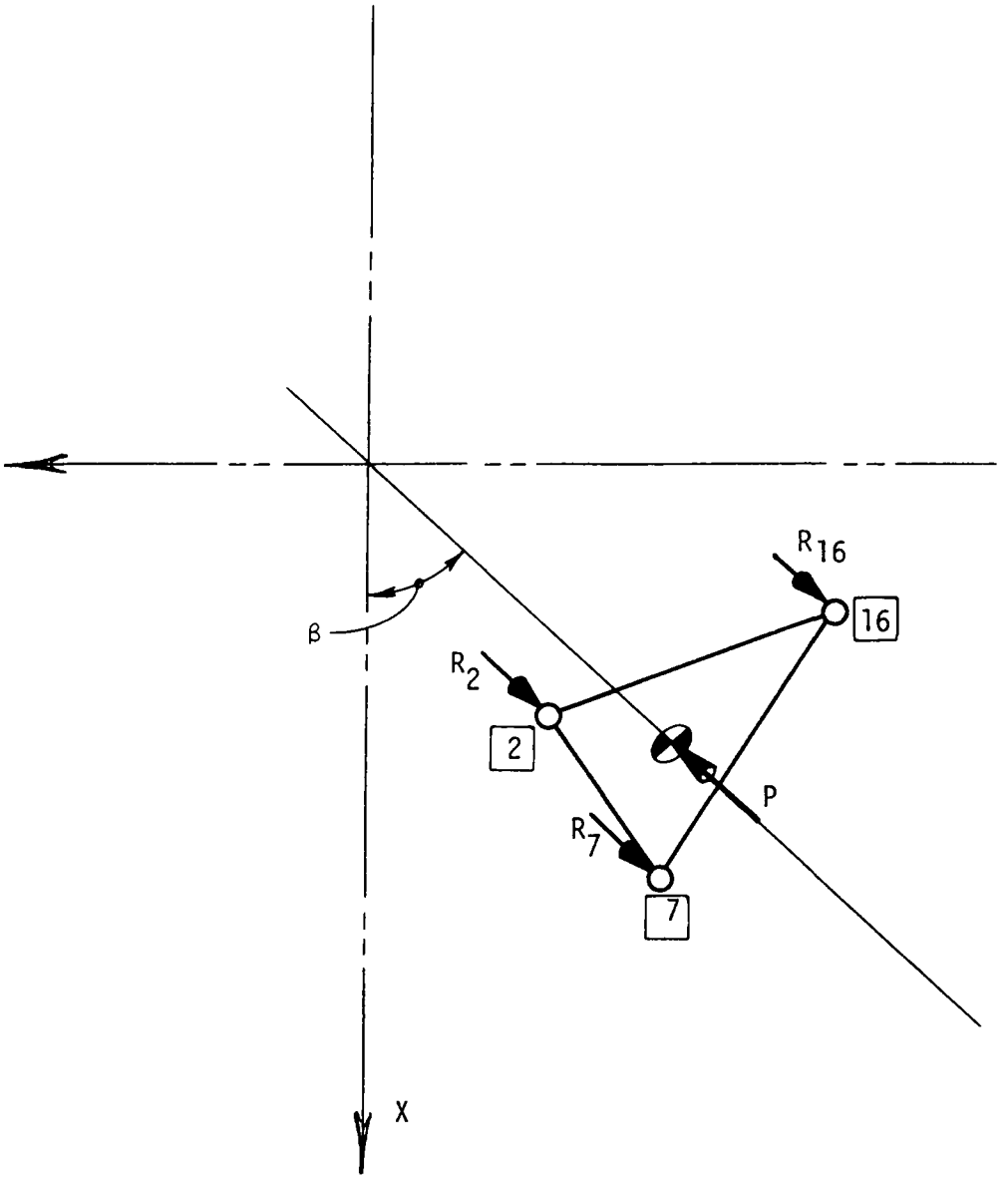

FIG. B.7 - Calculation of Horizontal Components of Joint Loads in X-Z Plane

APPENDIX C

RESULTS OF THE AUTOMATED DESIGN OF DEMONSTRATION PROBLEM NO. 1 SUBJECTED TO DESIGN LOAD COMBINATIONS

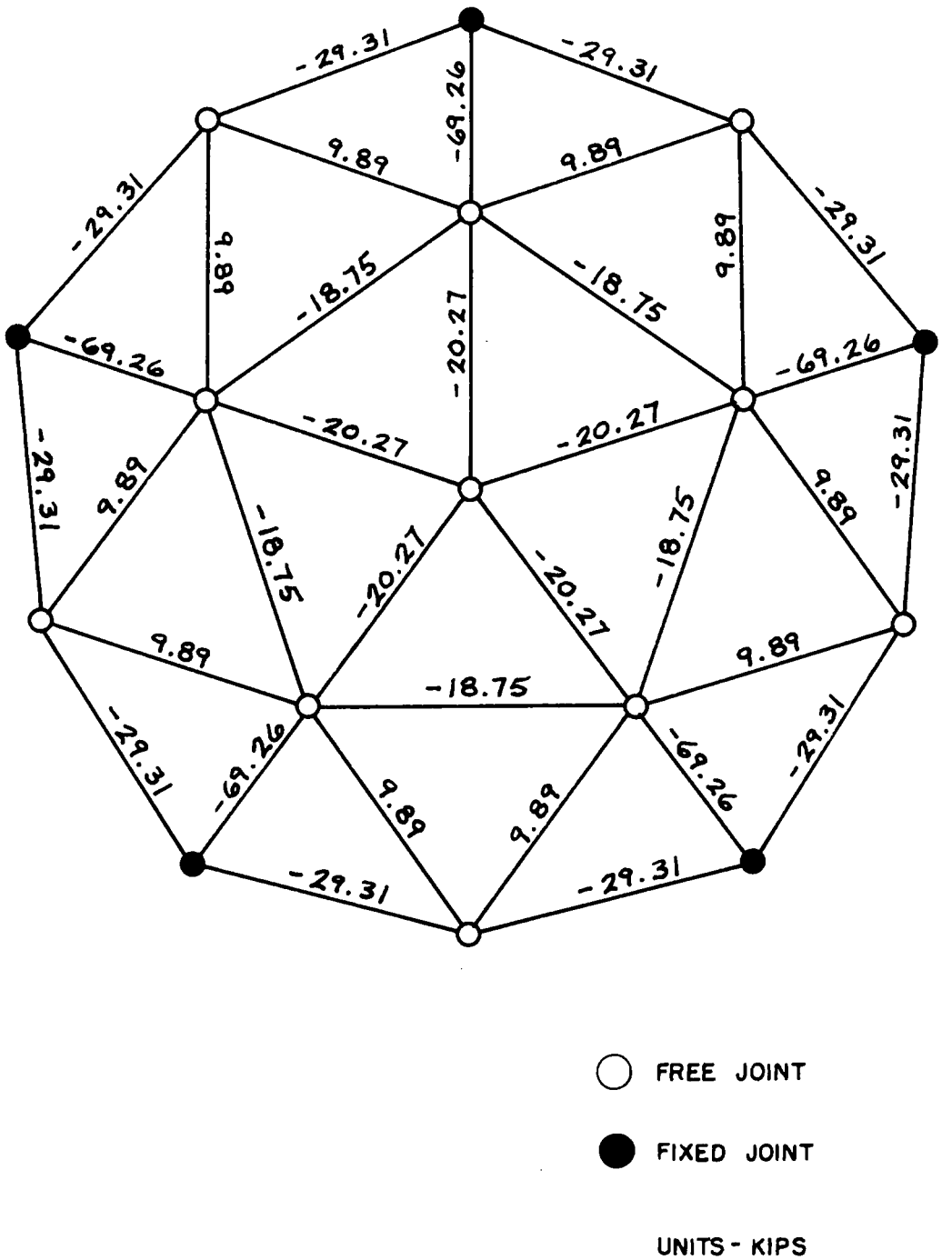

FIG. C.1 - AXIAL LOADS DUE TO DEAD LOAD + SNOW LOAD

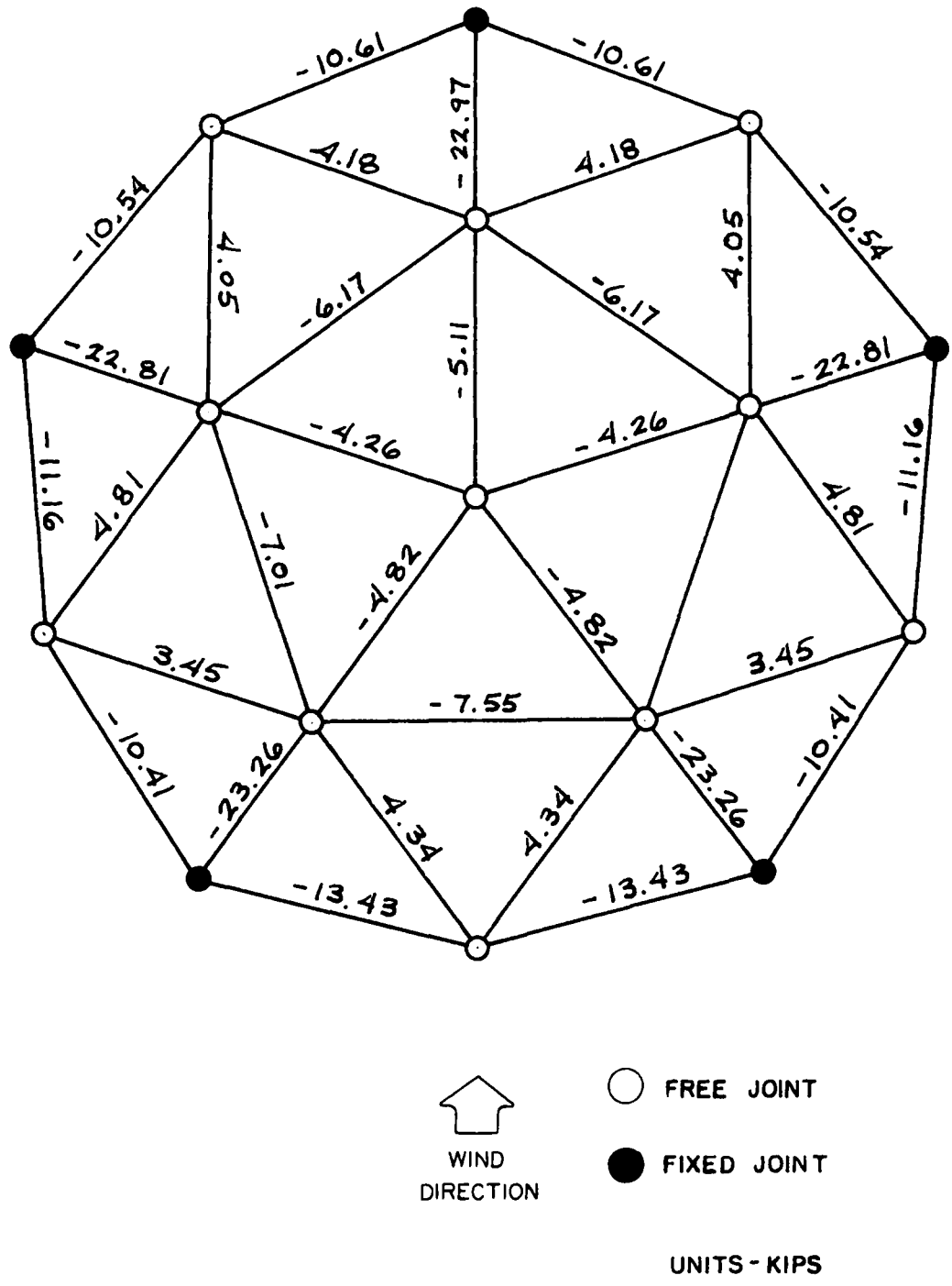

FIG. C.2 - AXIAL LOADS DUE TO 75% (DEAD LOAD + WIND LOAD)

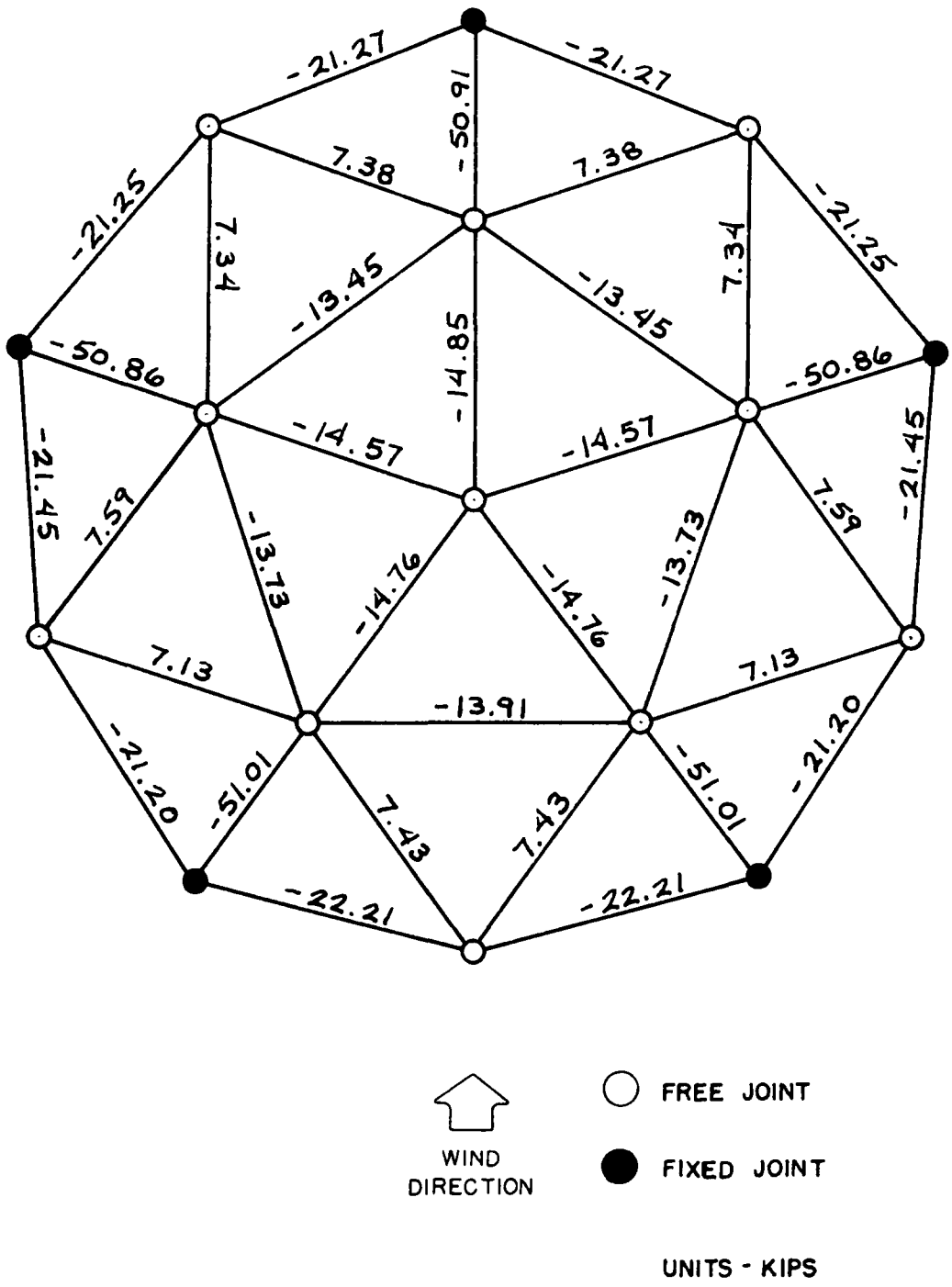

FIG. C.3 - AXIAL LOADS DUE TO 75% (DEAD LOAD + SNOW LOAD + WIND LOAD/3)

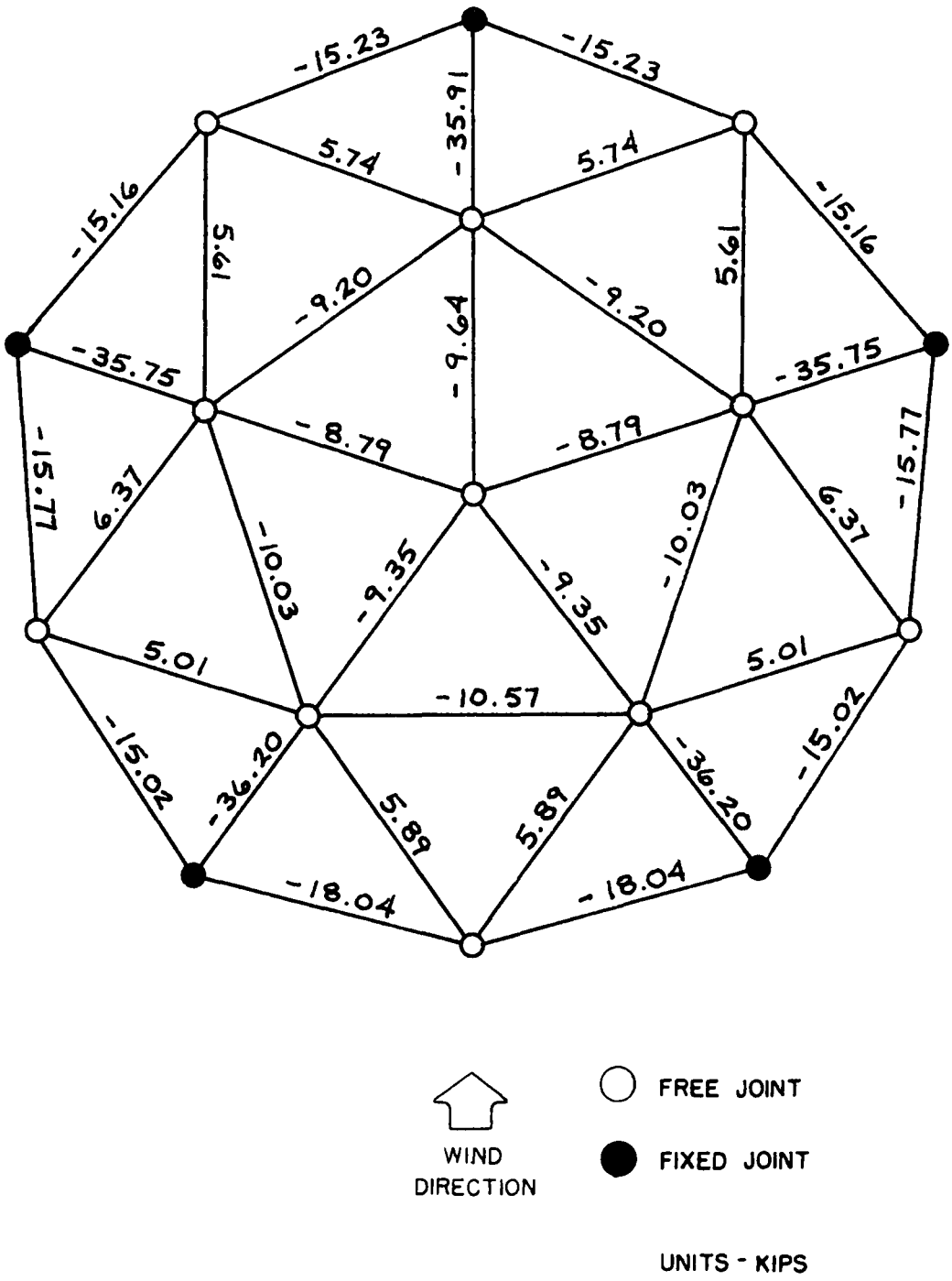

FIG. C.4 - AXIAL LOADS DUE TO 75% (DEAD LOAD + SNOW LOAD/2 + WIND LOAD)

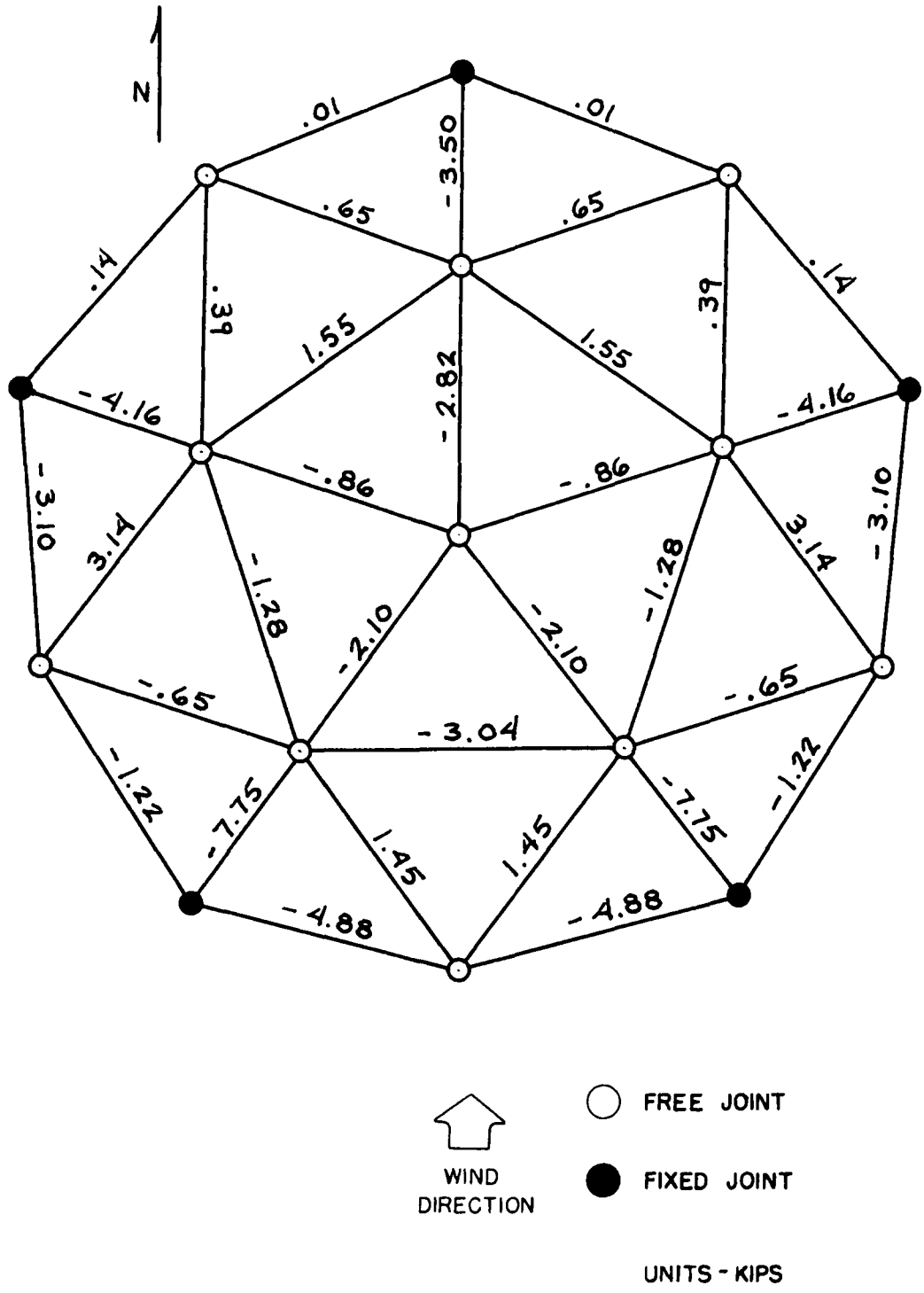

FIG. C.5 - AXIAL LOADS DUE TO 75% (UNBALANCED SNOW LOAD + WIND LOAD)

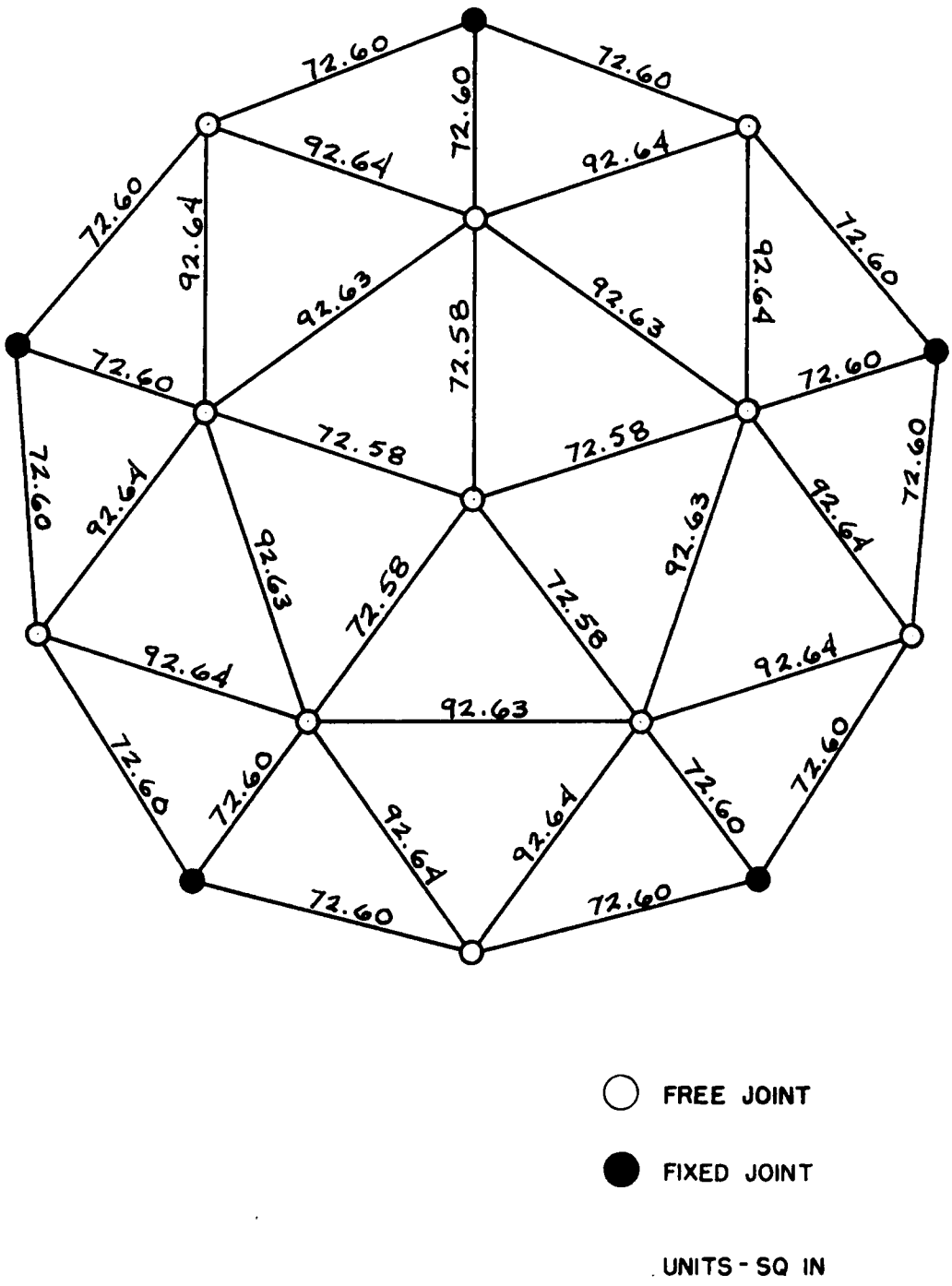

FIG. C.6- INITIAL CROSS-SECTIONAL AREAS FOR DEMONSTRATION PROBLEM NO. I

The vita has been removed from the scanned document

DESIGN AND AN AUTOMATED PARMETRIC STUDY OF GEODESIC DOMES

by

Cecil Allen Jones

(ABSTRACT)

An automated parametric investigation of geodesic domes is conducted in this study. A brief description of the stiffness method of matrix structural analysis is included in addition to a discussion of the fully-stressed design procedure via the stress-ratio method. Automated solution algorithms based on the stiffness method are utilized in the development of WATFIV/FORTRAN computer codes to analyze space trusses and space frames.

Several geodesic dome demonstration problems are formulated and subjected to axisymmetric and asymmetric loads to ascertain the three-dimensional load distribution characteristics of these structures. Shallowness effects are investigated and a demonstration problem is modified to determine the load distribution characteristics in a geodesic dome evenly supported about its base perimeter. Analysis results are recorded and presented along with commentary and conclusions. Several suggestions for further study are also provided.

The WATFIV/FORTRAN computer code for space truss analysis is modified to include a stress-ratio algorithm for an automated fully-stressed design procedure. Numerical results obtained from a computer-aided design of a geodesic dome demonstration problem are provided in the appendix.